21962

NATIONAL LIBRARY
OTTAWA

BIBLIOTHÈQUE NATIONALE
OTTAWA

NAME OF AUTHOR...... Lawrence A. Schienbein

TITLE OF THESIS...... The Design of Single Slotted Flap Airfoil Sections for Low Reynolds Numbers

UNIVERSITY........ Alberta

DEGREE FOR WHICH THESIS WAS PRESENTED...... Ph.D.

YEAR THIS DEGREE GRANTED...... 1974

Permission is hereby granted to THE NATIONAL LIBRARY OF CANADA to microfilm this thesis and to lend or sell copies of the film.

The author reserves other publication rights, and neither the thesis nor extensive extracts from it may be printed or otherwise reproduced without the author's written permission.

(Signed).....

PERMANENT ADDRESS:
#808
105 Dunbrack St.
Halifax, N.S.

DATED..... Nov. 4 1974

INFORMATION TO USERS

THIS DISSERTATION HAS BEEN
MICROFILMED EXACTLY AS RECEIVED

This copy was produced from a micro-
fiche copy of the original document.
The quality of the copy is heavily
dependent upon the quality of the
original thesis submitted for
microfilming. Every effort has
been made to ensure the highest
quality of reproduction possible.

PLEASE NOTE: Some pages may have
indistinct print. Filmed as
received.

Canadian Theses Division
Cataloguing Branch
National Library of Canada
Ottawa, Canada   K1A ON4

AVIS AUX USAGERS

LA THESE A ETE MICROFILMEE
TELLE QUE NOUS L'AVONS RECUE

Cette copie a été faite à partir
d'une microfiche du document
original. La qualité de la copie
dépend grandement de la qualité
de la thèse soumise pour le
microfimage. Nous avons tout
fait pour assurer une qualité
supérieure de reproduction.

NOTA BENE: La qualité d'impression
de certaines pages peut laisser à
désirer. Microfilmée telle que
nous l'avons reçue.

Division des thèses canadiennes
Direction du catalogage
Bibliothèque nationale du Canada
Ottawa, Canada   K1A ON4

THE UNIVERSITY OF ALBERTA

THE DESIGN OF SINGLE SLOTTED-FLAPPED AIRFOIL
SECTIONS FOR LOW REYNOLDS NUMBERS

by

(C)   LAWRENCE A. SCHIENBEIN

A THESIS

SUBMITTED TO THE FACULTY OF GRADUATE STUDIES AND RESEARCH
IN PARTIAL FULFILMENT OF THE REQUIREMENTS FOR THE DEGREE
OF DOCTOR OF PHILOSOPHY

DEPARTMENT OF MECHANICAL ENGINEERING

EDMONTON, ALBERTA

FALL, 1974

THE UNIVERSITY OF ALBERTA

RELEASE FORM

NAME OF AUTHOR ..... Lawrence A. Schimpton

TITLE OF THESIS ..... The Design of Single Slotted-Flapped Airfoil Sections for Low Reynolds Numbers

DEGREE FOR WHICH THESIS WAS PRESENTED ..... Ph.D.

YEAR THIS DEGREE GRANTED 1974

    Permission is hereby granted to THE UNIVERSITY OF

ALBERTA LIBRARY to reproduce single copies of this

thesis and to lend or sell such copies for private,

scholarly or scientific research purposes only.

    The author reserves other publication rights, and

neither the thesis nor extensive extracts from it may

be printed or otherwise reproduced without the author's

written permission.

(Signed) ..... *[signature]*

PERMANENT ADDRESS:

    # 808

    105 Dunbrack

    Halifax, N.S.

DATED ..... Sept. 3, 1974

UNIVERSITY OF ALBERTA

FACULTY OF GRADUATE STUDIES AND RESEARCH

The undersigned certify that they have read, and recommend to the Faculty of Graduate Studies and Research, for acceptance, a thesis entitled "The Design of Single Slotted-Flapped Airfoil Sections for Low Reynolds Numbers" submitted by Lawrence A. Schienbein in partial fulfilment of the requirements for the degree of Doctor of Philosophy.

....
Supervisor

....

....

....

....
External Examiner

Date .. 25 Oct 1974

ABSTRACT

The problems associated with the design of a
slotted-flap airfoil for high lift and low drag at low
numbers ($\approx 10^6$) were investigated and a single slotted-flap
airfoil was designed using a simplified design technique.

A basic design philosophy was developed; the main
points being the proper choice of the basic airfoil section
and the modification of the flap section to achieve the
desired loading. The maximum lift coefficient for low drag
was determined by the onset of flow separation on the main
section while the flap was designed to remain unstalled.

The effects of the boundary layer on the lift and
the pressure distribution were accounted for by a camber
change related to the calculated boundary layer displacement
thicknesses.

A maximum usable lift coefficient of 2 was found
for the slotted-flap airfoil designed in the course of the
project.

ACKNOWLEDGEMENTS

TABLE OF CONTENTS

TABLE OF CONTENTS (Continued)

LIST OF TABLES

LIST OF FIGURES

LIST OF FIGURES (Continued)

LIST OF SYMBOLS

α	airfoil angle of attack
δ_f	flap deflection angle
δ	boundary layer thickness
δ^*	boundary layer displacement thickness
ρ	density
θ	boundary layer momentum thickness
ν	coefficient of kinematic viscosity
c	airfoil chord length (flap retracted)
b	wing span
s	planform area of a wing
x	chordwise displacement or displacement along the surface
y	displacement normal to the airfoil chord or normal to the surface
u	local velocity in the boundary layer
s	displacement along the airfoil surface
u	subscript referring to the upper surface or the suction side
l	subscript referring to the lower or the pressure side
U	local velocity outside the boundary layer
U_∞	free stream velocity
D	profile drag per unit span
D_i	induced drag
L	lift per unit span
$C_D = \dfrac{D}{\frac{1}{2}\rho U_\infty^2 c}$	profile drag coefficient

xii

$C_{Di} = \dfrac{D_i}{\frac{1}{2}\rho U_\infty^2 S}$ induced drag coefficient (s.= planform area)

$C_L = \dfrac{L'}{\frac{1}{2}\rho U_\infty^2 c}$ lift coefficient

C_f skin friction coefficient

C_{Lf} lift coefficient of the flap based on the retracted airfoil chord

$C_p = 1 - \left(\dfrac{U}{U_\infty}\right)^2$ pressure coefficient

$R = \dfrac{U_\infty c}{\nu}$ Reynolds number

$R_{\delta^*} = \dfrac{U\delta^*}{\nu}$

$R_\theta = \dfrac{U\theta}{\nu}$

$A_R = \dfrac{b^2}{s}$ aspect ratio

$\dfrac{x}{c}$ nondimensional chordwise displacement

$\dfrac{\theta}{c}$ nondimensional momentum thickness

$H = \dfrac{\delta^*}{\theta}$ shape factor

$H^* = \dfrac{\delta - \delta^*}{\theta}$ entrainment parameter

$U' = \dfrac{dU}{dx}$

CHAPTER I

INTRODUCTION

1.1 Introduction to the Project.

The purpose of this project was to investigate the problems involved in the design of a single slotted-flap airfoil section at low Reynolds numbers, to develop a design method and to demonstrate the design method by designing and testing a slotted-flap airfoil section.

The design method discussed in the following chapters represents a unique contribution to flapped airfoil design in which specific emphasis has been placed on satisfying the requirements of high speed and low speed flight in the low Reynolds number range. ($R = 10^6$ to 3×10^6.)

In the course of the project:

(1) Three main computer programs were developed for the design process (see Appendices A, B, and D).

(2) A design philosophy was developed and the method was tested by designing and testing a slotted-flap airfoil section.

(3) The design of single element airfoil sections for low Reynolds numbers was studied and some airfoils

1

were designed using a computer program of Truckenbrodt's[1] method (see Appendix C).

The remainder of Chapter 1 includes a general discussion of airfoil design, an introduction to slotted-flap airfoils, a discussion of the design requirements for the project, and an introduction to the analytical design tools (computer programs).

1.2   Introduction to Airfoil Design

In practical aeronautics the designer is interested in bodies where the component of the aerodynamic force acting on the body perpendicular to the direction of motion is much larger than the component acting in the direction opposite to that of motion. Such bodies are called airfoils.

The perpendicular force is called the lift and is of course desirable since it balances the weight of the aircraft. The force opposing motion is called drag. For powered aircraft the drag must be countered by the thrust to maintain level flight. In the case of powerless aircraft the ratio of drag-force to lift force is equal to the tangent of the glide angle.

The design of aircraft is based on the design of airfoil sections. An airfoil section is the cross section of a wing. The design of airfoil sections can be described as the design of a wing of uniform cross section,

constant chord and infinite span. In other words the design
of airfoil sections is two dimensional design.

The chord of an airfoil section is generally
taken to be the length of the longest line joining the
trailing edge and the leading edge although the chord may
be arbitrarily chosen.

The drag of an airfoil section is termed profile
drag and is made up of skin friction drag (viscous drag)
and form drag (pressure drag). Form drag is the result of
the displacement of the streamlines (and hence the alteration
of the pressure distribution) due to the formation of the
boundary layers. In practice the separate determination of
form drag and skin friction drag is not usually important
since the total profile drag can be computed directly using
boundary layer theory or can be measured using a pitot or
hot wire wake traverse.

The lift and profile drag of airfoil sections are
expressed in nondimensional coefficient form. The two-
dimensional lift coefficient, C_L is defined as

$\dfrac{L'}{\frac{1}{2}\rho v^2 c}$ where L' is the lift force per unit span, v is the
speed of the airfoil section (or the free stream speed if
the airfoil is fixed), ρ is the density of the fluid and
c is the airfoil section chord length. The profile drag
coefficient (C_D) is $\dfrac{D}{\frac{1}{2}\rho v^2 c}$ where D is the profile drag

per unit span.

Airfoils (or wings) are not of infinite span nor usually of constant chord and cross-section. Due to the finite span an additional source of drag exists. This drag is termed induced drag and owes its existence to the down-wash induced by the wing tip vortices. The induced drag coefficient (C_{Di}) is $D_i / \frac{1}{2}\rho v^2 s$ where D_i is the induced drag and s is the planform area of the wing. In general C_{Di} is proportional to $\frac{C_L^2}{\pi A_R}$ where the aspect ratio (A_R) is equal to $\frac{b^2}{s}$. (b is the wing span.

The total drag of an actual aircraft is made up of profile drag, induced drag and parasite drag (drag of the other aircraft components such as the fuselage). In airfoil design, parasite drag is not considered. However, the induced drag must be considered since the expected ratio of induced drag to profile drag will determine whether any extra effort should be expended in attempting to reduce the profile drag in the design of the airfoil section. (This is discussed further in section 1.3.)

Design for low speed flight (speeds less than about 250 miles per hour) permits the assumption that air is incompressible. However, the equally tempting assumption that air is an inviscid fluid leads to the paradoxical result that a moving airfoil section experiences neither

lift nor drag.

The application of potential flow theory
(inviscid and incompressible fluid flow) leads to the
prediction of zero profile drag since the property of
viscosity is responsible for this force. In order to
account for the existence of the lift force it was
necessary to introduce the concept of circulation. Circul-
atory flow when superimposed on the uniform incident flow
results in a lift force.

Every airfoil section exhibits a unique lift
coefficient for a given angle of inclination (angle of
attack) with respect to the free stream. In order to
apply potential flow theory to calculate the pressure
distribution and lift, a uniqueness criterion is required
to fix the value of the circulation for a given angle of
attack. Kutta observed that the flow tends to leave the
trailing edge of an airfoil smoothly. That is, the
stagnation streamline leaves the trailing edge and is
tangent to the camber line at that point. This trailing
edge condition (known as the Kutta Condition), when applied
to potential flow methods such as the singularity methods[2],
permits the circulation to be uniquely defined for a given
angle of attack.

When the potential flow calculation methods, such
as Theodorsen's Method[3], are applied to airfoil sections,

the results indicate that one airfoil section is as suitable
as any other in terms of the lift characteristics. That
is, the predicted curves of C_L versus α for all airfoils
will be similar. Only the angle of zero lift will in
general be different for cambered airfoil sections. (The
zero lift angle is equal to zero for all symmetrical
sections.)

In practice the lift curves (C_L versus α) for
all airfoil sections correspond closely to the theoretical
(potential flow) lift curves over only a limited range of
angles of attack. As incidence increases the deviation
from theory increases; a maximum C_L exists for all airfoil
sections for a given Reynolds number. (See for example
Figure 1.)

The deviation from theory is due to the growth
of boundary layers on the surfaces of the airfoil section.
The growth of the boundary layers depends primarily on
the pressure distribution and the Reynolds number. On the
upper surface (suction side) of the airfoil section, the
boundary layer thickness increases with incidence. Con-
sequently the streamline pattern (and therefore the pressure
distribution) is different than the theoretical so that
the lift coefficient is reduced from the theoretical value
of potential flow theory; the difference between experimental
and theoretical lift increases with incidence.
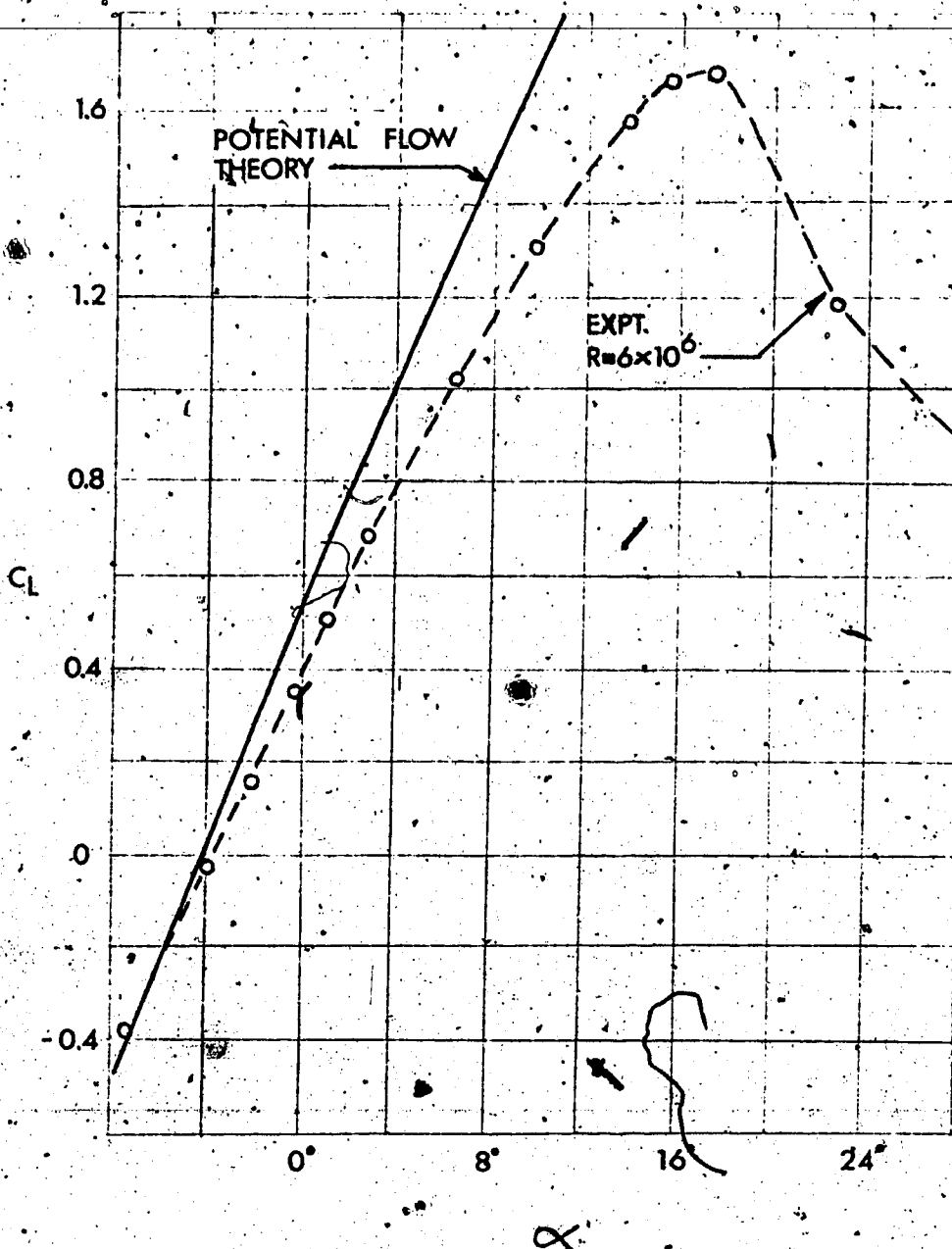
Figure 1. Comparison between Theoretical and Measured
Lift Coefficients for the NACA 4412 Wing
Section (Ref. 3)

Ultimately the boundary layer is no longer able to overcome the steep adverse pressure gradient associated with increasing incidence. The boundary layer will separate and the rate of increase of C_L with α decreases with α as the region of separated flow (on the suction side) expands. Eventually a maximum C_L is reached. This phenomenon is called trailing edge stall.

Since potential flow methods can predict neither the actual lift nor the drag characteristics the design of airfoil sections requires the application of boundary layer calculation methods to predict the drag based on the potential flow pressure distribution. Then the pressure distribution (and therefore the lift) can be corrected to account for the boundary layer. A very important part of boundary layer calculation methods are the methods of predicting boundary layer transition and separation.

The lift-drag characteristics of an airfoil section are described using the lift curve and the lift-drag polar (C_L versus C_D). Since C_L and C_D are functions of Reynolds number, a complete description usually consists of a number of curves for various Reynolds numbers. (Figures 1 and 5 are examples of these curves.)

Preventing boundary layer separation is the key to extending the low drag range or the range of useful lift coefficients for flight Reynolds numbers. Given a design

pressure distribution that will delay boundary layer
separation, inverse potential flow methods, such as that
of Truckenbrodt[1], can be applied to yield the airfoil
section shape that will exhibit the desired drag charact-
eristics. Boundary layer theory is applied not only to
predict the drag but also to find the boundary layer
displacement thickness distribution which is required to
correct the potential flow pressure distribution for the
effect of the boundary layer.

A discussion of the potential flow calculation
method used in this project (the method of distributed
vorticity) is found in Appendix A. Appendix B is a
discussion of boundary layer analysis and the methods
employed in the project. Appendix C is a discussion of
airfoil design for specified design pressure distributions.

1.3   The Design of Slotted-Flap Airfoil Sections

The design of airfoil sections is complicated
by the fact that aircraft operate over a range of speeds.
Therefore a single element wing section must be designed
as a compromise between the requirements of high speed and
low speed. The wing section lift-drag characteristics
when applied to an aircraft are, in reality, an envelope of
lift-drag polars for the range of flight Reynolds numbers
rather than one polar for a particular Reynolds number.
(The lift-drag polar for the Phoenix sailplane[4] is shown

in Figure 2 as an example.)

The desired high speed characteristics of an airfoil section are low profile drag and small pitching moment while good low speed performance requires high lift coefficients, low drag and a gentle stall.

For powered aircraft, the use of a wing section capable of providing high lift at low speeds results in a lower take-off speed and hence a shorter take-off run. At the same time the power required for take-off can be reduced if the drag coefficient is minimized. On the other hand sailplanes require high lift and low drag at low speeds in order to reduce the sinking speed while circling in thermals.[5]

Good high speed performance is best achieved with an airfoil section of small camber while high lift at low speeds requires a highly cambered section. Increasing the camber of an airfoil results in an upward displacement of the low drag range so that at low lift coefficients (high speed flight) the profile drag is increased. In other words, attempting to improve the low speed performance of an airfoil by an increase in the camber results in a loss of performance at high speeds.

For low speed aircraft operating in the range $R = 10^6$ to 2×10^6 for sailplanes and $R = 2 \times 10^6$ to 4×10^6 for powered aircraft, good performance requires
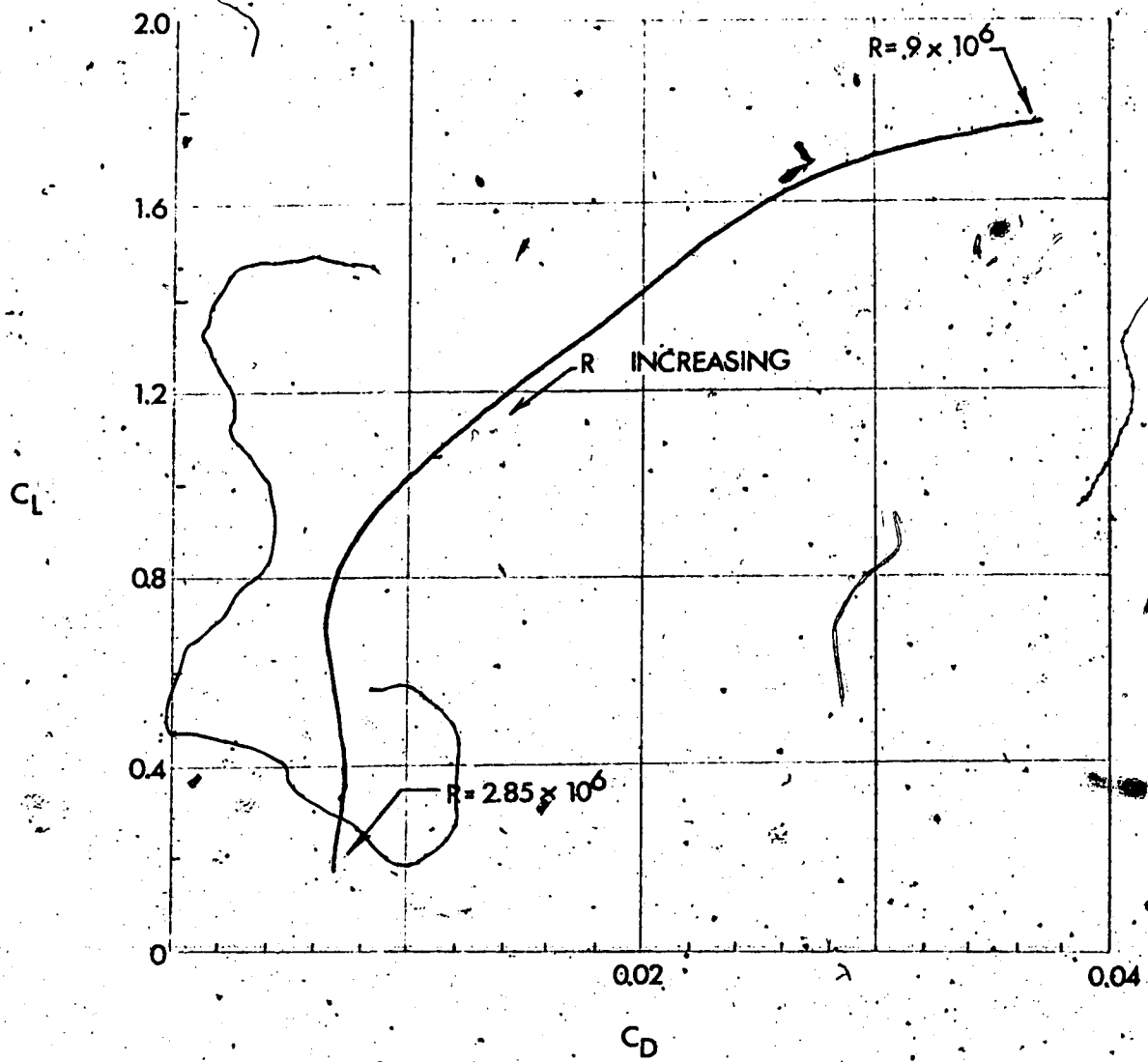
Figure 2. Flight Lift-Drag Polar for the Wing Section used on the Phoenix Sailplane

the lowest possible stalling speed and the lowest possible

profile drag. To improve performance, the maximum lift
coefficient must be increased while at the same time the
drag coefficient is minimized. Ideally this should be
accomplished without sacrificing the high speed performance.
This problem has been explored extensively by airfoil
designers to find the best compromise for a single element
section. The work by Wortmann[6] perhaps best illustrates
this but many other investigators have designed airfoils
for the best compromise for a particular case (see Reference
7 for example). Some investigators have looked at extreme
cases such as maximum possible lift (Liebeck[8]) or minimum
possible drag (Wortmann[6]).

The use of variable geometry or multi-element
airfoils should make it possible to design for a wider
range of conditions in that high speed characteristics
need not be seriously compromised in favor of low speed
or vice-versa. Flaps and slats have been used for this
purpose since the early days of aviation.

In the last 50 years a number of camber
modifying devices have been proposed and tested including
the plain flap, leading edge flap, the drooped nose, the
split flap and the slotted-flap.[9] The slotted-flap has
proven to be the most successful means of increasing the
maximum lift coefficient of airfoil sections while at the

same time extending the low drag range[9] because large scale flow separation on the flap is delayed by air flow through the slot. In other words, the slot permits the development of a new boundary layer on the suction side of the flap and this boundary layer is better able to overcome the steep adverse pressure gradient on the flap without separating.

Three possible design routes can be defined for the design of slotted-flap airfoils:

(1) Design a flap which detaches from the trailing edge. The only variable is the slot shape and the flap deflection angle.

(2) Simultaneously design both the flap and the main section, implying varying the geometry of both sections freely.

(3) Design a flap that provides a specified pressure distribution over the upper surface of the flap. Here the flap shape is variable but the main section shape is fixed.

The efforts of the NACA[9] have consisted mostly of studying the relationship between lift, drag, flap position, flap deflection and flap chord length. Their work has in general followed the first route as described in the preceding paragraph, consisting mainly of extensive testing of a wide variety of airfoil-flap combinations at

Reynolds numbers above 3×10^6.

The prospect of designing slotted-flap airfoils for both high lift and low drag can be traced to the work of Stratford[10], Wortmann[6], and Liebeck and Ormsbee.[11] Wortmann and Stratford proposed the concept of optimum pressure recovery and boundary layer development on an airfoil for minimum drag. Liebeck and Ormsbee developed a method for the optimization of airfoil shapes for maximum lift.

Recently Chen[12] has applied the work of Liebeck and Ormsbee to the design of multi-component airfoil sections. Chen's method can be described as following the second design route stated previously. This technique does not take into account the high speed requirements in the design of the airfoil sections.

The third possible approach to the design of slotted-flap airfoils is to design for a specified pressure distribution on the flap by modifying the camber of the flap section. This is the most practical approach because the main section and the flap remain structurally compatible. That is, the flap will retract smoothly because the thickness distribution remains fixed. In this regard two-element airfoils such as those designed by Chen are impractical because the two elements are structurally incompatible. (See Figure 3.)
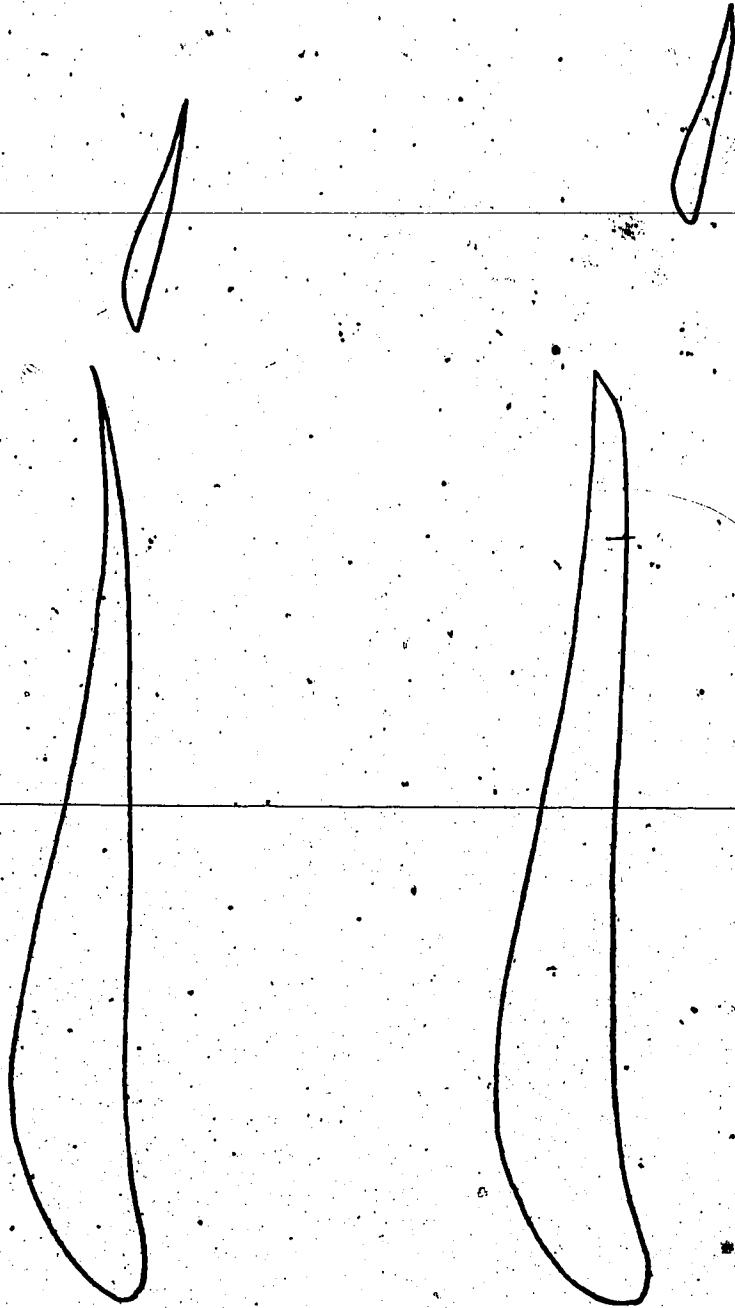
Figure 3. Two-Element Airfoil Shapes Optimized for Maximum Lift (Ref. 12)

1.4 The Design Requirements

The main objective in the design of single slotted-flap airfoil sections is to extend the low drag range to higher lift coefficients. In addition to the benefits of such a wing section in improving performance, as discussed in the last section, the suppression of separation on the flap at high lift coefficients allows the flap to act as a useful control surface beyond the actual stall of the wing section as a unit. This is a very significant benefit because it allows control of the aircraft to be maintained when the wing is stalled.

The reduction of profile drag is still a desirable objective even at high lift coefficients where the induced drag coefficient is usually the largest part of the total wing drag coefficient. For example at $C_L = 1.5$ and with wing aspect ratio of 25, the induced drag coefficient is about 0.03. At $R = 10^6$ to 2×10^6 however, the profile drag coefficient for a high lift single slotted-flap airfoil may easily exceed 0.06.[13] Hence a reduction in profile drag coefficient from 0.06 to say 0.02 represents a 45% reduction in the total drag. Similarly for a wing aspect ratio of ten, which is typical of light aircraft, the induced drag coefficient at $C_L = 1.5$ is about 0.07. Here a reduction in the profile drag coefficient from 0.06 to 0.02 represents a 30% drag reduction.

The design of a slotted-flap airfoil represents an overconstrained problem for which an optimum solution cannot be found. A design can be termed successful if it provides the desired performance while satisfying the mechanical and structural requirements.

For light aircraft it is desirable to design a two-element wing for one flap deflection angle and one flap position only in order to reduce the size, complexity and the weight of the flap deflection mechanism.

The main effect of low Reynolds numbers on the design of flapped airfoils is to limit the flap loading and hence the maximum lift coefficient. A realistic but significant design objective at a Reynolds number of 10^6 is to attempt to obtain the lowest possible profile drag up to a lift coefficient of two[14] with a single slotted-flap airfoil section. At the same time the flap should retract smoothly to give a single element airfoil possessing good high speed performance at a Reynolds number of about two to four million.

1.5 Analytical Tools

In airfoil design, the designer must be able to calculate the potential flow pressure distribution over the airfoil section, the lift coefficients, the profile drag coefficients and the correction to the lift due to the boundary layer.

The surface singularity methods, (distributed source and distributed vorticity) as applications of potential flow theory, are ideally suited to the calculation of pressure distributions over multi-element airfoil sections. The advent of the digital computer has made the application of these methods (which generally involve thousands of computational steps) relatively easy. The distributed vorticity method has the advantage of requiring significantly less computing time than the surface source method. For this project Wilkinson's[2] version of the distributed vorticity method was programmed for the single element and for the single slotted-flap airfoil. This method is discussed at length in Appendix A.

For design purposes the prediction of the position of boundary layer separation, the variation of displacement thickness, the growth of the momentum thickness and the extent of laminar and turbulent boundary layers on the airfoil surface are the only boundary layer features that are of interest.

One of the main emphases of this project was to assess current boundary layer calculation methods and to devise a boundary layer analysis computer program incorporating the best techniques in the light of the requirements of the preceding paragraph. These techniques and the reasons for their selection are discussed in Appendix B.

The boundary layer analysis computer program is capable of computing the growth of the momentum thickness and the displacement thickness, and is capable of predicting the positions and mode of boundary layer transition and separation. Particular emphasis was placed on the problem of short laminar separation bubble transition[15] since for Reynolds numbers of about 10^6 this becomes the most probable mode of transition.

The boundary layer analysis program uses the pressure distributions generated by the distributed vorticity method. The program was extensively tested. Airfoil sections used in testing included the FX-67-K-150,[14] FX-67-K-170 and the GU-25-5(11)8[16] for which reliable experimental results exist. In all cases the program succeeded in predicting the profile drag, the position and mode of laminar-turbulent transition and the limits of the low drag range in good agreement with published results.

In the early stages of the project much work was done on the problem of the design of single element low drag airfoils. Several designs were attempted for Reynolds numbers of 10^6 to 3×10^6 using a computer program of Truckenbrodt's method.[1] Two of the designed airfoils as well as a general discussion of the design procedure for low drag at low Reynolds numbers is presented in Appendix C.

CHAPTER II

The Design Method

This chapter outlines the proposed design method. Each step of the design process is discussed along with the logical basis for the step (design philosophy), the application of the method and other design considerations.

The first three sections of the chapter consider the three main steps of the method: selection of the basic airfoil shape, preliminary flap design and position and optimizing the flap shape. Section 2.4 deals with the problem of correcting the theoretical lift-drag characteristics to take into account the effect of the boundary layer.

The design of the slotted-flap airfoil (based on the FX-67-K-170 airfoil section) in the course of the chapter is a vehicle to demonstrate the design method as it is discussed. (Chapter III compares the experimental and theoretical results for this airfoil section.) The method is, however, applicable to any other existing airfoil exhibiting the basic requirements.

2.1 The Basic Airfoil Section

2.1.1 Low Drag Airfoil Sections for Low Reynolds Numbers

Wortmann[6] has shown clearly that the optimum suction side pressure distribution on an airfoil is one that permits the maximum extension of the laminar boundary layer by recovering the pressure in the minimum distance. Pressure can be recovered over the shortest distance by using a pressure distribution which causes the development of a turbulent boundary layer that is about to separate over its entire length. Such a boundary layer, as proposed by Wortmann[6] and Stratford[10], suffers the minimum momentum loss. Hence the airfoil section experiences the minimum drag.

In connection with optimizing multi-element airfoil sections for maximum lift, Chen[12] has shown that any form of pressure recovery other than the above will not provide the maximum lift for a given pressure recovery. Wortmann has stressed the drag reduction benefit of the zero shear stress pressure distribution. It should be emphasized that the combination of low drag and high lift is only possible at Reynolds numbers where the laminar boundary layers can persist for long distances (i.e. R 10^6 - 3 x 10^6 approximately).

Based on the preceding ideas, Wortmann[17] and others have designed a large number of low drag airfoil sections for low Reynolds numbers. These airfoils can be classified

very generally into three groups: high lift, laminar and high speed. The groups represent the results of three sets of design conditions. In general each group is distinguished physically by a general shape but more specifically by the location of the low drag range. Figure 4 shows a typical airfoil section for each class and typical design velocity distribution.

The high lift group of airfoils have a mid-range lift coefficient of at least 0.6 while the high speed group is typified by a design lift coefficient of about 0.2. Airfoil sections of the laminar group generally possess the lowest minimum profile drag since the design pressure distribution attempts to stress the laminar boundary layer on both suction and pressure sides. For this group, the center of the low drag range usually lies in the lift coefficient range 0.4 to 0.6.

For the low drag airfoils the limits of the low drag range are indicated by the appearance of a nose suction peak on either the suction side or the pressure side. On a high lift airfoil, for example, at high incidence, the nose suction peak on the suction side causes the development of a nonoptimum turbulent boundary layer and flow separation which grows in extent as incidence increases. Typically the rapid pressure rise at the nose results in the formation of a long bubble type of flow separation at large incidences.
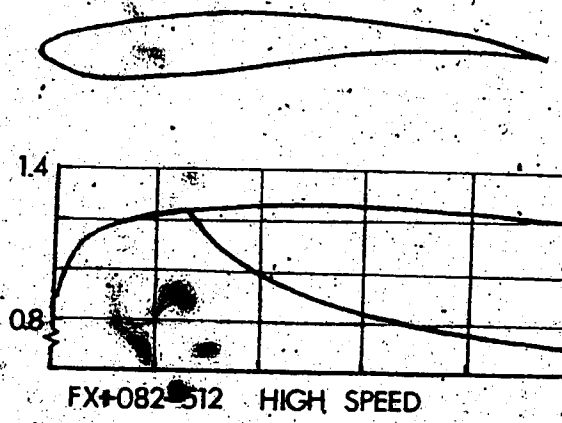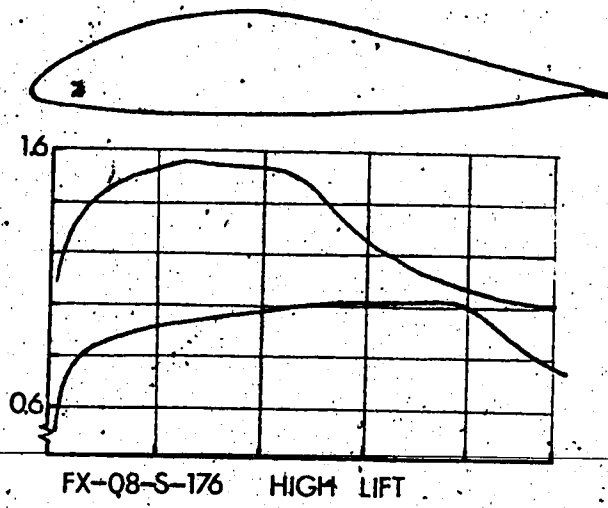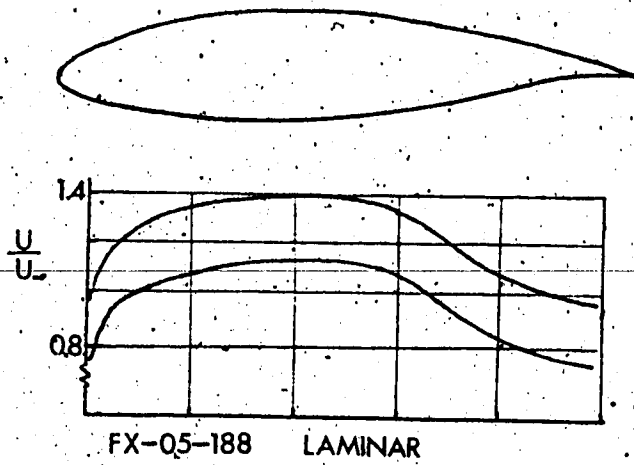
Figure 4. Low Drag Airfoil Sections and Design Pressure Distributions. (References 6 and 17)

As the incidence decreases below the design incidence a suction peak develops on the pressure side leading edge which eventually promotes transition to a turbulent boundary layer and a rather abrupt drag increase. However the flow remains basically attached over a range of incidences so that a secondary drag plateau is formed. Eventually, of course, flow separation begins and the drag rises sharply. Figure 5 shows the $C_L - C_D$ curve for the NACA 8-H-12 airfoil[17] and is typical of the high lift group.

2.1.2 <u>The Choice of a Basic Airfoil Section</u>

The effect of a small flap deflection on the pressure distribution over a flapped airfoil is shown in Figure 6. It is interesting to note that the load on the main section has increased substantially although the actual magnitude of the pressure recovery is less than that on the flap section. Moreover if the main section exhibits a "roof-top" type of pressure distribution with a short recovery distance, substantial flow separation will not occur until the nose suction peak develops. Given this situation, the suction side boundary layer on the flap may well be separated if the flap is overloaded. In this case the flap loading determines the performance of the system.

The pressure distribution on the flap remains basically constant for varying incidence at a fixed flap deflection angle. In effect the flap operates at only
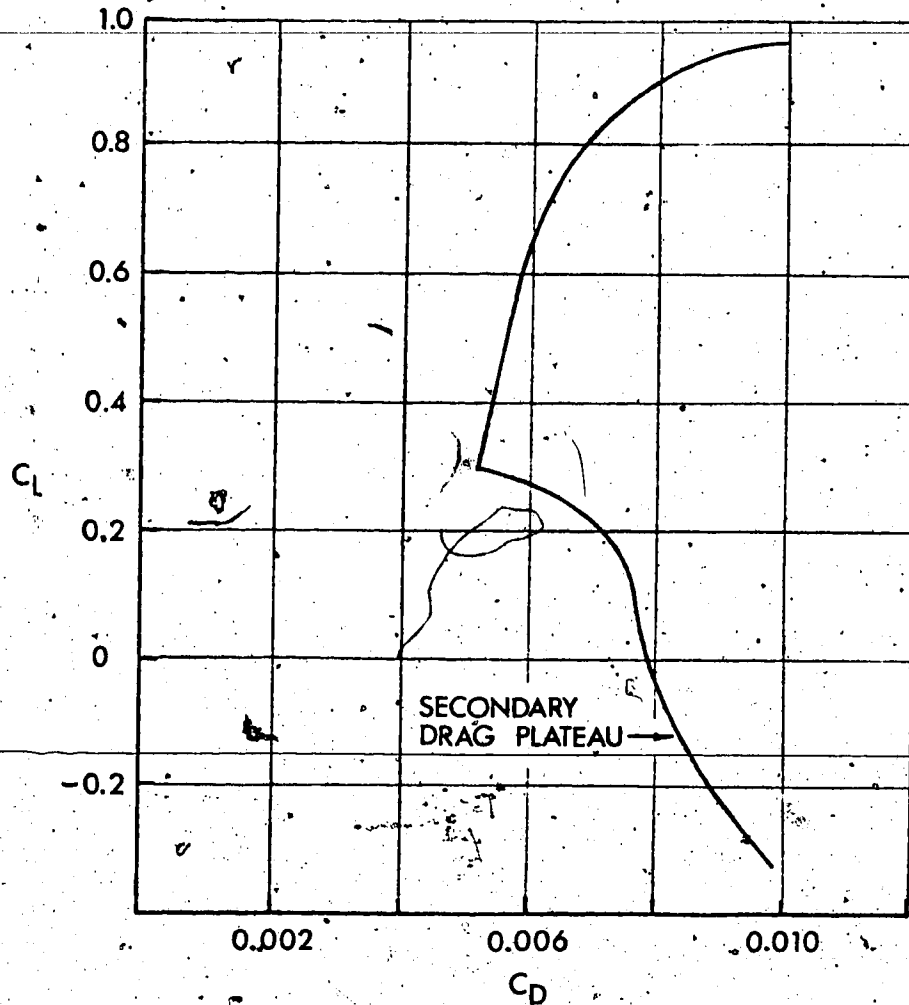
Figure 5. Lift-Drag Polar for the NACA 8-H-12 Airfoil
Section (R = 1.8 x 10^6)
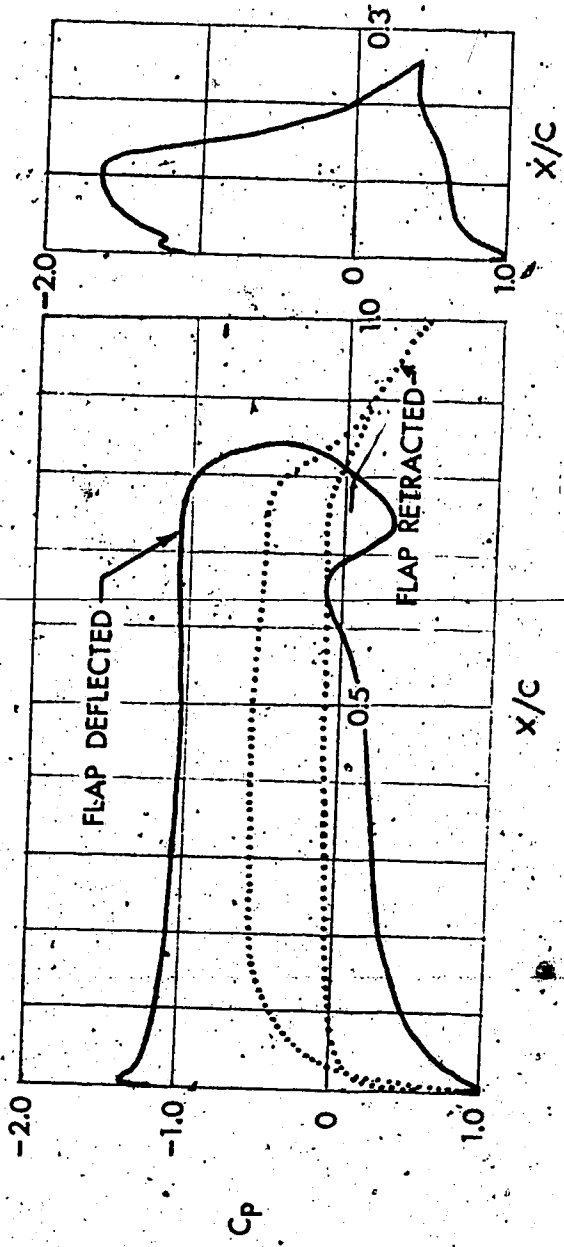
Figure 6. Theoretical Pressure Distributions on a 25% Chord Slotted-Flap Airfoil Designed in the Course of the Project

one incidence because the streamline pattern around the
flap is determined by the geometry of the main section-
flap configuration which remains fixed. This means that
the pressure distribution on the flap can be optimized
for a given deflection.

On the other hand, the main section continues to
operate over a wide range of angles of attack so that
if a good single element airfoil is chosen as the basic
section, the main section geometry need not be modified
because it has already been optimized for minimum drag.

By optimizing the flap pressure recovery, the
separation may be eliminated on the flap so that the limit
of the low drag range will be delineated by the begin-
ning of separation on the main section. This permits
the good stalling characteristics of the main section to
be retained while at the same time the flap remains useful
as a control surface up to the stall.

The total lift of the flap and the main section,
when the suction peak develops at the nose of the main
section, is always greater than the lift of the airfoil
section alone for the same condition. This increase in lift
represents an upward displacement of the minimum drag lift
coefficient as distinct from the lift increment, which com-
monly refers to the increase in lift of the flapped airfoil
over the plain airfoil at the same angle of attack.

The preceding arguments suggest that in order to achieve high lift coefficients with small flap deflections and avoid separation an airfoil section of the high lift group should be chosen as the basic section. There are however, two problems associated with this group of airfoils that must be considered:

(1) The minimum drag coefficients of airfoils in this group are always larger than those associated with laminar airfoils.

(2) As stated previously, the drag coefficients at low lift coefficients are large since they lie outside of the low drag range.

The first problem constitutes an unavoidable design penalty. Problem two can be solved by turning the trailing edge region upward and this is discussed in Section 2.3.

Although it is possible to design high lift airfoils, using the method discussed in Appendix C, it makes more sense, considering the number of available profiles, to choose an already existing airfoil.

Three airfoil sections designed by Wortmann[14,17] which possess the characteristics desirable for use as basic high lift sections for a slotted-flap were considered. Table 1 is a comparison of the important characteristics of these airfoils. Clearly the differences are slight.

The FX-67-K-150 and the FX-67-K-170 are overall

Table 1. Comparison of some Characteristics of
Three Airfoil Sections for $R = 1.5 \times 10^6$

Airfoil	Maximum C_L for Low Drag	Corresponding C_D	Minimum C_L for Low Drag	Corresponding C_D	Min C_D	C_D at $C_L = 0.2$
FX-67-K-150	1.25	0.0080	0.40	0.0064	0.0062	0.009
FX-67-K-170	1.27	0.0076	0.45	0.0065	0.0065	0.010*
FX-08-S-176	1.22	0.0084	0.55	0.0066	0.0066	0.0095

* estimated

slightly better than the FX-08-S-176. The FX-67-K-170 was chosen primarily because of the larger thickness to chord ratio (17% versus 15%) which helps when constructing a full scale structure, and greater thickness towards the rear which provides space for structure and mechanisms for the flap.

Figure 7. is a superposition of the three airfoil sections showing the degree of similarity in shape.

2.2 Preliminary Flap Design

2.2.1 Flap Size and Shape

The design of a flap is perhaps more of an art than a science. The shape of the trailing edge portion of the airfoil determines to a large extent the size and the shape of the flap since the flap must retract smoothly.

There are, nevertheless, some guidelines available:

(1) The flap should be highly cambered if flap deflections are small. Vesely[13] achieved a lift increment of 0.65 for a flap deflection of only 10° with a highly cambered 35% chord flap on an NACA section of the 63 6xx family.

(2) For small deflections, where boundary layer development can be calculated in the normal way, the flap Reynolds number determines the load capacity of the flap. At low Reynolds numbers there is little benefit derived from increasing flap chords from say 25% to 30%. This problem is discussed in the next section.

FX-08-S-176

FX-67-K-170

FX-67-K-150
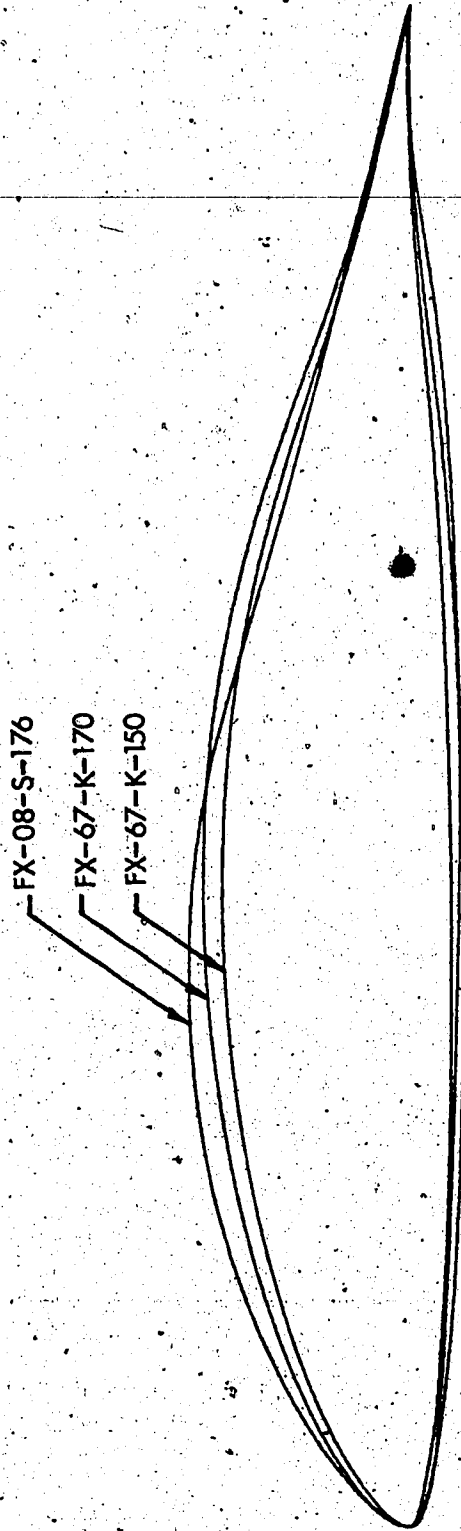
Figure 7. Superposition of Three High-Lift Airfoil
Sections

(3) The results of extensive NACA testing[9] show that
little gain in maximum lift arises from exceeding
a flap chord of about 35%.

(4) For a given lift increment the increased pitching
moment is less for a large chord flap than for a
small chord flap since lift is more evenly
distributed.

The preliminary flap, then, should have a chord
length of about 35% of the retracted chord; it should be
highly cambered to permit a high flap loading for a small
deflection. For small flap deflections it is possible to
predict the behavior of slotted flap airfoils fairly
reliably by assuming that the boundary layers on both the
main section and the flap section develop independently.[18]

A freehand study of possible flap sections com-
bining high camber, maximum thickness and reasonable
thickness distribution shows that for the FX-67-K-170
airfoil, a flap of 35% chord is reasonable.

The flap design procedure described below is prelim-
inary; the shape is further modified to give the desired
pressure recovery.

The flap profile shape was constructed as shown in
Figure 8. Freehand sketches help to establish the points of
tangency T_1 and T_3, the center C_2 and the radius R_2.
Perpendicular AB and the arc of radius R_2 are constructed.
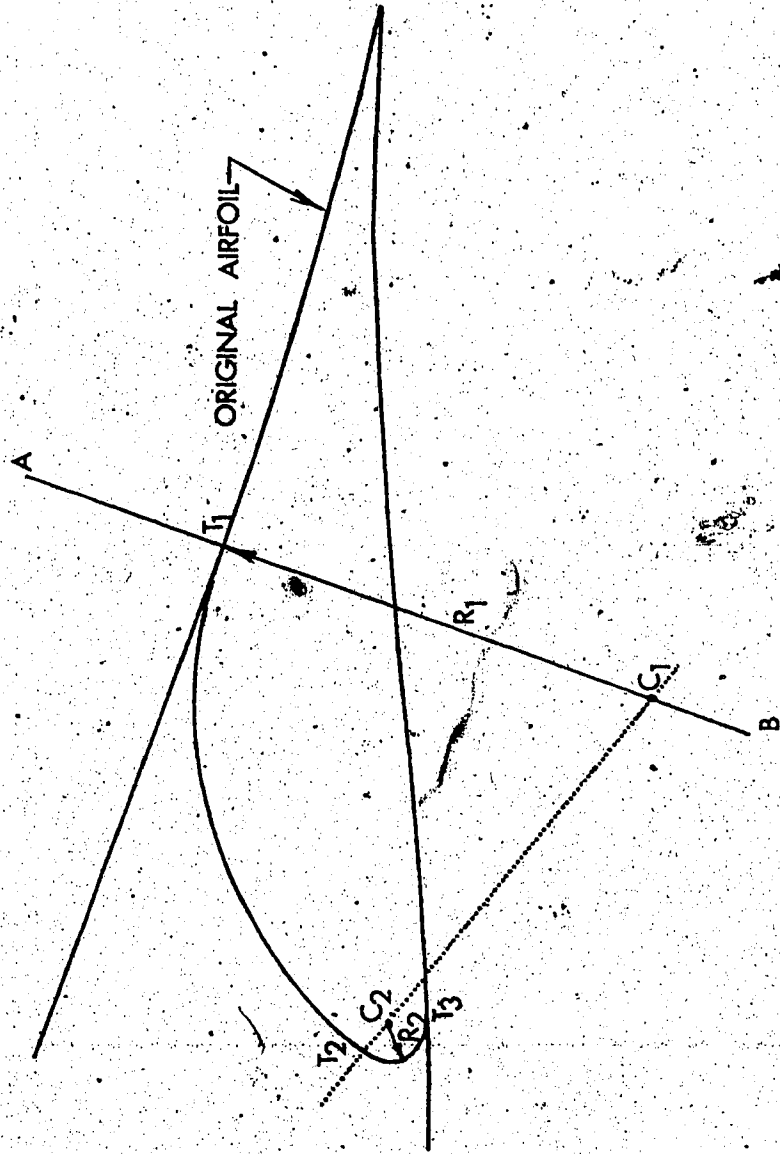
Figure 8. Geometric Construction of the Flap

After a few trials the radius R_2 is found which is tangent
to the surface at T_1 and tangent to the smaller arc at
some point T_2. The accuracy of the construction is checked
by noting if T_2, C_2, and C_1 lie on a straight line. If
they do, the two arcs are indeed tangent at T_2.

Should the construction give an unsuitable shape
(perhaps a bulbous nose or a poor distribution of thickness)
then a new shape can be sketched and the process repeated.
If the chord is reasonable T_1 will generally remain fixed
but R_2 and C_2 must be changed.

With some practice the entire procedure could take
only a few minutes assuming that the airfoil trailing portion
has already been drawn.

Admittedly the construction of the flap in the
manner described is largely arbitrary and subjective. At
the same time it represents a necessary step in the practical
design procedure; the benefit of the above procedure is that
the resulting flap is structurally compatible with the main
section.

2.2.2 Gap Size and the Optimum Flap Position

Experimental results[9,19] show that for a given
flap deflection, a unique flap position exists at which the
lift coefficient is a maximum. In fact lines joining posi-
tions of equal lift form a series of concentric rings of
irregular shape. The center of these rings is of course the
location of maximum lift.

Foster, Irwin and Williams[18] found the potential theory lift to be a weak function of horizontal position of the flap in agreement with experimental results. In both cases a definite maximum lift can be found. During the course of the current research this finding was checked using the computer program to calculate lift on a slotted flap airfoil.

Foster, Irwin and Williams also found that for some flapped airfoils potential flow calculations will yield a vertical position of the flap at which the lift coefficient is a maximum. With other flapped sections the lift coefficient increases with decreasing gap and no maximum can be found. (Figure 9 shows gap and overlap.) (Flapped airfoils tested in this project proved to be of the latter type.) Foster, Irwin and Williams postulate that the flow around the wing and the flap is determined mainly by the inviscid (potential) solution. They further suggest that should no optimum gap exist for gaps greater than that for which the boundary layers in the slot merge, then the optimum gap (maximum C_L) will be at or near the smallest gap at which the boundary layer on the flap and the main section at the slot exit are just separate. Their experimental results verify that, at least for the airfoil tested, the total lift varies with flap position in a manner similar to that predicted by inviscid theory provided that the boundary
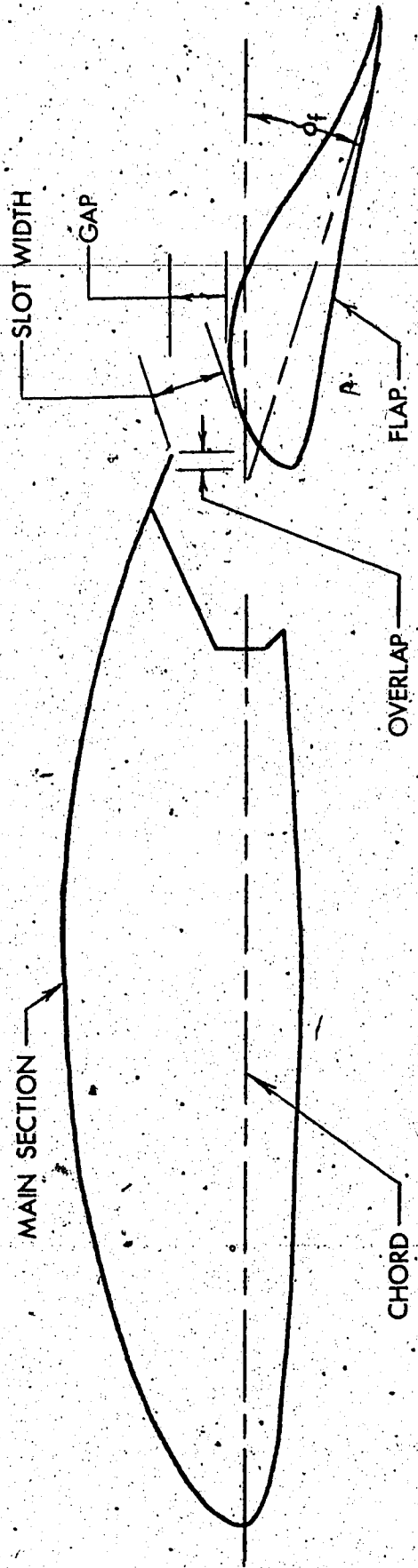
Figure 9. Description of the Flap Positioning Terminology
For a Single Slotted-Flap Airfoil

layer on the flap and on the wing main section are every-where separated by a region of freestream pitot pressure, however small.

Optimum flap overlap (i.e. horizontal position) for a given deflection can be found by computing the potential lift for various overlaps. This procedure will always yield an optimum horizontal position. However it is difficult to determine the optimum gap (i.e. vertical position) reliably without resorting to wind tunnel testing. Although potential flow results may indicate an optimum vertical position the pressure distributions computed using the method of distributed vorticity (as used in this project) become unreliable in the slot area if the slot spacing becomes smaller than the point vortex spacing. Consequently a potential optimum, if it exists at all, cannot be found.

In order to avoid the confluent boundary layer[20] a substantial core of potential flow is required at the slot exit, therefore optimizing the gap according to the Foster, Irwin, Williams criterion is largely irrelevant.

Using the flat plate formula for a turbulent boundary layer and assuming the slot is faired in, the thickness of the boundary layer on the main section side of the slot can be estimated. This formula gives a thickness of 2% of the retracted airfoil chord length for a main section chord length of 82% of the retracted chord. Since

the boundary layer on the pressure side will be laminar up to the slot entry, this estimate is probably conservative.

The boundary layer on the flap develops from the stagnation point to the slot exit in a generally favorable pressure gradient. Using the flat plate formula for the laminar boundary layer, the boundary layer thickness at the slot exit is about 0.06% of the retracted chord. This is negligible.

A gap which gives a slot exit width of 4% of the retracted chord will undoubtedly provide for a substantial core of potential flow at a Reynolds number of 10^6 based on the retracted chord.

2.2.3 The Slot Shape and Predicted Drag

In actual practice the deflection of the flap on a slotted flap wing leaves the exact slot shape undefined as shown in Figure 10 (a cross section of the model tested). Referring to this figure it is clear that a vortex or a combination of vortices must exist in the gap. Sufficient circulation is provided by the vortex or vortices for the flow to leave A smoothly.[21] (Analogously, the circulation of an airfoil is adjusted to make the flow leave the trailing edge uniformly.)

Clearly the drag coefficient predicted by the boundary layer computer program will be too low since the trapped vortex or vortices must be sustained by the air

DESIGN POSITION

DEFLECTION - 20°
GAP   0.02C
OVERLAP   0.01C

A

GAP REQUIRED FOR FLAP NOSE

SLOT FAIRINGS TESTED
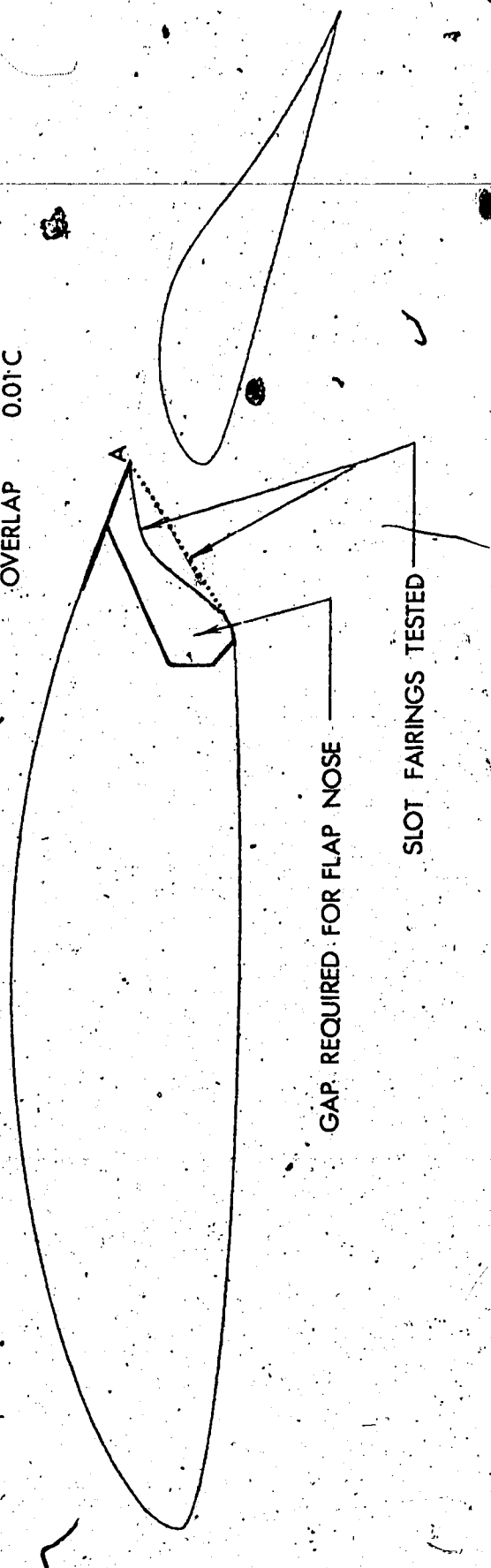
Figure 10. A Cross Section of the Model Showing the
Designed Flap in the Design Position and Two
Slot Fairings

flowing through the slot. If the average pressure coefficient in the separated region is only 0.1 less than the average pressure coefficient over the nose, then the resultant drag force coefficient will be 0.01 based on an effective area of 10% of the chord. This contribution to the drag could easily account for the difference between experimental results and those predicted by the program assuming a faired slot.

Because the method of distributed vorticity is incapable of handling regions of small thickness, fairing of the slot was necessary to generate pressure distributions using the computer program. Other researchers have faired in the main section trailing portion for the purpose of calculating the pressure distribution. To compare theoretical results with experimental results the model should be faired as well. However practical single slotted-flap airfoils, if they are to have fully retractable flaps, cannot be easily designed to provide for a slot fairing.

The effect of main section fairing was tested for two different fairings shown in Figure 10. Figure 11 shows the computed inviscid-pressure distributions. The results show significant changes in the pressure distribution in the neighborhood of the slot.

The suction peaks shown at the nose of the designed flap are not large enough to promise long bubble.
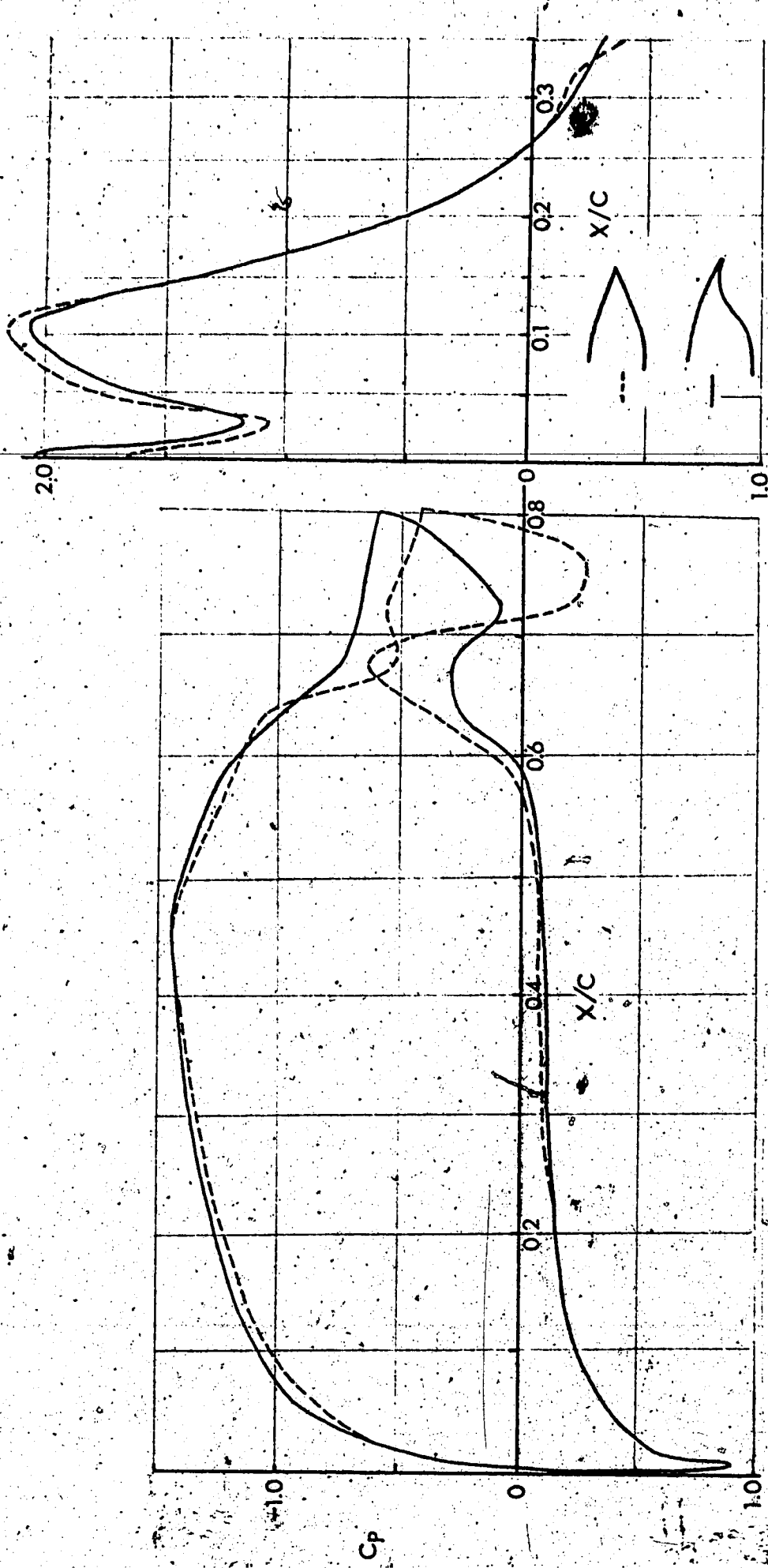
Figure 11. The Effect of a Change in Slot Shape on the
Calculated Inviscid Pressure Distributions
($\alpha = 0^o$ and $\delta_f = 15^o$)

separation or short bubble transition. In this regard the high peaks found by Foster, Irwin, and Williams[18] are not supported by other experimental results[20,22] and are no doubt the result of slight flattening in the flap nose region. Surface discontinuities, especially in the neighborhood of the nose, can easily cause large suction peaks. This can be demonstrated using the pressure distribution computer program.

2.3 Optimizing the Flap Loading

2.3.1 Flap Deflection and the Maximum Lift of the Flap

The optimum pressure distributions suggested by Wortmann and Stratford are applicable to the flap section as long as the assumption of an independently developing boundary layer is valid. Minimum momentum loss and maximum lift are the benefits of the optimum pressure recovery.

Chen[12] and Wortmann[6] show clearly the relationship between Reynolds number, total pressure recovery and pressure recovery distance, provided transition has occurred just prior to the beginning of the pressure recovery. Very simply the relationship is that for a fixed pressure recovery distance and Reynolds number there exists a maximum possible pressure that can be recovered without boundary layer separation.

The application of the ideas of Wortmann and

Stratford to the determination of maximum flap loading is not straightforward. An iterative procedure using a series of flap deflections and taking into account boundary layer displacement thickness effects must be adopted.

Theoretical results tend to verify the fact that if the pressure recovery on the flap is greater than that allowed by the optimum recovery then the boundary layer will separate. However since some less than maximum pressure recoveries will often result in flow separation as well, the optimum pressure recovery criterion must first be applied to the theoretical results to determine approximately the maximum flap loading (i.e. flap deflection). For this flap deflection the theoretical boundary layer results will likely indicate some boundary layer separation, however by modifying the camber the pressure distribution can be brought closer to the optimum and the separation will be eliminated.

The procedure for determining the maximum flap loading is best explained in relation to the actual flapped airfoil being designed. Since the flap lift is essentially independent of the angle of attack for a given flap deflection, it is only necessary to calculate the pressure distribution and boundary layer development once for each flap deflection.

Figure 12 shows the theoretical inviscid pressure distribution on the flap for deflections of 12° and 15° as
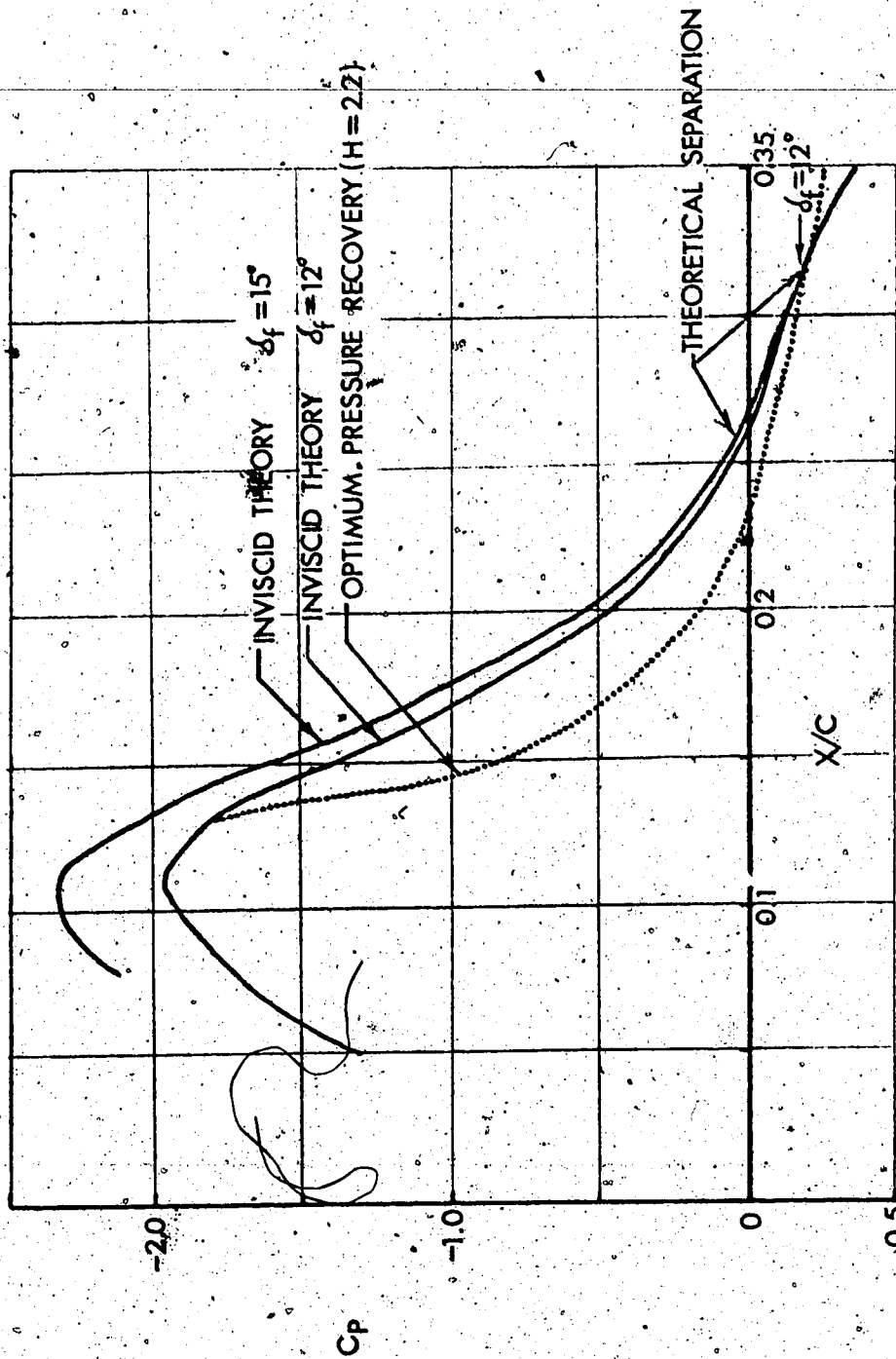
Figure 12. Theoretical and Optimum Flap Suction Side
Pressure Distributions for Two Deflection
Angles (α = 3.4o)

INVISCID THEORY $\delta_f = 15°$

INVISCID THEORY $\delta_f = 12°$

OPTIMUM PRESSURE RECOVERY (H = 2.2)

THEORETICAL SEPARATION

$\delta_f = 12°$

C_p

X/C

0.35

0.2

0.1

0

-1.0

-2.0

0.5

well as the location of separation and the optimized pressure recovery according to Wortmann's data. From the figure it is clear that 12° is close to the maximum possible deflection or in other words the loading represented by 12° is close to the maximum allowed. At this deflection the boundary layer separates very near to the trailing edge and the pressure recovery from the point of transition is slightly more than the optimum recovery. (Wortmann's optimum recoveries seem to be conservative. This is discussed later.)

From Figure 12 it is also clear that the flap shape must be modified from about the location of the pressure minimum back to the trailing edge to obtain the optimum pressure recovery distribution.

It is important to note that the flap shape fixes the general location of the pressure minimum and therefore indirectly limits the flap loading. For the flap under consideration the loading is very close to the optimum (based on the work of Chen) and no substantial gain in lift is possible by reshaping the flap to move the peak suction position. However the loading can be increased by a small amount of local reshaping of the nose to give a peak suction plateau ("rooftop") rather than a region of steadily decreasing pressure from the nose to the minimum pressure point. (This was demonstrated by Foster, Irwin and Williams.)

Two flap modifications were tried; the resulting

theoretical inviscid pressure distributions for about equal

pressure recoveries are shown in Figure 13. Both modific-

ations remove the flow separation and from Figure 14 it can

be seen that a constant shape factor boundary layer develops

which is near to separation. The boundary layer development

is also characterized by the linear increase in the momentum

loss thickness which is typical of the optimum pressure recovery.

Having modified the flap, the flap retracted

performance is now modified. Previous study of the FX-08-S-176

airfoil demonstrated that a small upturning of the tail had

two beneficial effects:

(1) The low drag "bucket" was moved to lower C_L's.

(2) The pitching moment was reduced by the appearance

of a loop in the trailing edge pressure distri-

bution typical of the design pressure distributions

for helicopter blades.

Similar effects should be expected from the mod-

ifications to the FX-67-K-170 airfoil, however theoretical

results suggested that the FX-67-K-170 is a more critically

designed section where slight modifications to the geometry

have serious effects. Theoretical results for this airfoil

using the larger flap modification indicate that flow

separation will occur at all angles of attack; results for

the smaller modification show a narrowing and lowering of

the low drag range to about $0.05 < C_L < 0.70$ with little
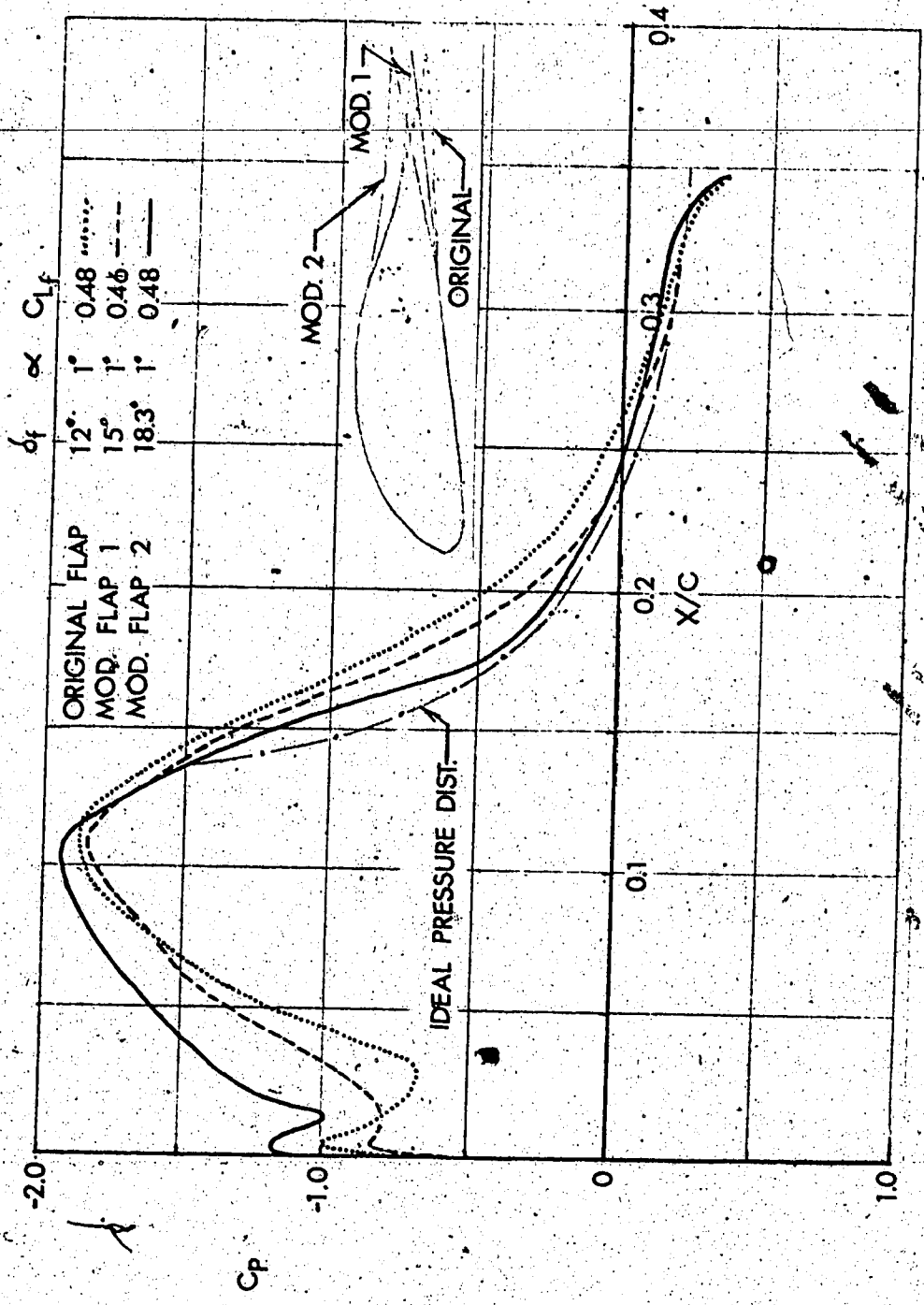
Figure 13. Theoretical Inviscid Suction Side Flap Pressure Distributions for the two Flap Modifications.
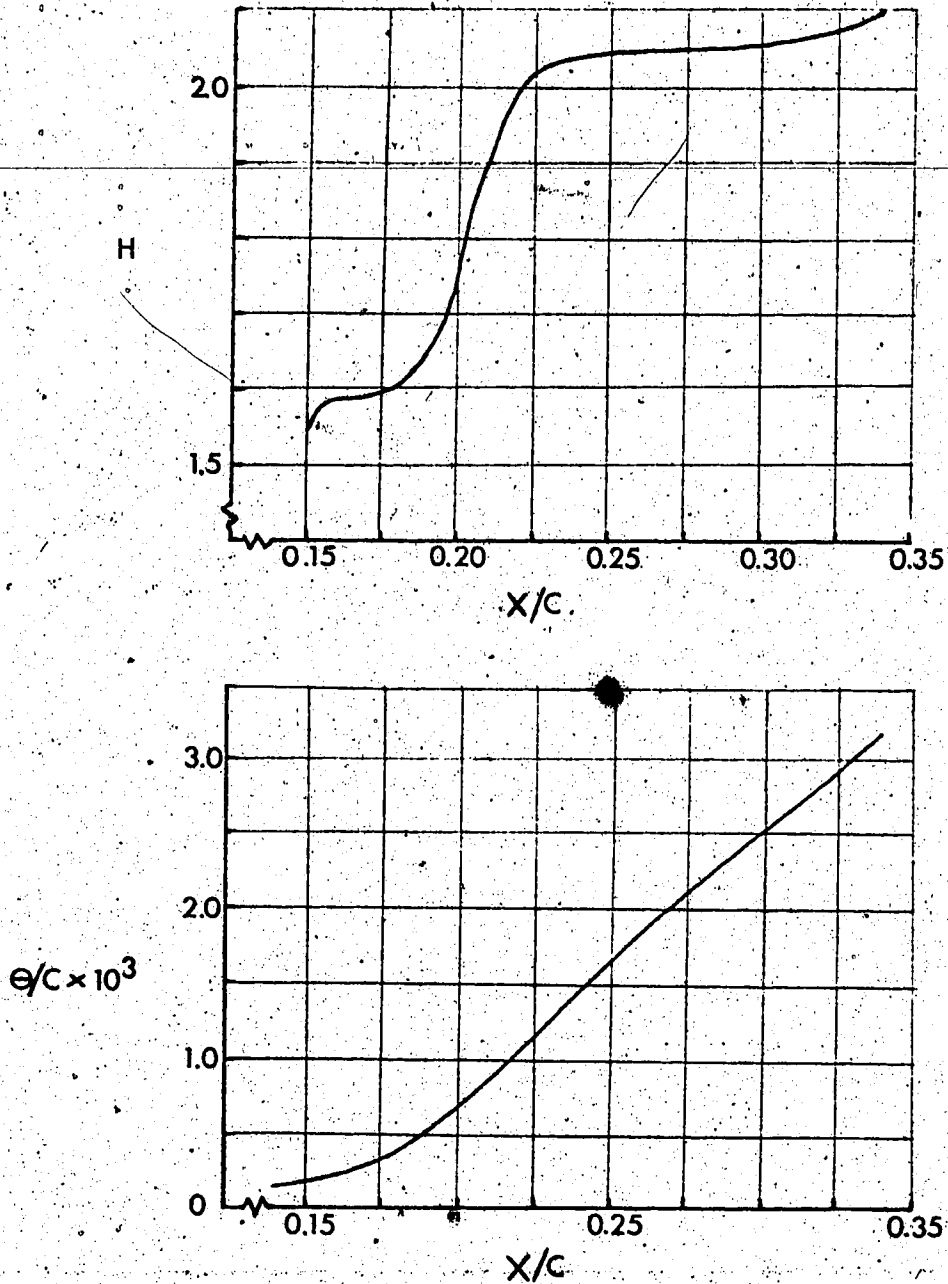
Figure 14. Computed Shape Factor and Momentum Thickness Development on Modified Flap Number One Based on the Theoretical Inviscid Pressure Distribution

change in the profile drag for $R = 2 \times 10^6$.

It is not surprising that modifications to the trailing portion of this airfoil have large effect since changing the pressure recovery from the optimum must lead to an increase in the boundary layer shape factor (H) and probable separation at incidences where separation did not occur before. While modification number two gives the lower flap drag coefficient (because it gives a closer to optimum pressure recovery), modification number one must be used since the resulting airfoil retains a reasonable low drag range in the retracted configuration.

2.3.2 The Optimum Pressure Recovery

Wortmann's method of calculating the optimum pressure recovery requires that the boundary layer momentum thickness at the beginning of pressure recovery be known along with the flow velocity at that point and the Reynolds number based on the profile chord. The following equation determines the velocity at a chordwise point x in the pressure recovery region

$$\frac{U_x}{U_1} = \frac{1}{\left[1 + \frac{\beta}{\theta_1}\frac{(x-x_1)}{c}\right]^m}$$

where, β is the slope of the graph of momentum thickness (θ) versus x for a given shape factor (H) and Reynolds number (R). Subscript 1 refers to the values at the beginning of pressure

recovery and c is the airfoil chord.

$$m = 0.33 - \frac{C_f}{6\beta}$$

$$C_f = 0.074 \ R^{-0.20}$$

Details of the derivation of these relations can be found in reference 6.

Clearly the maximum pressure recovery depends on the denominator $\left[1 + \frac{\beta}{\theta_1} \frac{(x-x_1)}{c}\right]^m$. Using Wortmann's results, m is found to be around 0.20 for a turbulent boundary layer with a large constant shape factor (about 2.2). Applying these results to the flap (considered a separate airfoil) it is clear that in order to attain a small value of $\frac{U_{te}}{U_1}$ (i.e. a large pressure recovery) $\frac{\beta}{\theta_1}\left(\frac{x_{te}-x_1}{c}\right)$ must be large.

If $\frac{x_{te}-x_1}{c}$ is fixed as it is for the flap, the magnitude of the maximum pressure recovery depends on β/θ_1. (The subscript te refers to the trailing edge point.)

Experience with this method shows that Wortmann's method will give constant shape factor boundary layer development but that the shape factor used to compute the pressure recovery is not the shape factor computed by Head's[23] method. The calculated shape factor (using the boundary layer program) was always found to be less than that used to find the pressure distribution.

The preceding suggests that Wortmann's data which was derived from Truckenbrodt's quadrature method will yield conservative pressure recoveries. In other words larger pressure recoveries (without flow separation) are possible in a given distance and for an initial pressure coefficient, than those predicted by Wortmann.

The ratio β/θ_1 can be increased if the calculated θ_1 is used rather than θ_1 calculated assuming a laminar boundary layer development in a uniform pressure up to transition. For example, using the following relation to compute θ_1 for the flap,

$$\frac{\theta_1}{c} = \frac{0.664}{\sqrt{R}} \sqrt{\frac{U_\infty}{U_1} \frac{x_1}{c}}$$

where $c = 0.35$ ft., $R = 0.35 \times 10^6$, $\frac{U_\infty}{U_1} = \frac{1}{1.673}$ and $\frac{x_1}{c} = \frac{0.13}{0.35}$, θ_1 is found to be 0.0002 feet. This compares to $\theta_1 = 0.00015$ feet calculated by the boundary layer computer program using Thwaites'[24] method. (Boundary layer calculations are discussed in Appendix B.)

2.3.3 The Pressure Distribution and Boundary Layer Transition on the Flap

At a Reynolds number 0.35×10^6 based on flap chord, a laminar boundary layer development in a favorable pressure gradient and a steep pressure recovery, it is not surprising that transition to the turbulent boundary layer is by means of the short laminar separation bubble.

Theoretical boundary layer results show that this mode of transition exists up to at least $R = 3.5 \times 10^6$ based on the designed 35% flap chord.

For the purpose of calculating the turbulent boundary layer development and the optimum pressure recovery it is assumed that when the short bubble exists, transition takes place over the length of the bubble (which is of the order of one per cent of the chord length) and that the momentum thickness of the reattached turbulent boundary layer is about equal to the momentum thickness of the boundary layer at separation.

The design pressure distributions for low drag airfoils include a so-called instability region or in other words a region of slightly increasing pressure immediately upstream of the final pressure recovery and occupying perhaps 20% of the chord length. The purpose of this region is to ensure that normal transition due to the growth of boundary layer instabilities occurs prior to the major pressure recovery. This region is vital for $R = 10^6$ to 3×10^6.

However on the flap at $R = 0.35 \times 10^6$, based on the flap chord, the inclusion of an instability region will ot promote transition and transition will always occur by ns of the short bubble. (The criterion for bubble nsition is discussed in Appendix B.)

2.4 The Effect of the Boundary Layer

2.4.1 The Viscous Correction Method

Methods of potential flow calculation, such as the method of distributed vorticity, give the pressure distribution about an airfoil section that would exist if air was inviscid. The effect of viscosity is to modify the flow pattern by means of the boundary layer. This change in streamline pattern implies a change in circulation. Experimental results confirm that the actual lift is less than the theoretical inviscid lift. This difference in lift is small for high Reynolds numbers and low lifts, however reductions can amount to 10 - 15% of inviscid lift coefficients at high lifts coefficients and low Reynolds numbers.

With experience lift reductions can be reliably estimated and since calculated drag based on inviscid pressure distributions varies little from the actual drag, it is possible to estimate actual lift drag polars quite accurately for most purposes.

The accurate theoretical calculation of lift and drag including the effects of viscosity is more desirable.

Powell[25] and others have considered the problem in detail by considering the three effects of a boundary layer on an airfoil section: the change in the airfoil thickness distribution, the change in the camber-line position and the change in the angle-of-incidence. These

effects follow from the assumption that an airfoil defined by the addition of the measured displacement thickness to the actual airfoil will have an inviscid pressure distribution almost identical to the pressure distribution existing over the actual airfoil in viscous flow. In order to apply Powell's method an iterative procedure must be followed since the calculation begins with theoretical displacement thicknesses rather than measured values. The inviscid pressure distribution becomes stable after a number of iterations and this is taken to be the actual viscous flow pressure distribution.

For this project a simplified viscous correction procedure was attempted based on these assumptions:

(1) For a given camberline, a change in thickness distribution does not change the lift substantially.

(2) For most airfoil sections and for airfoils with flaps at small deflections the effect of the wake is small when correcting for viscosity.

The method of superposition of velocities discussed by Abbott and Von Doenhoff[3] suggests that the pressure distribution over an airfoil is made up of three parts; the pressure distribution over the symmetrical wing section at zero angle of attack (zero lift), the pressure distribution over the mean line at the ideal angle of attack and the increment resulting from the angle of attack for the symmetrical

wing section.

Since the change in thickness distribution (due to the addition of displacement thickness) is small, this effect on the pressure distribution can be ignored.

Changes in mean line shape cause the largest changes in pressure distribution and lift. For this project the mean line shape was modified (for both airfoil and flap) simply by adding the displacement $\Delta y = (\delta^*_u - \delta^*_l)/2$ (computed at given chordwise positions) to the y coordinates of the profile. The effect, for both main section and flap, is to turn the tail upwards. The change in angle of attack is automatically accounted for by the computer program since the angle of incidence is referred to a fixed coordinate system. (It is not based on the original airfoil chord.)

The accuracy of the method depends on:

(1) the accurate calculation of inviscid pressure distributions.

(2) the accurate calculation of displacement thickness.

Displacement thicknesses calculated for the inviscid pressure distribution tend to increase rapidly in the neighborhood of the trailing edge. Experimental results show a reduction in the rate of increase of displacement thickness in the neighborhood of the trailing edge. The inaccuracy of theoretical results is accounted for by the steep pressure recovery predicted by potential flow theory.

near the trailing edge. This recovery is never found experimentally. The reliability of the method depends on the ability of the user to modify the theoretical displacement thicknesses in the neighborhood of the trailing edge.

In using this method it is assumed that the displacement thicknesses used are approximately equal to the "experimental" displacement thicknesses. This implies that the pressure distribution and lift calculated for the modified airfoil are very close to the actual viscous flow pressure distribution and lift.

The method was tested by using it to predict the lift reduciton for two airfoils: the GU-25-5(11)8.[16] and the NACA 4418[3]. Results for the two airfoils sections are shown in Figure 15. The theoretical lift curve with viscous correction for the NACA 4418 airfoil does not correspond to the experimental results. This may be the result of the experimental results being low, the theoretical inviscid results being high or a combination of the two.

2.4.2 Application of the viscous Correction Method on the Design Method

From Figure 16 it is clear that the actual pressure recovery on the flap including the correction for viscos (for the design flap deflection of 15 degrees) is less than the design inviscid pressure recovery.
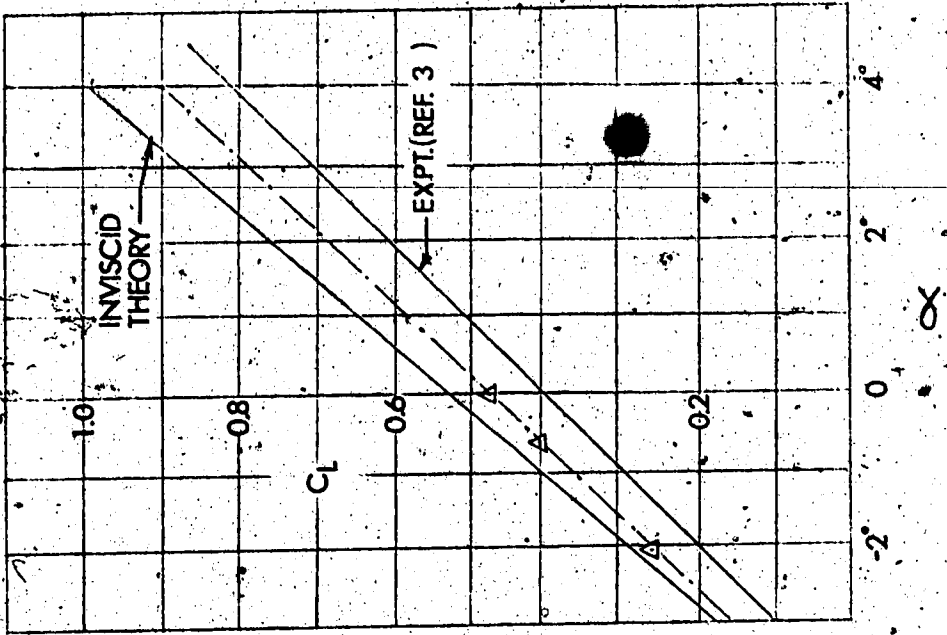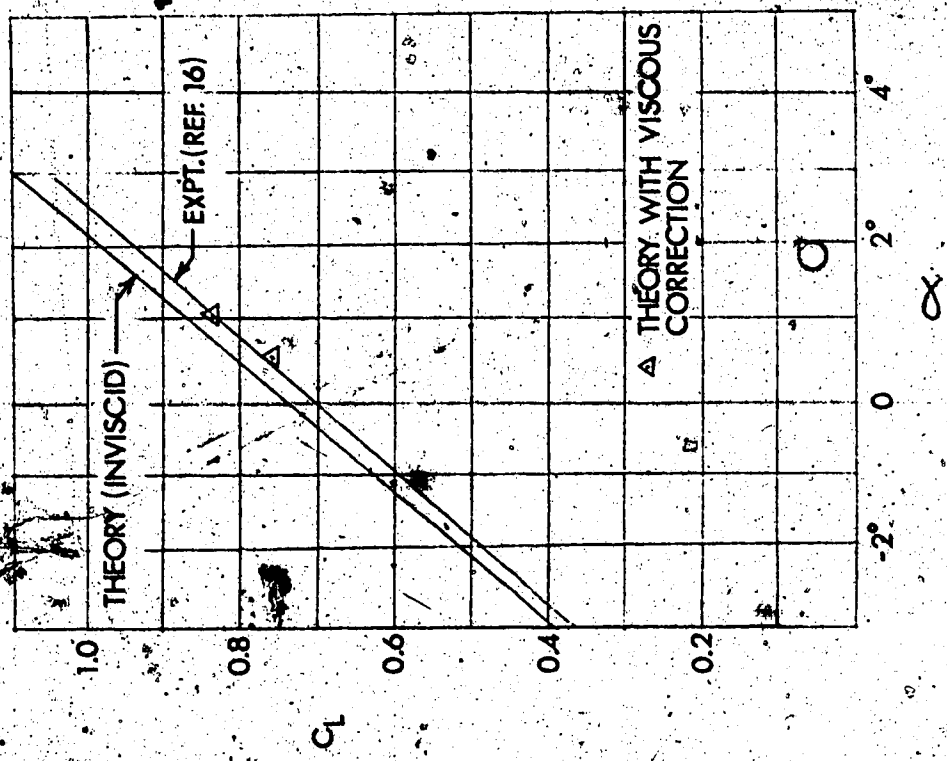
Figure 15. Theoretical and Experimental Lift Curves for the NACA 4418 and the GU-25-5(11)8 Airfoils
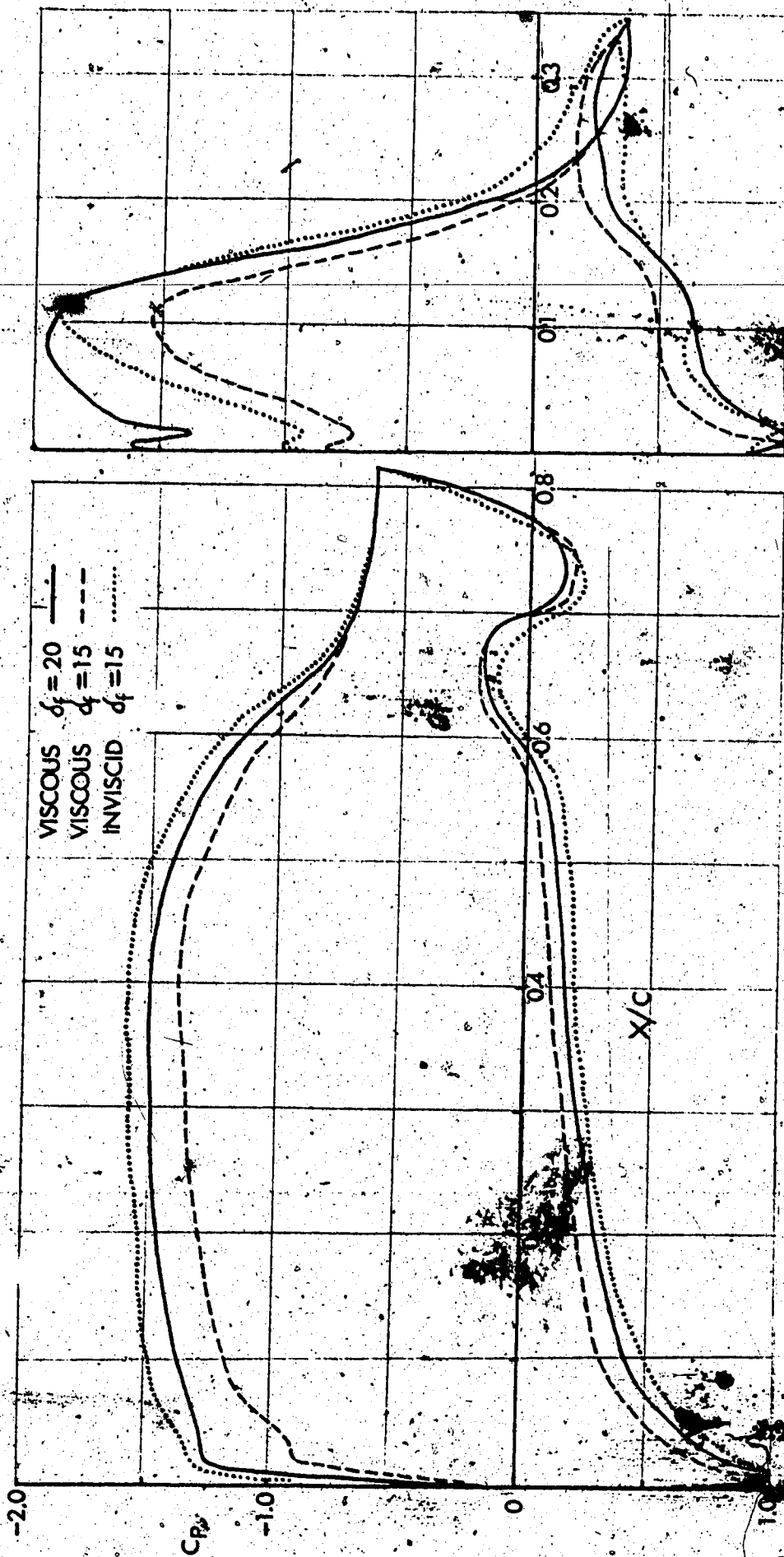
Figure 16. Theoretical Pressure Distributions over the Designed Slotted-Flap Airfoil ($\alpha = 3°$) for $R = 10^6$ and $C_L = 1.66$

Assuming that the mean line modifications due to viscous effects are about the same for small variations in the flap deflection at a given angle of incidence, the increase in the flap deflection required to achieve the optimum viscous/pressure recovery can be estimated. The procedure is to take the modified shape at a fixed angle of attack (say 3°) and deflect the flap (while maintaining the position) until the calculated pressure recovery on the flap is about equal to the design pressure recovery. Figure 16 shows the pressure distributions for $\delta_f = 20^O$ and $\alpha = 3^O$. The pressure distributions obtained after making corrections for boundary layer displacements and increasing the flap deflection to 20° are believed to be a good approximation to those which would be obtained experimentally.

Since the pressure distribution obtained for the section modified to account for the boundary layer (at $\delta_f = 20^O$) is very close to the inviscid pressure distribution for $\delta_f = 15^O$, it can be assumed that the drag for the modified case is about the same as the drag calculated using the inviscid distribution. The lift curve slopes for these two conditions should be about equal. For $\alpha = 3^O$, the computed lift coefficient (including viscous effects) is 1.66 for $\delta_f = 20^O$.

The angle of incidence at which flow separation begins on the main section is assumed to be six degrees since this is the critical angle for the inviscid case at $\delta_f = 15^O$. The maximum low drag lift coefficient is then equal to two.

CHAPTER III

EXPERIMENTAL RESULTS

The theoretical lift and drag results for the designed airfoil presented in this chapter are for a Reynolds number of 10^6 in the flap extended case to represent a typical low speed Reynolds number and for $R = 2 \times 10^6$ in the flap retracted case to represent a typical cruise condition.

The lift-drag characteristics of the new slotted flap wing section were measured in the University of Alberta aeronautical wind tunnel by D. J. Marsden, R. W. Toogood and G. Kiss[26]. (See Appendix E.)

Figure 17 compares the theoretical and corrected experimental results for the airfoil in the retracted configuration. The experimental results show that the low drag range is broader than was predicted by the theoretical analysis. The analysis program is not capable of computing drag for an airfoil with a separated boundary layer, and therefore the theoretical lift curve was terminated at the lift coefficient where separation begins. The analysis program predicted a slow increase in the extent of the separated region beyond the first occurrence of separation at a predicted lift coefficient
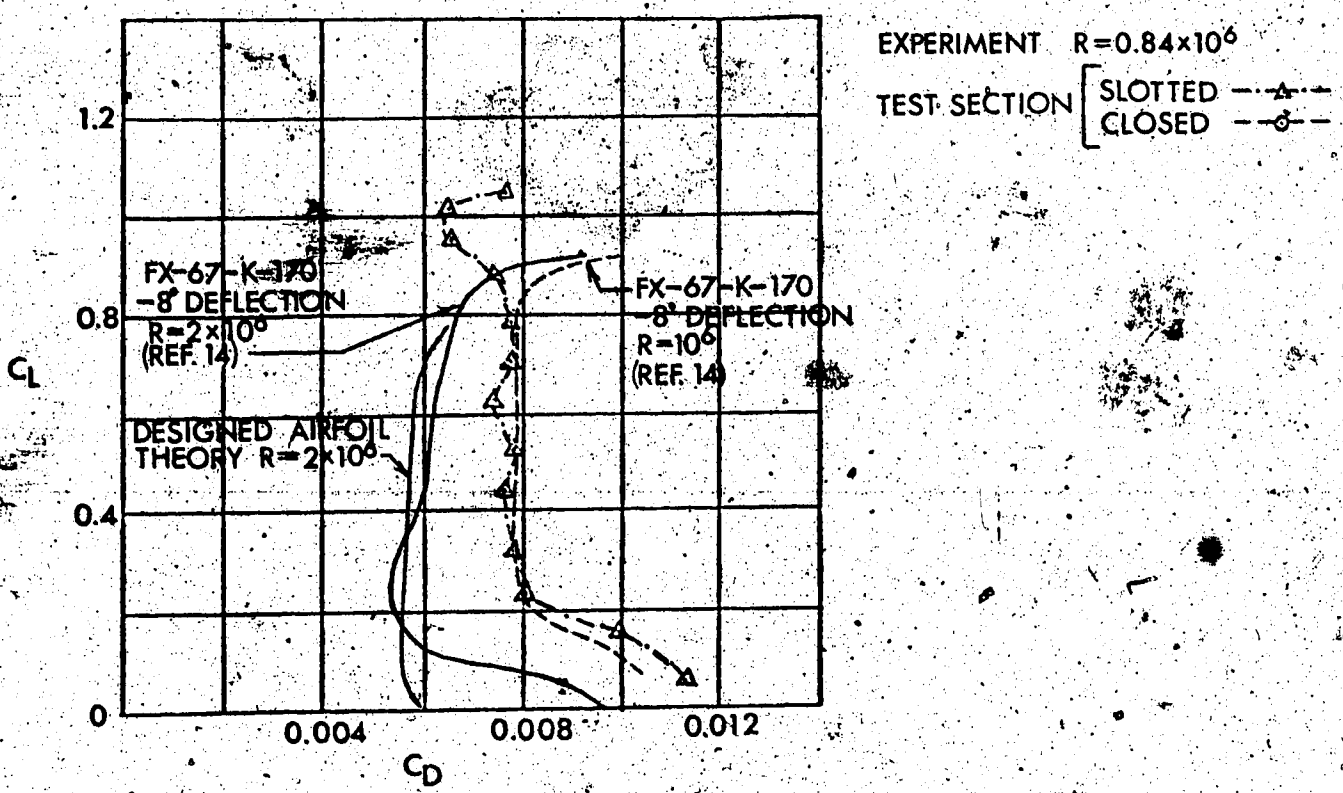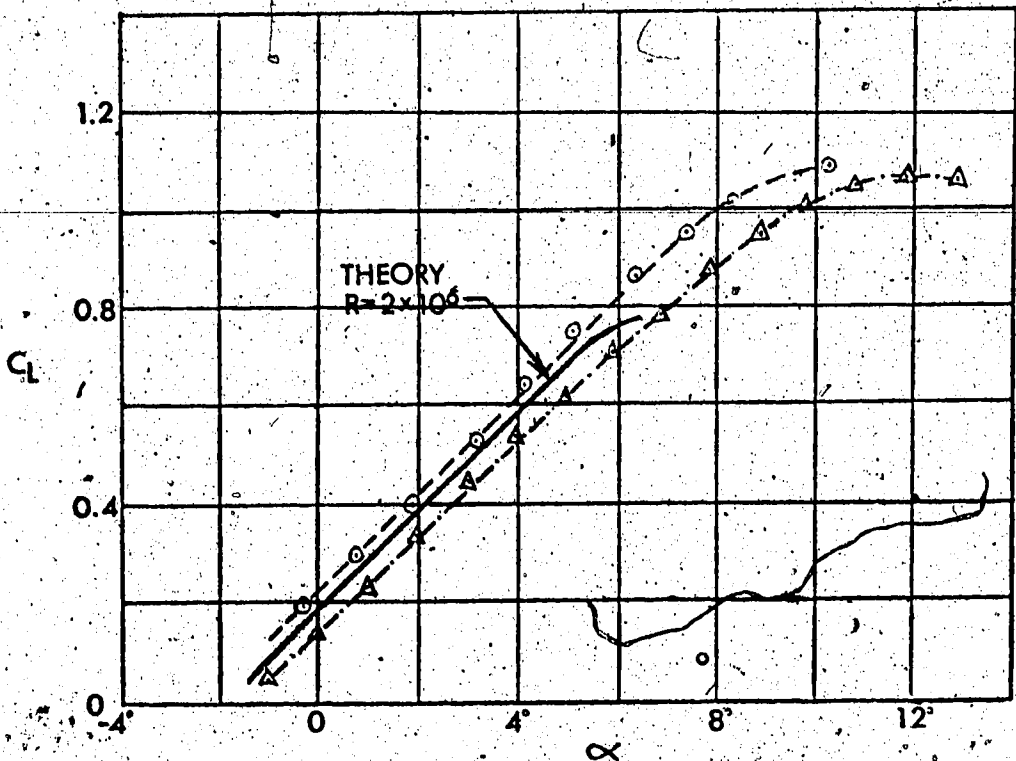
Figure 17. Results for the Slotted-Flap Airfoil in the Retracted Configuration

of 0.7. It may be that the separation criterion used was overly sensitive in this case.

A comparison of corrected wind tunnel results for a closed section with results for the 75% open area slotted top showed the open top section produced values of lift coefficient that were too low. More recent unpublished results by Williams at the University of British Columbia indicate that the open area ration should only be 60%.

The good agreement shown in figure 17 between published experimental results [14] for the FX-67-K-170 airfoil and theoretical results obtained here indicates the theory works well for this aerofoil. Wind tunnel results obtained here at a Reynolds number of 8.4×10^6 are compared in figure 17 with published results at nearly the same Reynolds number. The good agreement is an indication that the present experimental results are reliable.

Figure 18 comparies the theoretical and experimental lift and drag characteristics of the designed airfoil at the design flap deflection of 20°. The theoretical results include the correction for the effect of the boundary layer. While the lift coefficients agree fairly well (as well as can be expected from two dimensional model tests in a small scale wind tunnel), measured drag coefficients are considerably higher than those predicted by theory.

It is not unexpected that measured drag would be higher than predicted since no attempt was made in the theoretical analysis (as discussed in section 2.2.3) to account for the extra drag due to the separated flow that

THEORY R=10⁶

SLOTTED TEST SECTION
R=0.84×10⁶
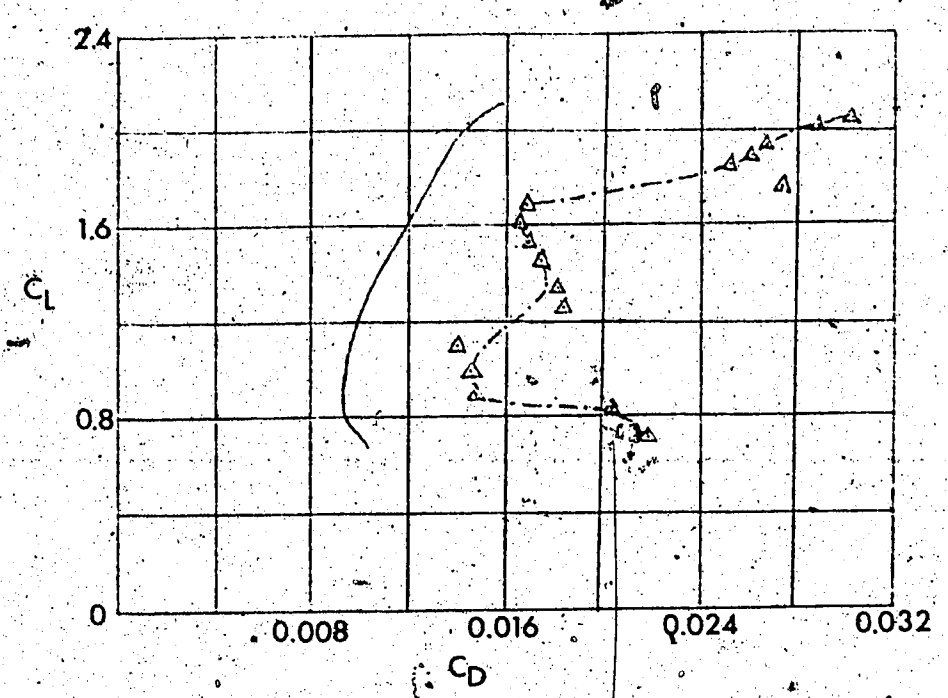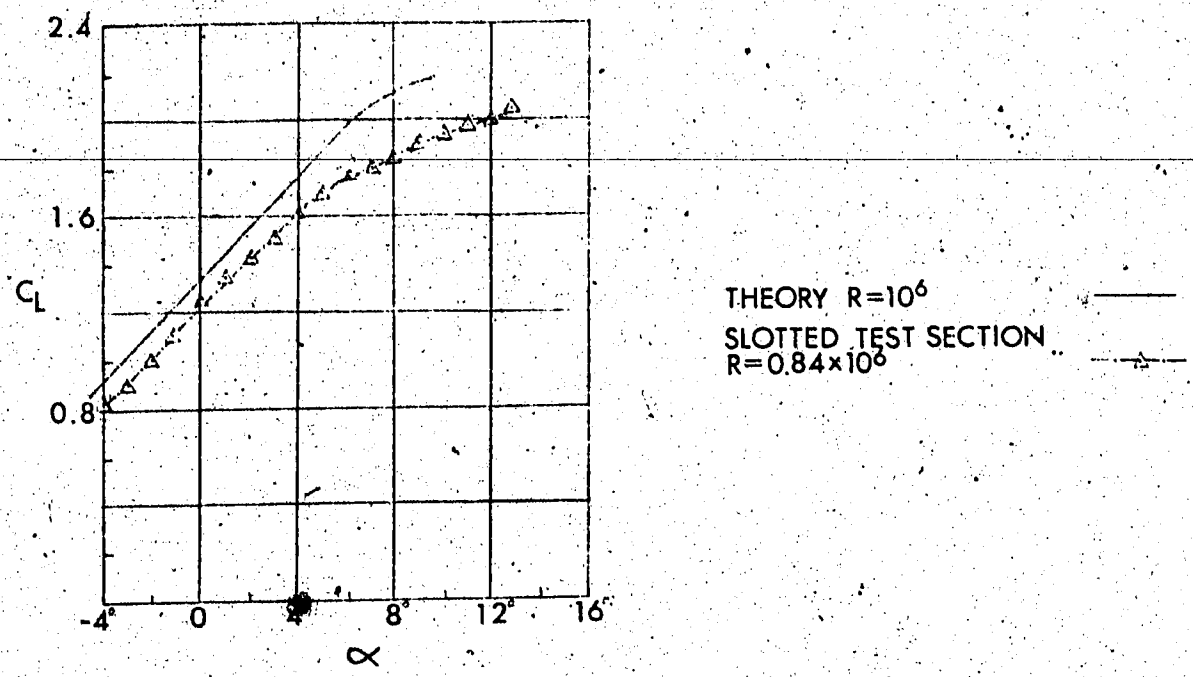
Figure 18. Results for the Slotted-Flap Airfoil in the
Flap Out Configuration

exists at the back of the main profile with the flap
extended. Flow visualization tests showed that a region
of separated flow does exist in the slot and that this
separated region is bounded by a free streamline such that
the flow leaves the trailing edge of the main section
smoothly.

The pressure in the separated region is less than
the free stream pressure and, as shown in section 2.2.3,
the associated form drag could be significant and could
account for the large measured drag coefficients when com-
pared to the theoretical drag coefficients which were
computed assuming a solid, faired in, slot.

While the measured drag coefficients are much
higher than predicted and probably somewhat higher than
would be encountered in flight, the overall lift-drag
characteristics (flap retracted and flap extended charact-
eristics taken together) represent a significant improvement
over existing airfoil characteristics. This is illustrated
in Figure 19 where the combined experimental results for
the designed section are compared with results for the
FX-67-K-170 airfoil[14] and an NACA 23012 airfoil with a
30% chord slotted flap[9].

The operating speed range is extended both at the
high speed end with the flap retracted (low C_L) and at the
low speed end of the range with the flap extended. The
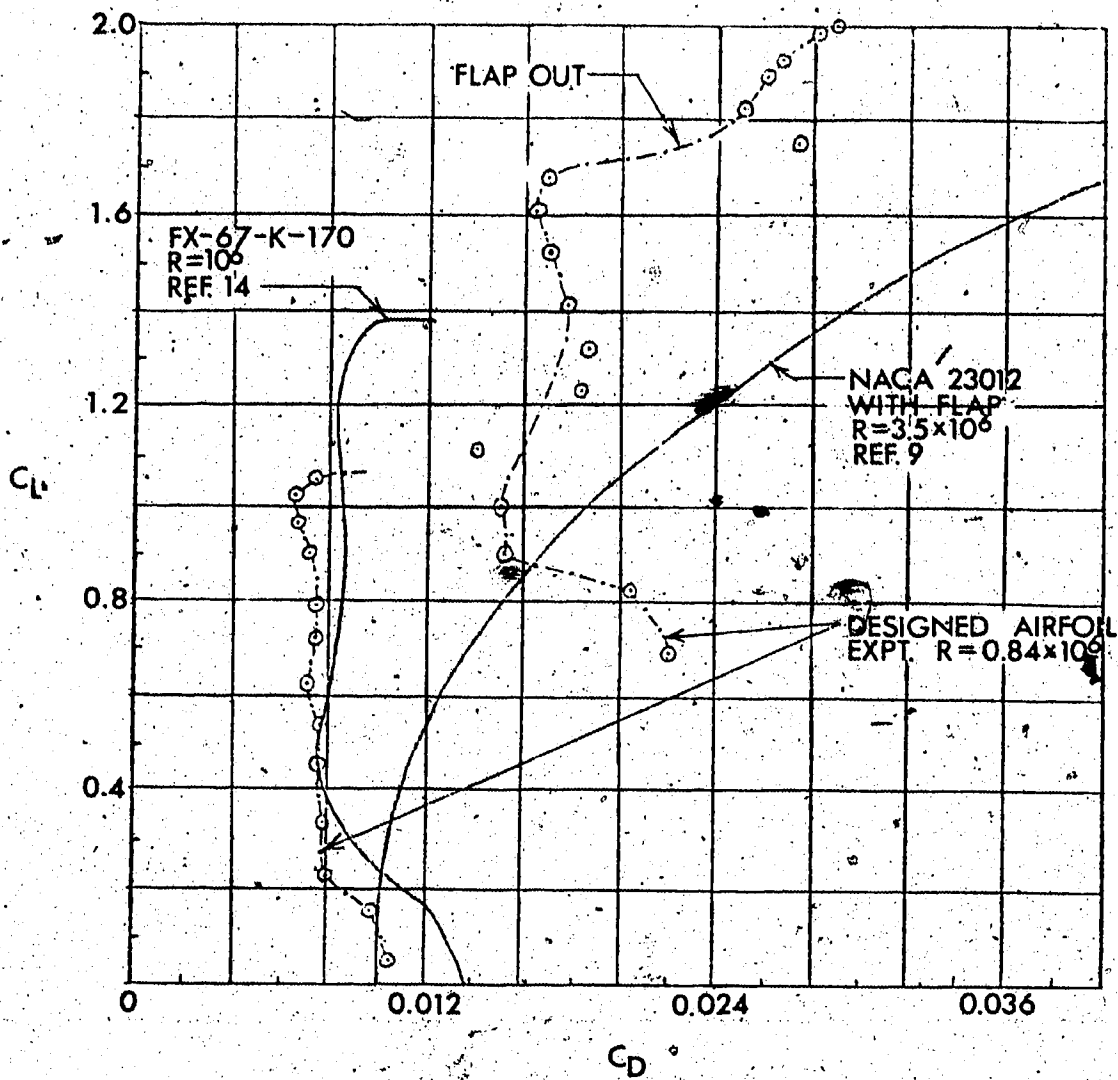
Figure 19. Comparison of the Characteristics of the Designed Airfoil with Two Other Airfoil Sections

extension of the C_L range above that of the original profile is a useable range in that C_D is only increasing slowly with α and the stall characteristics as shown in Figure 18 are very mild. A small increase in α when operating at high C_L will not result in a drastic increase in drag or a sudden loss of lift.

Flow visualization studies showed that the mode of transition from a laminar to a turbulent boundary layer on the suction side of the flap and the main section was by means of the short laminar separation bubble. This was predicted by the theoretical boundary layer analysis. The observed transition locations corresponded closely to the predicted locations of about 6.4 inches downstream of the nose for the main section and 1.6 inches downstream of the nose for the flap section.

Figure 20 is a comparison of the measured and theoretical pressure distributions for the flap extended configuration ($\delta_f = 20°$) at about the same C_L and Figure 21 compares the measured and theoretical (inviscid) pressure distributions for the retracted airfoil at $\alpha = 4°$.

The coordinates of the designed airfoil section are found in Table 2.
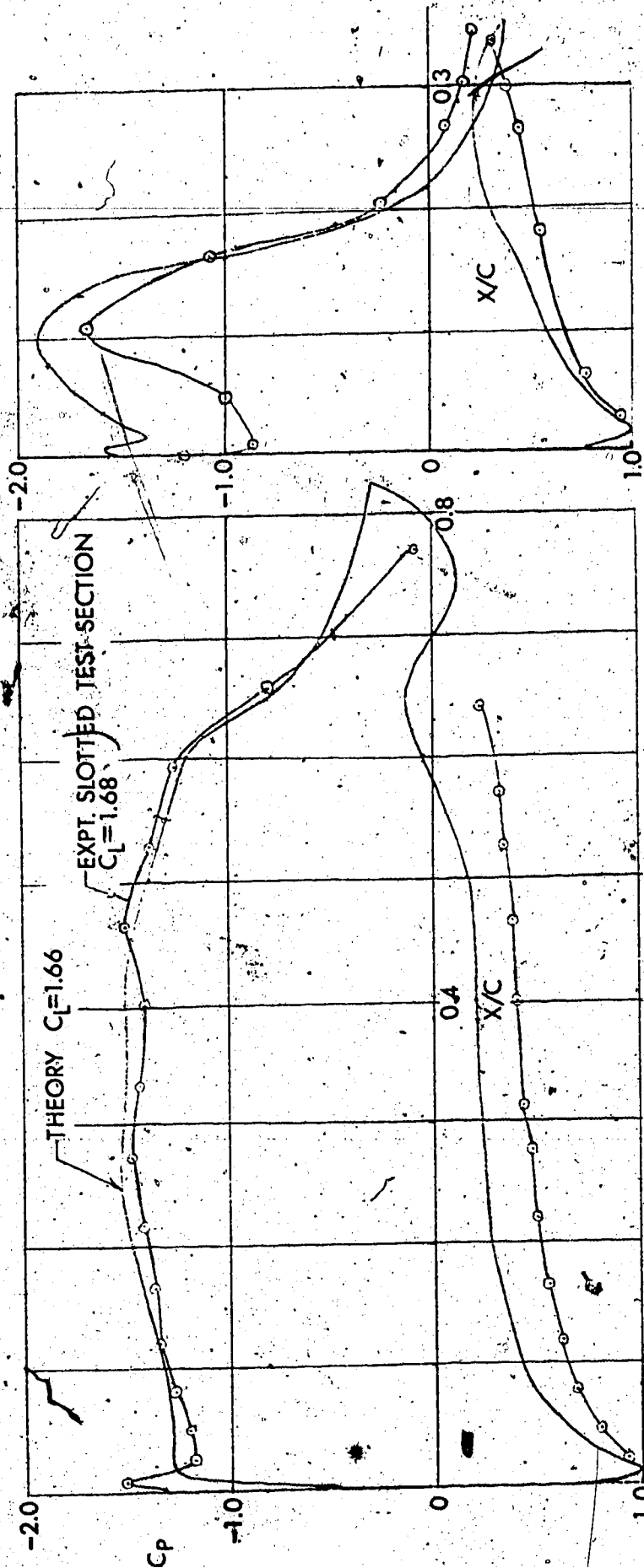
Figure 20. Comparison of the Calculated and Measured Pressure Distributions over the Slotted-Flap Airfoil ($\delta_f = 20°$)
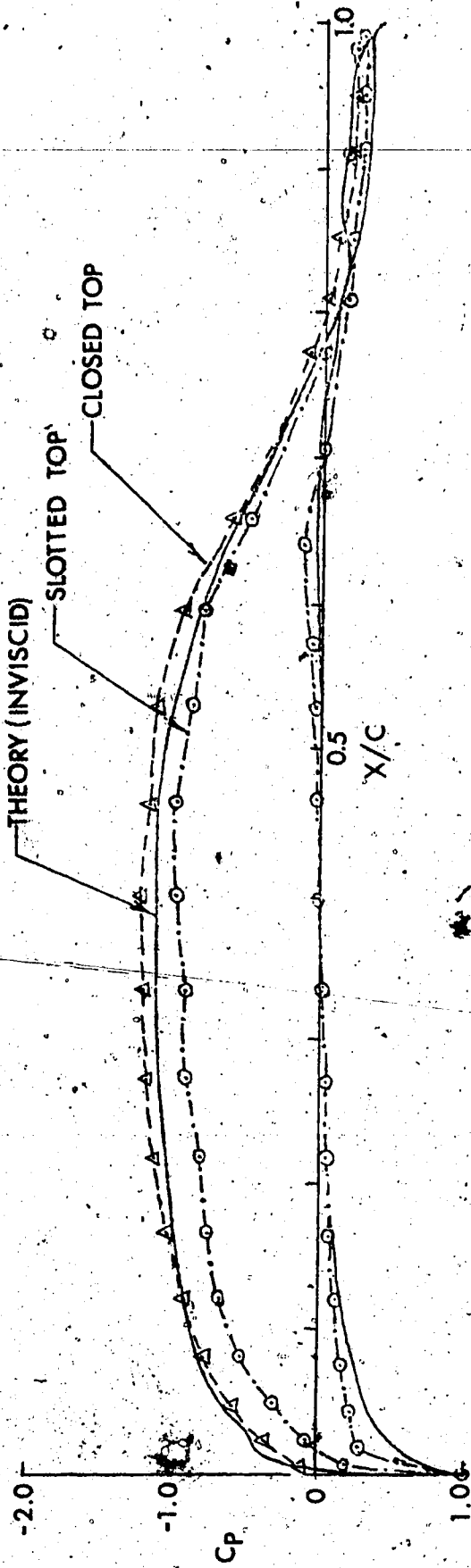
Figure 21. Comparison of Measured and Theoretical (Inviscid) Pressure Distributions with the Flap Retracted at α = 4°

Table 2. Coordinates of the Flapped Airfoil

Main Section

X	$Y_{up.}$	Y_{Low}
0	0	0
.00107	.00653	-.00217
.00428	.01192	-.00514
.00961	.02019	-.00815
.01704	.02760	-.012??
.02653	.03487	-.01???
.03806	.04309	-.015??
.05156	.05158	-.0182?
.06699	.06011	-.02062
.08427	.06856	-.02282
.10532	.07685	-.02490
.12408	.08490	-.02682
.14645	.09263	-.02856
.17033	.09994	-.03011
.19562	.10677	-.03146
.22221	.11305	-.03261
.25000	.11870	-.03354
.27866	.12365	-.03425
.30866	.12783	-.03474
.33920	.13119	-.03499
.37059	.13370	-.03501
.40245	.13526	-.03480
.43474	.13571	-.03435
.46730	.13490	-.03365
.50000	.13274	-.03272
.53270	.12919	-.03155
.56526	.12429	-.03012
.59755	.11808	-.02844
.62941	.11063	-.02654
.66072	.1026?	-.02437
.69134	.0926?	
.72114	.08259	
.75000	.07233	
.77779	.06229	
.80438	.05287	
.82090	.04762	

Table 2.   (Continued)

Flap Section

X	Y_{up}	Y_{Low}
0	-0.01250	-0.01250
.00250	-0.00385	-0.01750
.00500	+0.00069	-0.02000
.01000	+0.00729	-0.02200
.01500	+0.01250	-0.02340
.02000	0.01736	-0.02360
.04134	0.03291	-0.02187
.07114	0.04625	-0.01896
.10000	0.05350	-0.01572
.12779	0.05500	-0.01236
.15438	0.05099	-0.00914
.17967	0.04454	-0.00608
.20355	0.03756	-0.00319
.22592	0.03189	-0.00048
.26573	0.02387	0.00433
.29844	0.01906	0.00829
.32347	0.01660	0.01134
.34039	0.01533	0.01334
.34893	0.01461	0.01439
.35000	0.01454	0.01454

CHAPTER IV

Summary and Conclusions

The problem of designing a slotted-flap airfoil section does not lend itself to a neat optimized solution because of the conflicting structural and performance requirements. In the preceding chapters a design method has been put forward wherein a specific attempt has been made to satisfy the diverse structural and performance requirements in the design of a single slotted-flap airfoil section.

For practical applications, where minimizing profile drag is desirable, most of the flapped airfoil sections available are not suitable because substantial flow separation on the flap occurs for lift coefficients far below the maximum. The object of the present design method was to increase the low drag (unseparated) range of a single slotted-flap airfoil at low Reynolds numbers. A key element in the design philosophy is that the flow over the flap should be designed to remain unseparated for all angles of attack at a given deflection.

An important feature of the proposed method is that the flap can be designed for one optimum loading because the loading is basically independent of the angle of incidence. By comparison a normal wing section is designed to be a compromise to provide satisfactory pressure

distributions over a range of angles of incidence. In addition, the flap modification required to give the optimum pressure recovery is the modification required to lower the drag bucket with the flap retracted. This modification also results in a smaller pitching moment because of the loop in the pressure distribution in the neighborhood of the trailing edge when the flap is retracted.

One important advantage of the proposed design technique is the fact that most of the basic airfoil remains unaltered. For the specific design considered this means that the stalling characteristics of the FX-67-K-170 airfoil are transferred to the designed flapped airfoil section. The FX-67-K-170 airfoil exhibits a gradual stall with a small decrease in lift beyond the maximum. Consequently the maximum usable lift of this airfoil is very close to the maximum lift coefficient. That is, the airfoil can be operated very near the maximum C_L because a small increase in α will not result in a drastic increase in drag or sudden loss of lift. The maximum low drag lift coefficient for the designed flapped section was found to be two; this can be assumed to be very close to the maximum usable lift coefficient.

The design method presented in Chapter II can be summarized as follows:

(1) The airfoil chosen as the basic section should

have a high design C_L and a gentle stall character-
istic. In practice this implies an airfoil section
designed using the optimized Wortmann Stratford
pressure recoveries.

(2) The basic flap section should be highly cambered
to permit large lift increments for small flap
deflections. The thickness distribution must be
chosen to satisfy the condition that the flap is
compatible with the main profile in the retracted
configuration.

(3) The preliminary flap is modified by reflexing the
camber line from about the point of minimum pres-
sure (on the suction side) back to the trailing
edge. This procedure can be repeated to move the
suction side pressure distribution closer to the
optimum for the maximum loading. The flap will
then remain unstalled at all angles of attack for
the given design deflection and stalling will begin
with separation from the trailing portion of the
main section. The reflexing of the flap has the
effect of reducing the pitching moment of the
airfoil section when the flap is retracted.

The proposed design method is equally applicable to
design for higher Reynolds numbers although design at lower
Reynolds numbers, typical of light aircraft, has been shown

to be more critical.

The results presented in Chapter III demonstrate
that the application of the proposed design technique has
resulted in the design of an airfoil section for which a
worthwhile increase in the low drag range has been achieved.
The slotted-flap airfoil is competitive with plain flapped
airfoils in its application to low speed aircraft, and since
the slotted flap is more costly because of mechanical com-
plexity it will have to have substantially better performance
to justify its use. The designed airfoil, based on the
proposed method, offers improved performance over an
FX-67-K-170 airfoil with a 17% plain flap[14] which achieves
a maximum C_L of about 1.7.

The large discrepancy between measured and
calculated drag coefficient is due to the inability of the
present theory to take account of separated flow that occurs
in the slot for the flap extended configuration. This
additional drag will occur in practice unless some means
can be devised to fair in the back of the main profile
when the flap is extended. In spite of this approximately
50% increase in drag, a worthwhile extension of the low
drag range of the airfoil section was achieved.

In conclusion, a unique design philosophy for the
design of single slotted-flap airfoils at low Reynolds
numbers has been developed. An efficient and practical

approach has been evolved for the design of a slotted-flap that is structurally compatible with a good high speed airfoil section. It has been demonstrated, by applying the design method, that a worthwhile increase in the low drag range can be achieved for an airfoil section for the range of flight Reynolds numbers.

The proposed method of design represents an advance on design methods currently being used for airfoil design.

REFERENCES

1. Truckenbrodt, E., "Die Berechnung der Profilform bei vorgegebener Geschwindigkeitsverteilung", Ing. Archiv., Vol. 19, p. 365, 1951.

2. Wilkinson, D. H., "A Numerical Solution of the Analysis and Design Problems for the Flow Past one or more Aerofoils or Cascades", ARC R. & M. 3545, 1967.

3. Abbott, I. H., and Von Doenhoff, A. E., Theory of Wing Sections, Dover Publications, New York, 1958.

4. Raspet, A., and Gyorgyfalvy, D., "Der 'Phonix' - eine Losung fur optimalen Uberland-Segelflug", Z. Flugwiss, 8 (1960), 9, p. 260.

5. Marsden, D. J., "Prospects for Increased Performance of Sailplanes", CASI Journal, April 1971, pp. 151-152.

6. Wortmann, F. X., "A Contribution to the Design of Laminar Profiles for Gliders and Helicopters", Z. Flugw. 3 (10), pp. 333 - 345, 1955.

7. Eppler, R., "Laminar Profiles for Gliders", Z. Flugw. 3 (10), p. 345, 1955.

8. Liebeck, R. H., and Ormsbee, A. J., "Optimization of Aerofoils for Maximum Lift", AIAA 69-739, 1969.

9. Cahill, J. F., "Summary of Section Data on Trailing-Edge High-Lift Devices", NACA Report 938, 1949.

10. Stratford, B. S., "The Prediction of Separation of the Turbulent Boundary Layer", Journal of Fluid Mechanics, Vol. 5, p. 1, 1959.

11. Liebeck, R. H., and Ormsbee, A. I., "Optimization of Airfoils for Maximum Lift", Journal of Aircraft, Volume 7, Number 5, 1970, pp. 409-415.

12. Chen, A. W., "The Determination of the Geometries of Multiple-Element Airfoils Optimized for Maximum Lift Coefficient", Ph. D. Thesis, University of Illinois, 1972.

13. Vesely, J., "The Contribution of Aerodynamics to the development of Recent Sailplanes in Czechoslovakia", OSTIV Publication 5, 1956.

14. Althaus, D., Stuttgarter Profilkatalog I, Experimental Results from the Laminar Wind Tunnel of the Institut fur Aero und Gasdynamik der Universitat Stuttgart, 1972.

15. Tani, I., "Low-Speed Flows Involving Bubble Separations", Progress in Aeronautical Sciences, Vol. 5, p. 70, 1964.

16. Kelling, F. H., "Experimental Investigation of a High-Lift Low-Drag Aerofoil", ARC C.P. 1187, 1968.

17. Wortmann, F. X., "Experimental Investigations on new
Laminar Profiles for Gliders and Helicopters",
Z. Flugw., 5(8), pp. 228 - 243, 1957.

18. Foster, D. N., Irwin, H.P.A.H., and Williams B.R.,
"The Two-Dimensional Flow Around a Slotted Flap",
ARC R. & M. 3681, 1970.

19. Holtzclaw, R. W., Weisman, Y., "Wind-Tunnel Investigation
of the Effects of Slot Shape and Flap Location on
the Characteristics of a Low-Drag Airfoil Equipped
with a 0.25-Chord Slotted Flap", NACA MR A4L28.

20. Stevens, W. A., Goradia, S. H., and Braden, J. A.,
"Mathematical Model for Two-Dimensional Multi-
Component Airfoils in Viscous Flow", NASA CR 1843.

21. Ringleb, F. O., "Separation Control by Trapped Vortices",
Boundary Layer and Flow Control, Volume 1,
pp. 265-294, 1961.

22. Seebohm, T. "Boundary Layer, Transition, and Wake
Measurements at Low Mach Number for an Aerofoil
with Single-Slotted Flap", McGill University Report
69-1, 1969.

23. Head, M. R. and Patel, V. C., "Improved   nment
Method for Calculating Turbulent Bo   Layer
Development", ARC R. & M. 3643, 1968.

24. Duncan, W. J., Thom, A. S.,   d Young, A. D., Mechanics
of Fluids, London, Edward Arnold (Publishers) Ltd.,
1970.

25. Powell, B. J., "The Calculation of the Pressure Distri-
    bution on a Thick Cambered Aerofoil at Subsonic
    Speeds Including the Effects of the Boundary Layer",
    ARC C.P. 1005, 1967.

26. Marsden, D. J., Private Communication, 1974.

27. Seebohm, T., Private Communication, 1971.

28. Jacob, K. and Riegels, F. W., "The Calculation of
    the Pressure Distribution over Aerofoil Sections
    With and Without Flaps and Slots", RAE Library
    Translation 1101, 1965.

29. Riegels, F. W., Aerofoil Sections, London, Butter-
    worths, 1961.

30. Williams, B. R., "An Exact Test Case For the Plane
    Potential Flow About Two Adjacent Lifting Aerofoils",
    RAE T.R. 71197, 1971.

31. Rosenhead, L., Laminar Boundary Layers, Oxford, Clarendon
    Press, 1963.

32. Curle, N. and Skan, S. W., "Approximate Methods for
    Predicting Separation Properties of Laminar
    Boundary Layers", Aeronautical Quarterly, Vol. 8,
    p. 257, 1957.

33. Schlichting, H., Boundary Layer Theory, Fourth Edition,
    McGraw-Hill, 1962.

34. Liu, C. Y. and Sandborn, V. A., "Evaluation of the
    Separation Properties of Laminar Boundary Layers",
    Aeronautical Quarterly, p. 235, August 1968.

35. Crabtree, L. F., "Prediction of Transition in the
    Boundary Layer on an Aerofoil", J. Royal. Aero.
    Soc., Vol. 62, p. 525, 1958.

36. Owen, P. R., and Klanfer, L., "On the Laminar Boundary
    Layer Separation from the Leading Edge of a Thin
    Aerofoil", ARC C.P. 220, 1953.

37. Seebohm, T., "Prediction of the Flow Round Aerofoils
    Using Potential Flow and Boundary Layer Theory.
    Progress Report", McGill University Memorandum
    68-1, 1968.

38. Thompson, B. G. J., "A Critical Review of Existing
    Methods of Calculating the Turbulent Boundary Layer",
    ARC R. & M. 3447, 1964.

39. Head, M. R., "Entrainment in the Turbulent Boundary
    Layer", ARC R. & M. 3152, 1958.

40. Bradshaw, P., "Turbulent Boundary Layers", Journal of
    the Royal Aeronautical Society, Vol. 72, p. 451,
    1968.

41. Stanford Conference AFOSR-IFP, Computation of Turbulent
    Boundary Layers, 1968.

42. Thompson, B. G. J., "A New Two-Parameter Family of Mean
    Velocity Profiles for Incompressible Turbulent
    Boundary Layers on Smooth Walls", ARC R. & M. 3463,
    1967.

43. Sandborn, V. A. and Liu, C. Y., "On Turbulent Boundary-
    Layer Separation", Journal of Fluid Mechanics,
    Vol. 32, Part 2, p. 293, 1968.

44. Squire, H. B. and Young, A. D., "The Calculation of
    the Profile Drag of Aerofoils", ARC R. & M. 1838,
    1937.

45. Riegels, F., "Das Umstromungsproblem bei inkompressiblen
    Potentialstromungen", Ing. Archiv., Vol. 16, p. 373,
    1948.

46. Riegels, F., "Das Umstromungsproblem bei inkompressiblen
    Potentialstromungen", Ing. Archiv., Vol. 17, p. 94,
    1949.

47. Faulkner, S., Hess, L., Giesing, J. P., "Comparison
    of Experimental Pressure Distributions with those
    Calculated by the Douglas Neumann Program", Douglas
    Aircraft Report LB 31831, 1964.

48. Williams, C. D., "Theory for Wind Tunnel Wall Corrections",
    M. Sc. Thesis, University of British Columbia, 1973.

49. Pope, A. and Harper, J. J., Low-Speed Wind Tunnel Testing,
    New York, Wiley, 1966.

APPENDIX A

THE APPLICATION OF THE METHOD OF

DISTRIBUTED VORTICITY

The methods of distributed vorticity and distributed sources are both capable of handling the calculation of pressure distributions over multi-element airfoil sections. However the surface vortex method requires considerably less computing time[27].

For this project the method of distributed vorticity, as modified by Wilkinson[2], was chosen because of the time factor and the apparent accuracy and ease of application.

The basic equation of the method is:

$$-\frac{\gamma(s_p)}{2} + \frac{1}{2\pi} \oint \gamma(s) \, K(s_p,s) \, ds = -V_\infty \left[\cos \alpha \, (\frac{dx}{ds})_p + \sin \alpha \, (\frac{dy}{ds})_p \right]$$

This equation expresses the condition that the sum of the tangential component of the free stream velocity at a given point and the tangential component of the velocity induced by the continuous distribution of vorticity around the airfoil surface must equal the velocity at the point. (By specifying a zero internal tangential velocity boundary condition it is found that the external tangential velocity is equal to the vortex density at the point s_p where γ is the vortex density.) Clearly for a continuous distribution

82

the method is exact.

The method as proposed by Jacob and Riegels[28] and by Wilkinson involves two major approximations:

(1) The surface integral in the preceding equation is replaced by an approximation using the trapezoidal rule.

(2) The boundary condition is satisfied at a finite number of points only.

The integral in the preceding eqn. can be replaced by a summation as a result of trapezoidal integration. Using equal intervals of the angular parameter ϕ; the basic idea of continuous vortex distribution remains intact. The basic equation becomes:

$$\sum_{n=1}^{2N-1} \gamma_n K_{mn} = -2N (\cos \alpha \cdot x'_m + \sin \alpha \cdot y'_m)$$

where

$$\gamma_n = \gamma_s \frac{ds}{d\phi}, \quad x'_m = \frac{dx_m}{d\phi}, \quad y'_m = \frac{dy_m}{d\phi} \text{ and } \phi_n = \frac{n\pi}{N}$$

(where $n = 1, 2, \ldots 2N - 1$). The K_{mn} are the tangential velocities induced at point m by vortices of strength equal to one located at points n on the airfoil surface.

The strength of the vortex density at the trailing edge ($n = 0$) was set equal to zero to satisfy the Kutta condition. Without this condition the equations are linearly dependent and no unique solution is possible. Wilkinson pointed out that for sharp trailing edges $\frac{ds}{d\phi} \to 0$ as $\phi \to 0$ therefore

(1) specification of zero vortex strength at $\phi = 0$
does not correspond to zero velocity at $s = 0$ in
the real plane. (The velocity is undefined).

(2) the matrix of coefficients remains singular since
the K_{on} values (row one) are all zero.

Wilkinson proposed that another equation be re-
moved by setting the load at the point nearest the trailing
edge equal to zero. (ie. $\gamma_1 = -\gamma_{2N-1}$) In fact since the
actual velocity is $\gamma(s_\mu) = \dfrac{\gamma(\phi_\mu)}{s'(\phi_\mu)}$ the correct specification
is $\gamma(s_1) = -\gamma(s_{2N-1})$. The removal of this equation results

in a system of linearly independent equations that have a
unique solution.

The most common vortex point distribution is
according to the equation:

$$x_n = \frac{c}{2}(1 + \cos \phi_n) \text{ where } \phi_n = \frac{n\pi}{N} \text{ and } n = 1, \ldots, 2N-1.$$

x_n refers to the chordwise position of the point; the effect
of this distribution is to concentrate the points in the nose
region and the trailing edge region.

The large influence coefficients associated with
points having equal x values leads to large errors when
estimating the integral by the trapezoidal rule. To help
correct this, the $K_{\mu, 2N-\mu}$ coefficients are calculated using
an irrotationality device which very simply is that using
trapezoidal integration the sum of any column of influence

coefficients is constant (ie. the circulation around any closed curve not including the point in question must be zero since the flow is irrotational).

Wilkinson suggested further that the preceding point distribution be modified by introducing a constant k such that $\bar{x} = x_i[1 + (1 - k) \times (1 - x)]$. The intent of this modification was to move the points 1 and $2N - 1$ nearer the trailing edge so as to reduce the error in setting the velocities at these points equal. The effect for $k < 1$ is to concentrate points in the trailing edge region while retaining the equal angular spacing.

The last modification should improve the accuracy of the method since the concentration of points in the region of small thickness helps to more accurately approximate the integral. In principle (referring back to the two main approximations of the method) the accuracy must be improved as the total number of points increases.

The application of the vorticity method to multi-element sections is straightforward; the point spacing in the neighborhood of the slot (for a slotted flap) should not be greater than the minimum slot width.

The method of distributed vorticity as modified by Wilkinson was programmed for both the single element airfoil and the flapped airfoil pressure distribution calculations. Several airfoil sections and slotted flap sections were used to test the programs.

Evaluation of the results is difficult because:

(1) there are no results available of a systematic comparison of the currently used potential flow methods.

(2) comparison with experimental results must be done cautiously since the changes in pressure distribution due to the boundary layer, expecially near the trailing edge may be substantial. A permanently separated flow region may exist on the suction side near the trailing edge implying that inviscid pressure distributions are never realized. Pressures are difficult to measure near the trailing edge and most test results extrapolate pressure distributions in this region.

Some typical results are shown in Figures 22 through 25. Two conclusions were drawn from the results:

(1) The program works well for airfoils or multi-element sections with "normal" (ie wedge shaped) trailing edges.

(2) The program gives unreliable results for airfoils or flapped sections which exhibit cusped "hooked" trailing edges. Further to this, the reason for the poor results is likely that the assumed Kutta condition of zero loading at the trailing edge is incorrect for "hooked" sections. The results catalogued by Riegels[29] appear to substantiate this

DISTRIBUTED VORTICITY — — —
DISTRIBUTED SOURCE (REF. 47) ———

X/C

0.2

-2.0

-1.0

0

1.0

X/C

0.5

1.0

Cp

-2.0

-1.0

0

1.0
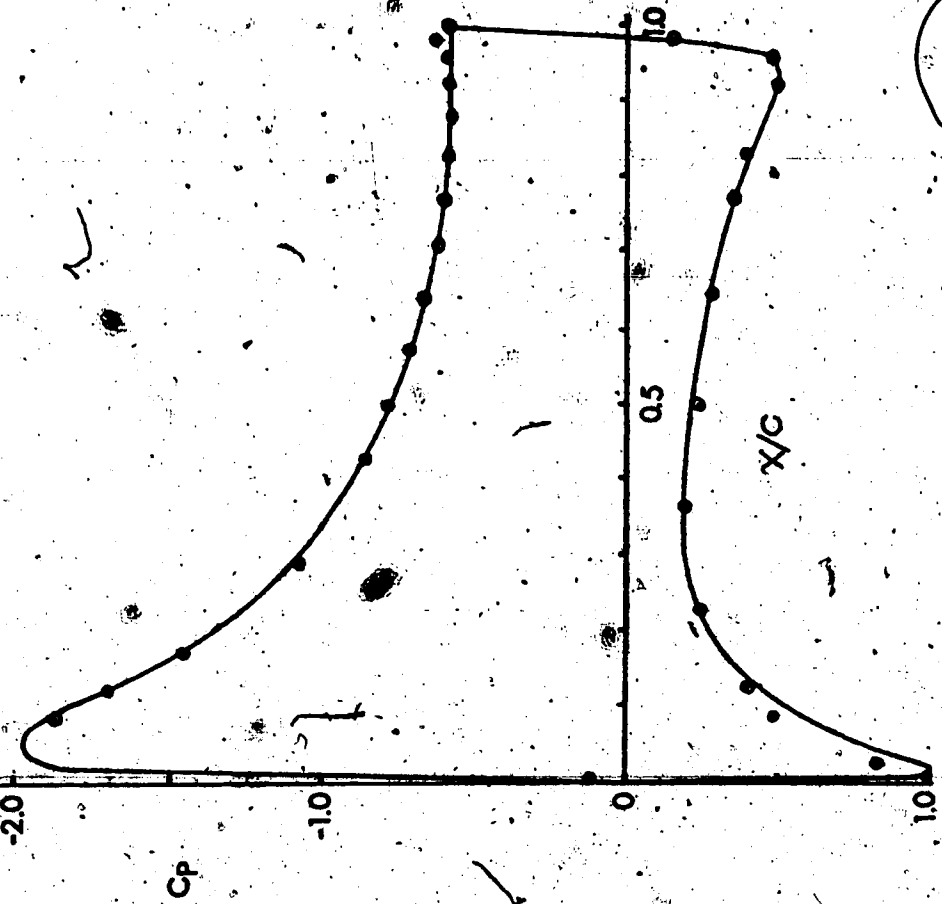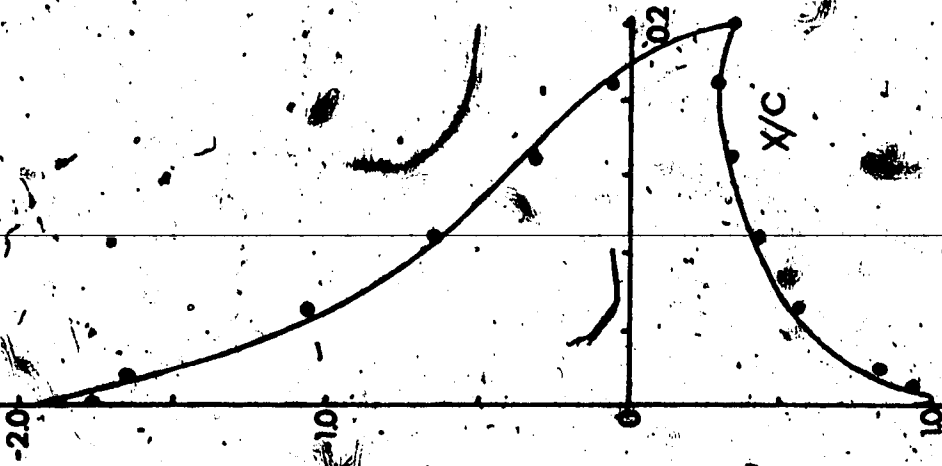
Figure 22.. Calculated Pressure Distributions on the NACA
23012 Airfoil with a 30% NACA 23012 Flap

VORTICITY METHOD ----
METHOD OF REF. 30 ——

C_P

x/c

Figure 23.   Comparison of the Calculated Pressure
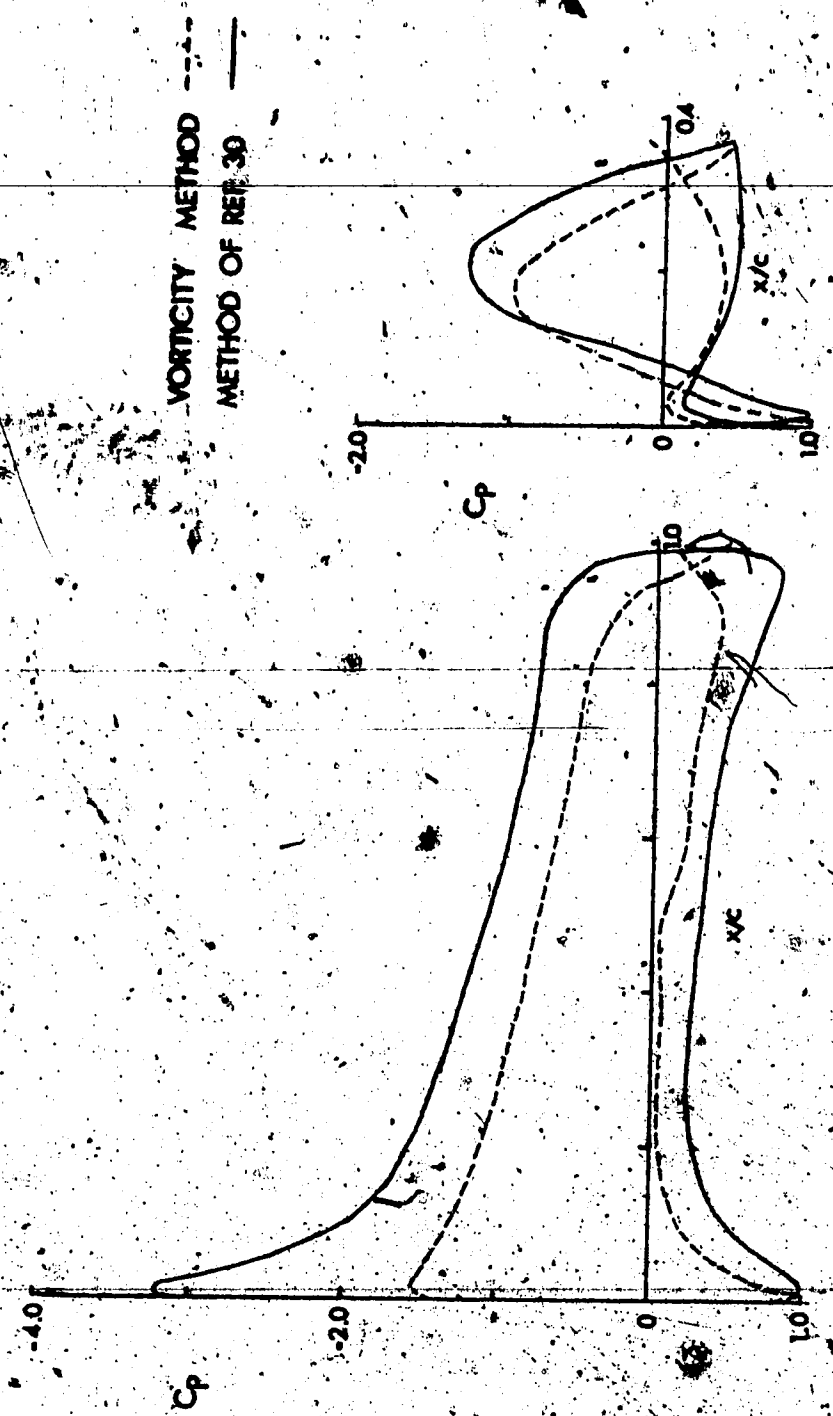Distributions on a Two-Element Airfoil
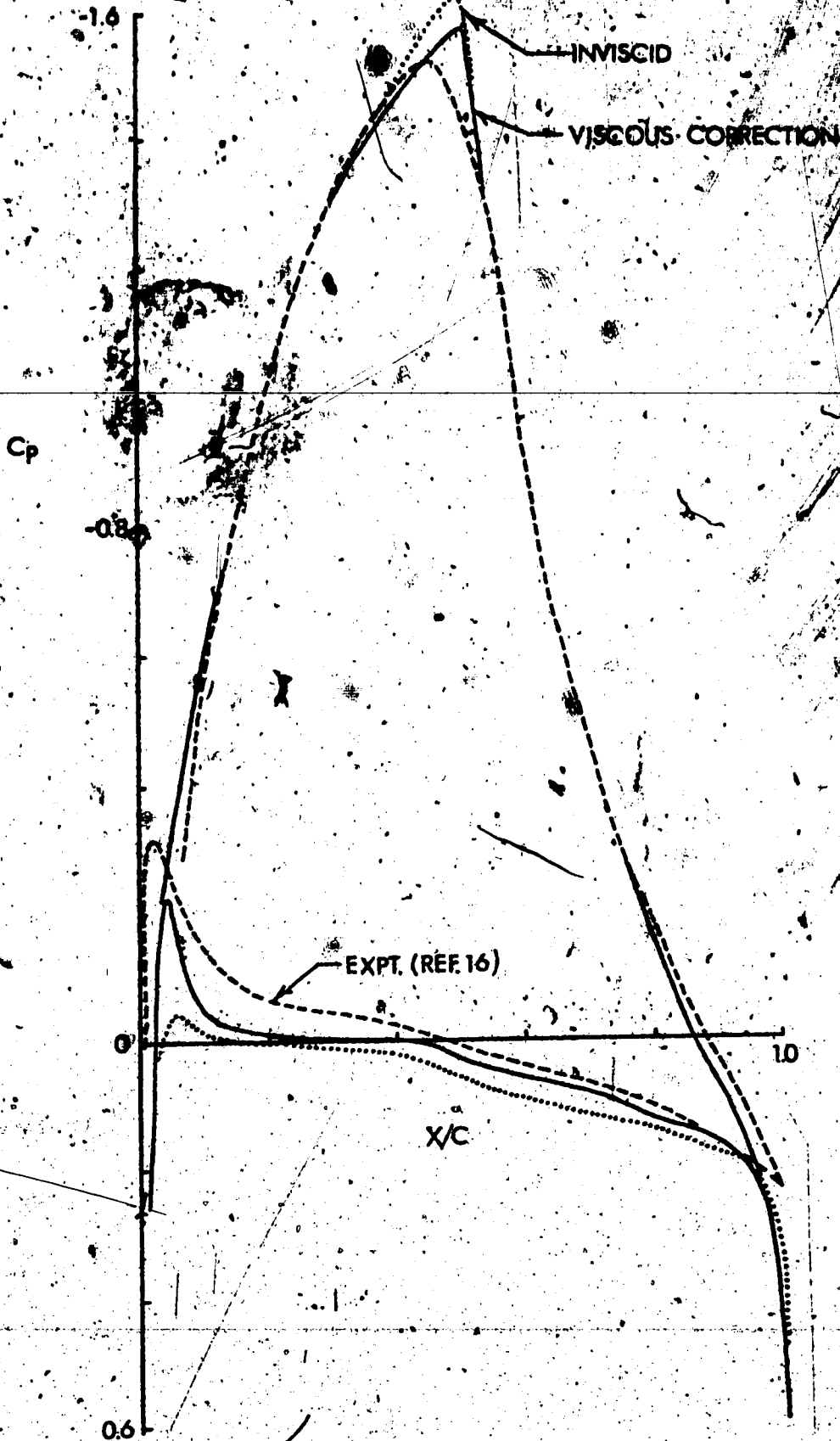
Figure 24. Comparison of Calculated Pressure Distributions on the GU-25-5(11)8 Airfoil ($\alpha = 0.6°$ and R = 0.63 x 10^{6})
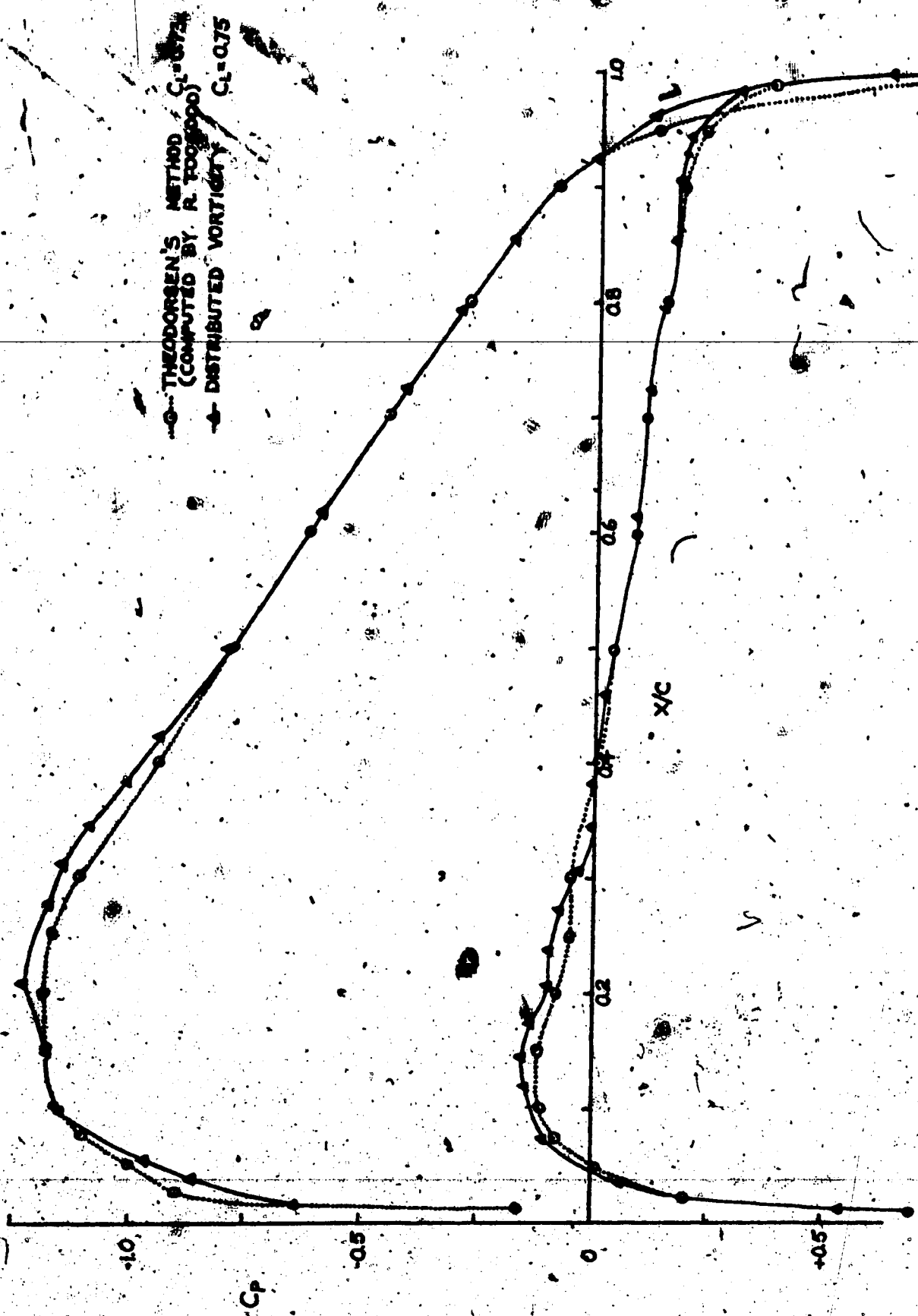
Figure 25. Comparison of Calculated Pressure Distributions on the NACA 4418 Airfoil (α = 2°).

hypothesis.

The usually good assumption that no pressure gradient exists across the wake at the trailing edge is probably incorrect because of the wake curvature at the trailing edge induced by the hook.

Sharp spikes in the pressure distribution at the trailing edge of the main section for a flapped aerofoil were also found by Stevens, Goradia and Braden using the method of distributed vorticity. The results of tests done using the Douglas Neumann Program and experimental results indicate that these spikes do not exist theoretically or experimentally.

The occurrence of a loop in the pressure distribution should be distinguished from the occurrence of a sharp peak. Loops in the pressure distribution are common for airfoils designed for small pitching moments.

Several airfoil sections were tested to determine the influence of the distribution coefficient (k) and the number of points on the pressure distribution and the lift coefficient. As indicated by Figure 26 the effect of decreasing k for the FX-61-163 "hooked" airfoil was to increase the lift coefficient and to move the pressure spike nearer the trailing edge. The lift coefficient also varied with N as shown in Figure 21. The results for the NACA 4424 airfoil show no spike in the pressure distribution (confirmed by experimental results) and a small variation in lift with k and N.
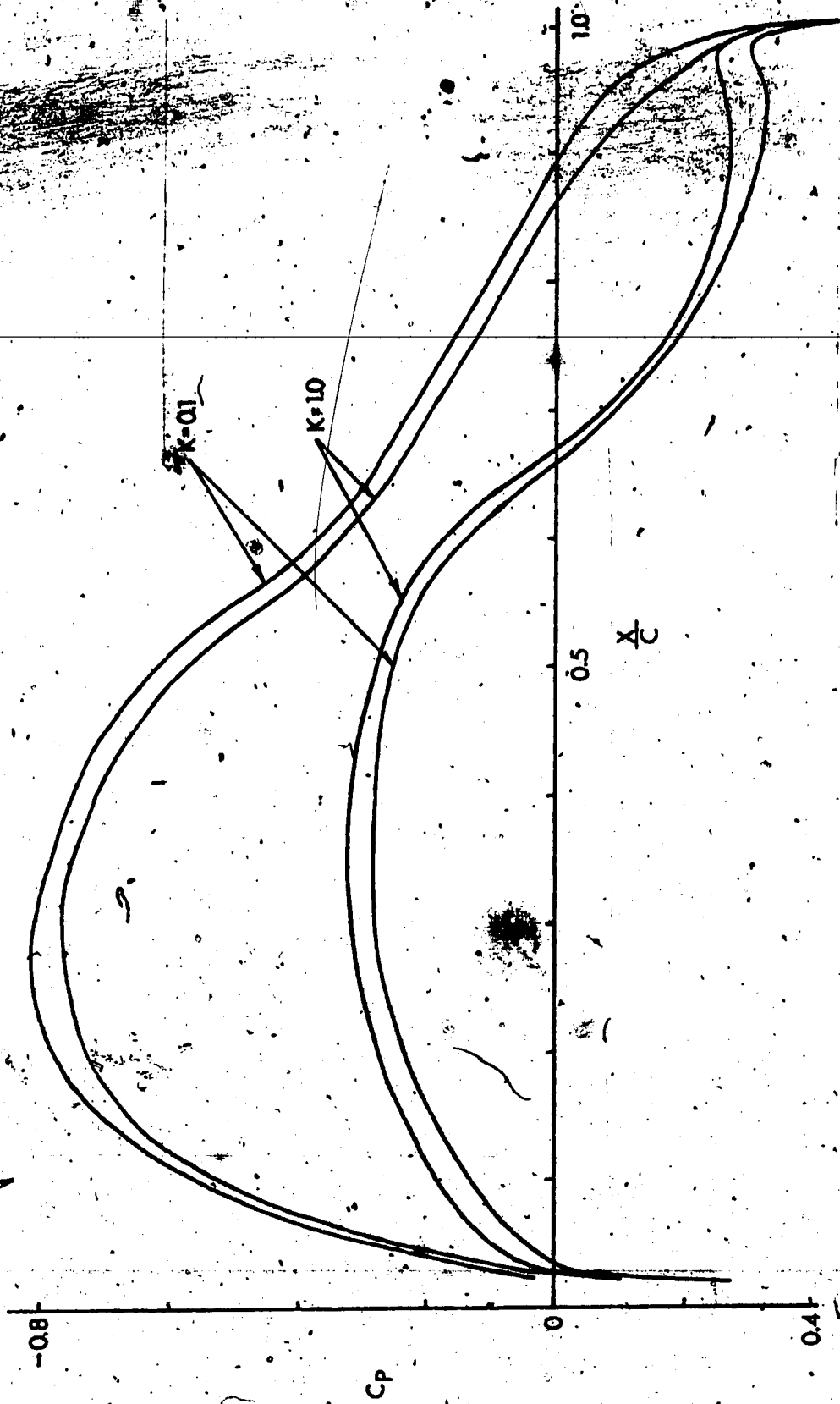
Figure 26. The Effect of Varying the Vortex Point Distribution Coefficient (k) on the Pressure Distribution of the FX-61-163 Airfoil ($\alpha = 0$ and $N = 40$)
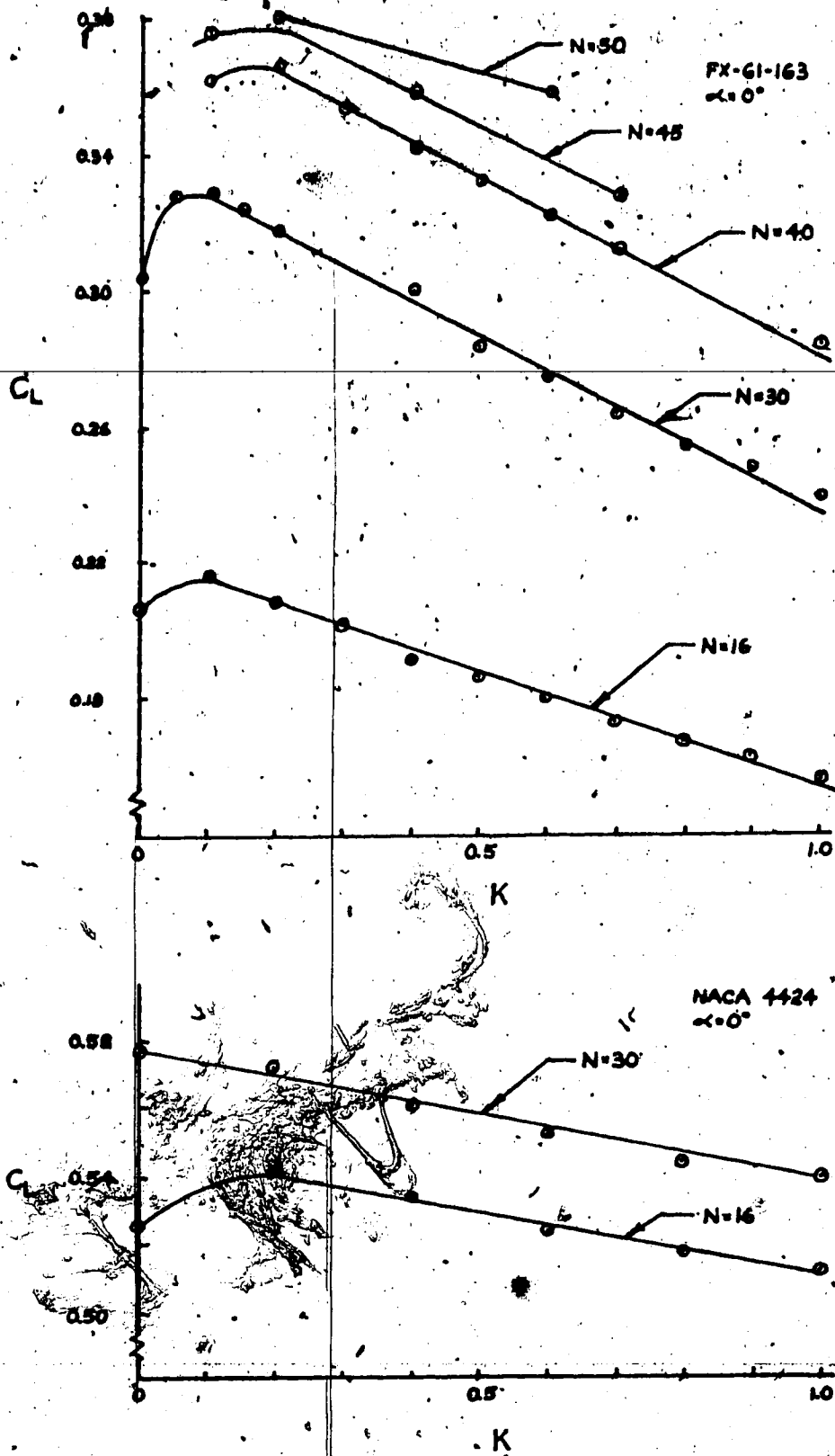
Figure 27. Variation of C_L with the Number of Vortex Points (N) and the Point Distribution Coefficient (k)

The distributed vorticity computer program was
assumed to give reliable results for the designed flapped
airfoil because the predicted lift coefficients were in line
with other slotted flap results for similar flap deflections.

The pressure distribution at the trailing edge of
the main section exhibits a steep pressure rise which should
be modified as shown by the dotted line in Figure 28. This
steep pressure recovery causes the prediction of flow separa-
tion for all the theoretical results. In addition the
occurrence of the loop means that the lift coefficient pre-
dicted for the main section is low.

Figure 28. Pressure Distribution on the Designed Main
Section with a Suggested Modification

APPENDIX B

LAMINAR AND TURBULENT BOUNDARY LAYER

CALCULATION AND THE PREDICTION OF

TRANSITION AND SEPARATION

Laminar Boundary Layer Calculation

Rosehead[31] suggests that an engineer may wish only to predict with sufficient ease and accuracy the features which interest him most: the position of separation, the distribution of skin friction and the variation of the displacement and momentum thicknesses of the boundary layer. Solutions of this type are characterized by a simplification of the boundary layer equations or the use of integral forms such as the momentum and energy equations.

Thwaites'[24] method is very suitable for general use in computing the important boundary layer parameters since it provides satisfactory accuracy with little computation. The estimate of the separation position is obtained more accurately by Curle and Skan's[32] modifications of Thwaites' method.

Thwaites' method makes use of the simplifying assumption that the laminar boundary layer profiles are a one parameter family. This assumption is good for favorable pressure gradients or weakly adverse pressure gradients. However the modification of Curle and Skan is required to

96

account for the case of strong adverse pressure gradients in order to find the point of separation.

Following is a brief summary and discussion of Thwaites' method.

Two non-dimensional parameters 1 and m are defined by the following equations:

$$1 = \frac{\theta}{U} \left(\frac{\partial u}{\partial y}\right)_{wall}$$

$$m = \frac{\theta^2}{U} \left(\frac{\partial^2 u}{\partial y^2}\right)_{wall}$$

Now $\nu \left(\frac{\partial^2 u}{\partial y^2}\right)_{wall} = \frac{1}{\rho} \frac{\partial P}{\partial x}$

and $\frac{\partial P}{\partial x} = -\rho U \frac{\partial U}{\partial x}$ so $m = -\frac{U'\theta^2}{\nu}$

m is related to the external velocity distribution (U) and is regarded as the form parameter (similar to the form parameter $\lambda = \frac{\delta^2}{\nu} U'$ of Pohlhausen's[33] method) if we assume a one parameter family of profiles. This implies that 1 and H are unique functions of m for all velocity profiles.

The momentum integral equation can be written as

$$\theta' + \theta(H + 2) \frac{U'}{U} = \frac{\nu 1}{U\theta}$$

Substituting for m

$$U \frac{d}{dx} (\theta^2) = 2\nu [m(H + 2) + 1] = \nu L(m)$$

Thwaites evaluated the expression represented by

the right hand side of the preceding equation for differing velocity profiles given by known exact solutions covering a wide range of pressure gradients and found that the resulting curves lay close to a straight line for which the equation was:

$$L(m) = 0.45 + 6m$$

This gives:

$$U\frac{d}{dx}(\theta^2) - 0.45\nu + 6U\theta^2 = 0$$

and

$$[\theta^2]_A = \frac{0.45\nu}{(U^6)_A} \int_0^A U^5 \, dx.$$

The plots of l and H as functions of m determined by Thwaites from the analysis of known solutions showed significant scatter for m > 0. This reflects the inadequacy of the assumption that the boundary layer profiles form a one parameter family. Certain exact solutions most relevant to the flow past aerofoils were selected as a guide, and based on these solutions a table of l and H as unique functions of m was established.

One result of this correlation is that a unique value of H must be assumed for separation of the laminar boundary layer where in fact H at separation has been found to vary between 4.04 and 2.6[33].

Curle and Skan[32] modified the H,l,m relationship so that the location of separation was more accurately predicted by Thwaites' method. It is interesting to note

that for the 11 pressure distributions for which exact
solutions were available the Curle and Skan modification
resulted in a very accurate prediction of the separation
point even though m calculated for these points, assuming
the linear relation L(M) = 0.45 + 6m, varied considerably.
While the value of H at separation predicted by Curle and
Skan is in error, the point of separation is predicted quite
accurately.

Curle and Skan's separation criterion is derived
in reference 32 and is a modification of Stratford's simpli-
fied formula. The criterion is that separation occurs when
the following is satisfied.

$$x^2 \, Cp \, \left(\frac{dCp}{dx}\right)^2 = 1.04 \times 10^{-2}$$

where $Cp(x) = .1 - \left(\frac{U}{U_m}\right)^2$ U_m is the maximum velocity and

$$x^2 = (x - x_0)^2$$

$$x_0 = x_m - \int_0^{x_m} \left(\frac{U}{U_m}\right)^5 dx$$ which allows for an initially

favorable pressure gradient.

Liu and Sandborn[34] plotted all available analytical
laminar boundary layer separation results and found H to be a
function of m at separation. They also showed that θ at sep-
aration determined by Thwaites' method is a good approximation,
so that in practice θ at separation can be calculated, and
the relation between $H_{sep.}$ and $m_{sep.}$ used to find $H_{sep.}$

In the computer program developed for this project
Curle and Skan's separation criterion is used to establish
the separation location. Thwaites' original relation between
H, l and m is used to find H although this is shown to be
a poor approximation for H.

The prediction of H at separation should probably
be made using the following table which is taken from the
curve drawn by Liu and Sandborn[34] based on the range over
which experimental profiles have been measured (H = 3 to
H = 4.04). Given $m = -\dfrac{\theta^2}{\nu} U'$ then H at separation can be
found by interpolation.

The important boundary layer results are the
values of θ and the point of separation. The parameter l
which involves skin friction is of little interest. The
shape factor H is required to predict the displacement thick-
ness δ^* which is needed to correct the inviscid pressure
distribution for viscous effects.

Transition

The most common modes of transition from a laminar
boundary layer to a turbulent boundary layer on an airfoil
are:

    (1)   transition resulting from the growth of instabilities.

    (2)   transition by means of the laminar separation
        bubble.

Most of the commonly used instability transition

Table 3. Correlation of $m_{separation}$ with $H_{separation}$ for the Laminar Boundary Layer

$m_{sep.}$	$H_{sep.}$
0.067	4.0
0.075	3.9
0.10	3.67
0.125	3.45
0.150	3.36
0.175	3.25
0.200	3.2
0.225	3.16
0.25	3.13
0.30	3.10
0.40	3.06

prediction methods are based on correlations of experimental data. For this program Crabtree's[35] criterion was chosen since it is based on a wide range of experimental data and is easy to apply. The basis of the method is a correlation of m (defined previously) at transition with Reynolds number based on the momentum thickness.

At low Reynolds number the point of laminar boundary layer separation usually precedes the point of theoretical transition on an airfoil. Experimental results show that under these conditions the flow will often reattach to the surface some distance downstream as a turbulent boundary layer. The region underneath the separated flow, between the points of separation and reattachment, is referred to as a "laminar separation bubble".

Experimental results suggest the existence of two bubble groups: short bubbles and long bubbles. A criterion was proposed independently by Tani, Owen and Klanfer, and Maekawa, and Atsumi[15]. Owen and Klanfer[36] proposed the following. For $R_{\delta*}$ greater than 400-500 at separation, a short bubble will exist with length of the order of 100 δ^*; for $R_{\delta*}$ less than 400-500 a long bubble will exist with length on the order of $10^4 \delta^*$.

The existence of a short bubble does not seriously disturb the pressure distribution. For the purposes of calculation, short bubble transition was assumed to occur within one calculation step (one percent of the chord).

Since no criterion exists for predicting the length of a long bubble, calculation must cease if long bubble formation is predicted. The presence of a long bubble makes the pressure distribution radically different from that in inviscid flow. A suction plateau of reduced level is formed which extends over the region occupied by the bubble length.

High lift airfoils of the FX-67-K-170 type exhibit a particular type of stalling behavior. At low Reynolds numbers the transition to turbulence is by means of a short bubble. The location of transition remains fairly stable with increasing incidence although eventually boundary layer separation begins near the trailing edge. With increasing incidence this region of separated flow expands and the airfoil stall is typical of the "trailing edge" type. Since the nose suction peak develops rapidly, the laminar boundary layer separation point moves quickly to the nose, with the formation of a long bubble. Because long bubbles grow rapidly with incidence, the angle of incidence for maximum lift is essentially the angle at which long bubble formation begins.

In the calculation program, the laminar boundary layer momentum thickness is matched to the turbulent momentum thickness at the point of transition. In addition the mass flows in the boundary layers must be equal. Since θ is known, it only remains to determine H^* ($H^* = \frac{\delta - \delta^*}{\theta}$) which is the mass flow parameter.

Pohlhausen's[33] laminar boundary layer profiles can be used to approximate δ at transition. Admittedly, at transition, a laminar boundary layer does not exist, however no other choice exists but to estimate the thickness by assuming a laminar layer. Fortunately Head's[23] turbulent boundary layer calculation method, used in this project, is quite insensitive to errors in the starting value of H^* and H.

The parameter H^* (at transition) can be used to find the shape factor H for the turbulent boundary layer at transition either by using correlations provided by Head or else by using an iterative method discussed by Seebohm[37]. The latter method was used in the computer program.

Calculation of the Turbulent Boundary Layer and the Prediction of Separation.

Thompson[38] conducted a critical review of the turbulent boundary layer methods in use and concluded that Head's[39] entrainment equation appears to give the best general level of agreement with experiment. Bradshaw[40] contends that the success of Head's method is based on the fact that, in contrast to most of the other integral methods, it is based on a clear physical hypothesis about turbulent flow.

Head's method was one of several considered at the Stanford Conference on the Computation of Turbulent Boundary Layers[41]. In a subsequent paper Head and Patel[23] presented an improved method which they consider to be "at least as

accurate as the best presented at Stanford while being
sufficiently simple to enable a hand calculation to be com-
pleted in an hour or two, and a computer calculation in a
very few seconds".

Based on its proven accuracy and speed, this
method was chosen as the turbulent boundary layer calculation
method.

Before considering the method it is valuable to
consider the physical hypotheses on which it is based.

Turbulent shear flows are dominated by large eddies
with a wavelength of about the same order as the thickness
of the boundary layer. Bradshaw[40] states that "the large
eddy observed in shear flow is basically a mixing jet, a slow
drift of rotational fluid with v/U no greater than 0.1, start-
ing from somewhere in the low velocity part of the flow and
moving towards the high velocity free stream". The outer
part of the turbulent boundary layer consists of a series of
billows or clumps or eddies of turbulent fluid which are res-
ponsible for the phenomenon of intermittency.

Bradshaw states that "a turbulent shear flow con-
sists of large eddies at various stages of their development
with a background of less successful perturbations" and
further that "in a real turbulent flow there will be a trans-
fer of turbulent energy to the smaller eddies which dissipate
it by viscosity and so the eddy will eventually die away after
having increased the boundary layer thickness by entraining

fluid from the free stream".

The outer boundary of the turbulent flow is normally defined by the outer boundaries of the turbulent clumps. The closer the billows are packed, the narrower the spread of intermittency. Hence the intermittency will be more and more confined to the region near the edge of the boundary layer. Entrainment is then reduced by closely packed billows and enhanced by a loose packing which permits a deeper penetration of the irregular boundary.,

The main hypothesis of Head and Patel is that an increase in the adverse pressure gradient beyond that of the equilibrium layer results in a reduction in entrainment while an increasingly favorable pressure gradient results in an increase in entrainment.

The preceding hypothesis seems reasonable. For example in a boundary layer proceeding to separation, the skin friction decreases rapidly while the displacement thick- ness increases rapidly. This implies a weak entrainment of free stream fluid into the boundary layer. In addition we can expect little growth of the large eddies because the shear in this boundary layer is decreasing and it is the mean veloc- ity profile which provides the turbulent energy for the growth of turbulent eddies.

The following discussion emphasizes the application of the method. References 23 and 39 provide a detailed dis- cussion.

Head's[39] original method assumed that the entrain-
ment of fluid into the boundary layer was independent of the
Reynolds number. In addition the quantity entrained per
unit area of the surface was thought to depend only upon the
boundary layer thickness, the velocity outside the boundary
layer and the distribution of velocity in the outer part of
the layer.

If the quantity of flow in the boundary layer per
unit time is Q then dQ/dx represents the amount of fluid
entrained by the boundary layer per unit length. The basis
of the method is then:

$$\frac{1}{U} \frac{d}{dx} [U(\delta - \delta^*)] = F(H^*).$$

Now $\frac{d}{dx} [U(\delta - \delta^*)] = \frac{dQ}{dx}$ and H^* is assumed to be a function of

the conventional form parameter H so that $H^* = G(H)$.

The functions F and G were determined on the basis
of limited experimental results. The drawing of a curve
representing the function $F(H^*)$ was a somewhat arbitrary
procedure however the justification is found in the accuracy
with which it enabled the form-parameter development to be
predicted in the examples.

However the assumption that entrainment is uniquely
related to H^* is over-simplified. The original entrainment
method is inadequate in the case of equilibrium flows and
flows where a strong adverse pressure gradient is followed
by a region of zero pressure gradient. The improved

entrainment method seeks to correct these deficiencies.

The accurate calculation of equilibrium flows (boundary layers where H is constant) is of particular interest since this type of turbulent boundary layer develops on the low drag airfoils discussed previously.

If the entrainment is written as $C_E = \frac{1}{U} \frac{dQ}{dx}$ and if the entrainment in the equilibrium layer is taken as datum, then for layers proceeding to separation the entrainment should be reduced, and for layers where H is decreasing it should be increased. The result is obtained by multiplying C_E for the equilibrium layer by a suitable function of some parameter that measures the departure from equilibrium conditions. The function chosen was $F(r_1) = C_E/C_{Eequil.}$ where the chosen parameter

$$r_1 = \left[\frac{1}{U} \frac{d(U\theta)}{dx}\right] \bigg/ \left[\frac{1}{U} \frac{d(U)}{dx}\right]_{equil.}$$

If $F(r_1)$ is determined, C_E can be found for given values of H and R_θ if $C_{Eequil.}$ is known as a function of these variables. Since H and H* vary slowly with x in equilibrium layers,

$$C_{Eequil.} = H^* \left[\frac{1}{U} \frac{d(U)}{dx}\right]_{equil.}$$

The relation between H* and ■ necessary to complete the relation is provided by Thompson's[42] profile data which also provides a new skin-friction relation to replace the Ludwig - Tillmann relation.

It is convenient to write the basic entrainment relation in the following way:

$$\theta \frac{dH^*}{dx} = H^* \left[\frac{1}{U} \frac{d(U\theta)}{dx} \right]_{equil.} [F(r_1) - r_1].$$

Practical calculation proceeds as follows:

(1) The momentum integral equation.

$$\frac{1}{U} \frac{d(U\theta)}{dx} = \frac{C_f}{2} - (H + 1) \frac{\theta}{U} \frac{dU}{dx}$$

is used to find the increment in $U\theta$ over a step. The skin friction relations given in graphical form can be approximated by the analytic relations:

$$C_f = \exp (aH + b)$$

$$a = 0.019521 - 0.386768c + 0.028345c^2 - 0.000701c^3$$

$$b = 0.191511 - 0.834891c + 0.062588c^2 - 0.001953c^3$$

$$c = \log_e R_\theta.$$

(2) $C_{Eequil.}$ is calculated and r_1 is calculated.

(3) $F(r_1)$ is calculated. $F(r_1) = \dfrac{1}{2r_1 - 1}$ for $r_1 \geq 1$

and $F(r_1) = \dfrac{5 - 4r_1}{3 - 2r_1}$ for $r_1 < 1$. H^*, H and $R\theta$ are known

at the transition point.

(4) The entrainment relation gives the increment in H^*.

(5) The values of $R\theta$ and H^* at the end of the step are used to find H (from the tables).

It can be seen that the success of the method depends on the validity of the hypotheses concerning turbulent boundary

layers and also on the accuracy of the functions C_f (R_θ, H) and $H(H^*, R_\theta)$. Thompson[42] established the preceding relations from an analysis of the incompressible turbulent boundary layers on smooth walls. The family of profiles that was proposed was checked against a broad spectrum of experimental profiles.

Sandborn and Liu[43] show that fully developed separation of the turbulent boundary layer cannot exist for H less than 2.7 and that intermittent separation cannot exist for H < 2.0. Separation has been commonly assumed to occur between H = 1.8 and H = 2.4.

Stratford's[10] separation criterion was tested in the computer program for the boundary layer development on the high-lift airfoil sections. Separation was predicted for H = 1.6. Since this is improbable and does not compare to the experimental results for these airfoils, the Stratford criterion is inapplicable.

The reason for the failure of the criterion is attributable to the fact that for airfoils of this type the turbulent flat plate profile assumed to exist at the beginning of the pressure rise would not be properly formed.

Using the method of Head and Patel it was found that erratic values of H were predicted when the factor H reached about 2.3. This suggests that the limits of Thompson's[42] profile data have been exceeded. Since Thompson's data compares well to experimental results, it can be concluded that

the failure of Head's method constitutes an adequate separa-
tion criterion particularly since the failure value of H is
greater than 2 which conforms to the result of Sandborn and
Liu.

The drag coefficient is determined from the Squire
and Young[44] relation which is well suited to theoretical
results. The results from stations slightly upstream of the
trailing edge are used since the large velocity jump very
near the trailing edge, not found experimentally, results in
erroneous calculations.

Because of the theoretical steep pressure recoveries
near the trailing edge, separation is nearly always predicted
over the last portion of the airfoil on the suction side. To
account for this, separation was not assumed to exist in reality
until the theoretical separation point had moved back to 93%
chord.

The method was tested on several airfoils and the
drag coefficients calculated for unseparated flow were found
to be very close to the experimental values. In addition the
drag was found to change very little after the pressure dis-
tribution had been corrected for viscous effects.

APPENDIX C

<u>THE DESIGN OF LOW-DRAG AIRFOIL SECTIONS</u>

The profile drag of a practical airfoil section cannot be less than the drag on a smooth flat plate at zero incidence with laminar boundary layers on both surfaces. Skin friction accounts for all of the profile drag on a flat plate whereas the profile drag of a wing section is composed of skin friction drag and pressure drag.

The pressure drag (or form drag) arises from the alteration of the potential flow pressure distribution about the airfoil by means of the boundary layer. A net pressure force results and acts in the direction opposing the motion of the airfoil. Because a flat plate has no thickness (in theory) only longitudinal shearing forces are possible.

The profile drag of a flat plate depends on the Reynolds number. Skin friction is of course dependent on velocity but more important the proportion of laminar boundary layer is determined by the location of transition. For low turbulence flow over a smooth surface with no pressure change, the transition point depends on the Reynolds number and moves upstream as the Reynolds number increases.

Up to a Reynolds number of about 3×10^5, the boundary layer is entirely laminar while at a Reynolds number of about 5×10^6 the boundary layer is almost completely

turbulent. This range defines the "transition" range within which drag reductions are possible by extension of the laminar boundary layer. Reynolds numbers of interest in this project (10^6 - 3×10^6) of course lie within this range.

Normally within the range of Reynolds numbers above one million, transition to turbulence is by the growth of boundary layer instabilities. However transition is also possible by means of laminar separation bubbles particularly for the situation of the leading edge suction peak on an airfoil at high incidence.

Instability type of transition is influenced by free-stream turbulence, surface roughness and pressure gradients, apart from Reynolds number. If surface roughness and turbulence are ignored, then transition can only be controlled by the pressure gradients.

The principle of the control of transition position is basic to the design of the low-drag airfoils. These airfoils exhibit a clearly defined almost uniform low-drag range because:

(1) over the low-drag lift coefficient range, the position of transition of both boundary layers remains fairly steady.

(2) the shape of the optimum pressure recovery distribution remains basically fixed.

Transition is confined to the so called "instability region". This is a region of uniform pressure or slightly increasing pressure just upstream of the primary pressure recovery; it is designed so that over the low-drag range transition will lie within it. Because of this, the boundary layer is fully developed at the beginning of the main pressure recovery for a range of lift coefficients and since the optimum pressure recovery is fixed, the boundary layer will grow in almost the same manner over the range of lift coefficients. At the same time since transition moves forward only slightly with increasing lift, the extent of laminar boundary layer is fairly constant. Older airfoil sections experience a gradual forward migration of transition with increasing incidence and consequently a poorly defined low-drag range.

The profile drag of an airfoil section is given by the Squire and Young formula:

$$C_D = \frac{2\theta_u}{c} \left(\frac{U_u}{U_\infty}\right)^{\frac{H_u+5}{2}} + \frac{2\theta_1}{c} \left(\frac{U_1}{U_\infty}\right)^{\frac{H_1+5}{2}}$$

The subscripts u and 1 refer to conditions at the trailing edge of upper and lower sides respectively. It is clear from this relation that drag is reduced by reducing θ_u and θ_1, and by increasing H if $\frac{U_1}{U_\infty}$ (or $\frac{U_u}{U_\infty}$) is less than unity. By maximizing H (by designing the pressure recovery for $H = H_{separation}$) θ_1 (or θ_u) is minimized. This was discussed

previously. For $H = H_{separation}$ and a fixed Reynolds number,
U (at the trailing edge) depends on the maximum value of U
(on the side of the airfoil being considered) and the length
of pressure recovery. This means that ordinarily the lowest
drag can only be achieved for airfoils designed for low lift
coefficients.

In theory the lowest possible drag would be
achieved by extending the laminar boundary layer to the max-
imum on both surfaces followed by optimized pressure recovery.
Alternatively pressure recovery might be restricted to one
side with a uniform pressure or gradually decreasing pressure
on the other side. At low Reynolds number, using the second
method, it is difficult (in practice) to get the desired lift,
the desired pressure recovery and the low trailing edge vel-
ocities simultaneously. Therefore, in practice, low-drag
airfoils are usually designed for at least some pressure
recovery on both surfaces.

The method of Truckenbrodt[1] is useful for the
design of airfoils from given pressure distributions.
Truckenbrodt's method is based on the work of Riegels[45,46]
involving the distribution of sources and vorticity along the
mean line. The main assumptions of the method are:

(1) The thickness distribution of the airfoil is related
to the mean velocity distribution over the airfoil.

$$U_m = \frac{U_u + U_l}{2}$$

(2) The mean line shape is determined by the velocity

deviation.

$$U_C = \frac{U_u - U_l}{2}$$

In addition airfoils designed by this method are designed such that the given pressure distribution exists for the ideal angle. In other words at the design lift the front stagnation point is at the nose.

The airfoil sections designed using this method exhibit the favorable characteristic that the design angle of incidence is nearly zero because the shape of the camber line is used primarily to generate the required lift.

An interesting problem arises from the application of Truckenbrodt's method to the design of airfoils employing optimized pressure recoveries. If the airfoils are designed for no pressure difference at the trailing edge, the resulting airfoil will usually have a small loop near the trailing edge. If however the pressure distributions are designed with a finite pressure difference at the trailing edge then the loop is eliminated. Furthermore these airfoils exhibit a cusped trailing edge with a pronounced "hook" typified by the NACA $66_2 - 415^3$, airfoil section.

Limited experimental results[29] support the existence of a pressure difference at the trailing edge for hooked airfoils. Airfoils for which the pressure difference (loading) diminishes to zero at the trailing edge are typified by the

NACA four digit series. This series does not exhibit the "hook".

The design problem then is to determine what pressure difference is possible at the trailing edge. Based on experimental data[29] for other airfoils, it appears that as the pressure difference at the trailing edge is increased, the designed airfoil becomes more severely cusped with a more pronounced "hook".

This suggests that lower drags may be possible because smaller pressure recoveries are possible at the same design lift. The pressure recovery regions can be reduced in length allowing the extension of the laminar boundary layer (at least at low enough Reynolds numbers).

A practical limitation on this procedure would be the difficulty in manufacturing the thin cusped highly cambered trailing edges.

Two low-drag airfoils were designed to gain experience with Truckenbrodt's method. These profiles and the design velocity distributions are shown in Figures 29 and 30.

For airfoil number one, the extent of the pressure recovery was the same on both surfaces and based on similar designs at $R = 3 \times 10^6$, the point of transition was expected to lie just upstream of the pressure recovery for the design pressure distribution. Theoretical results confirmed this prediction. The point of transition was calculated to lie
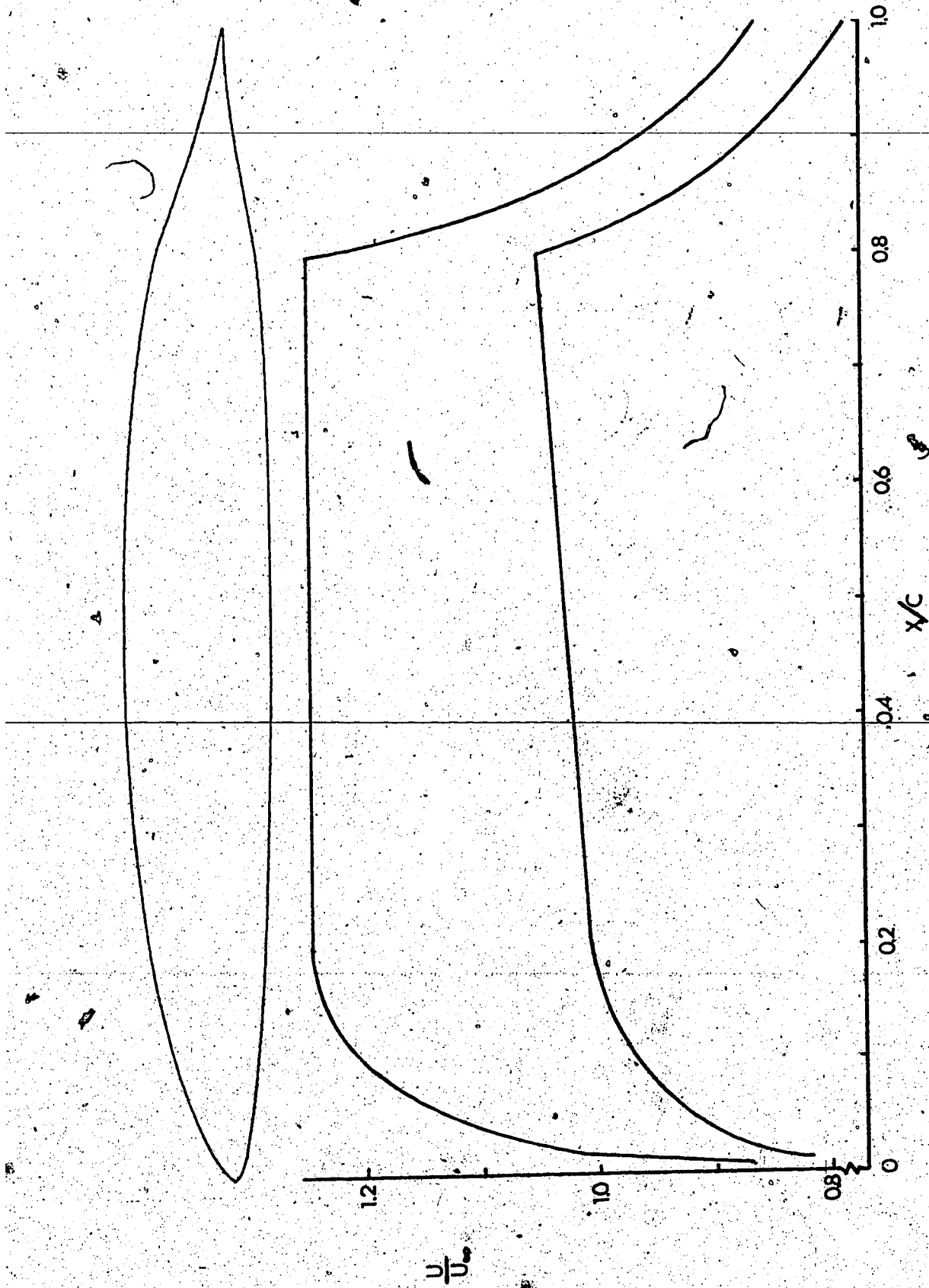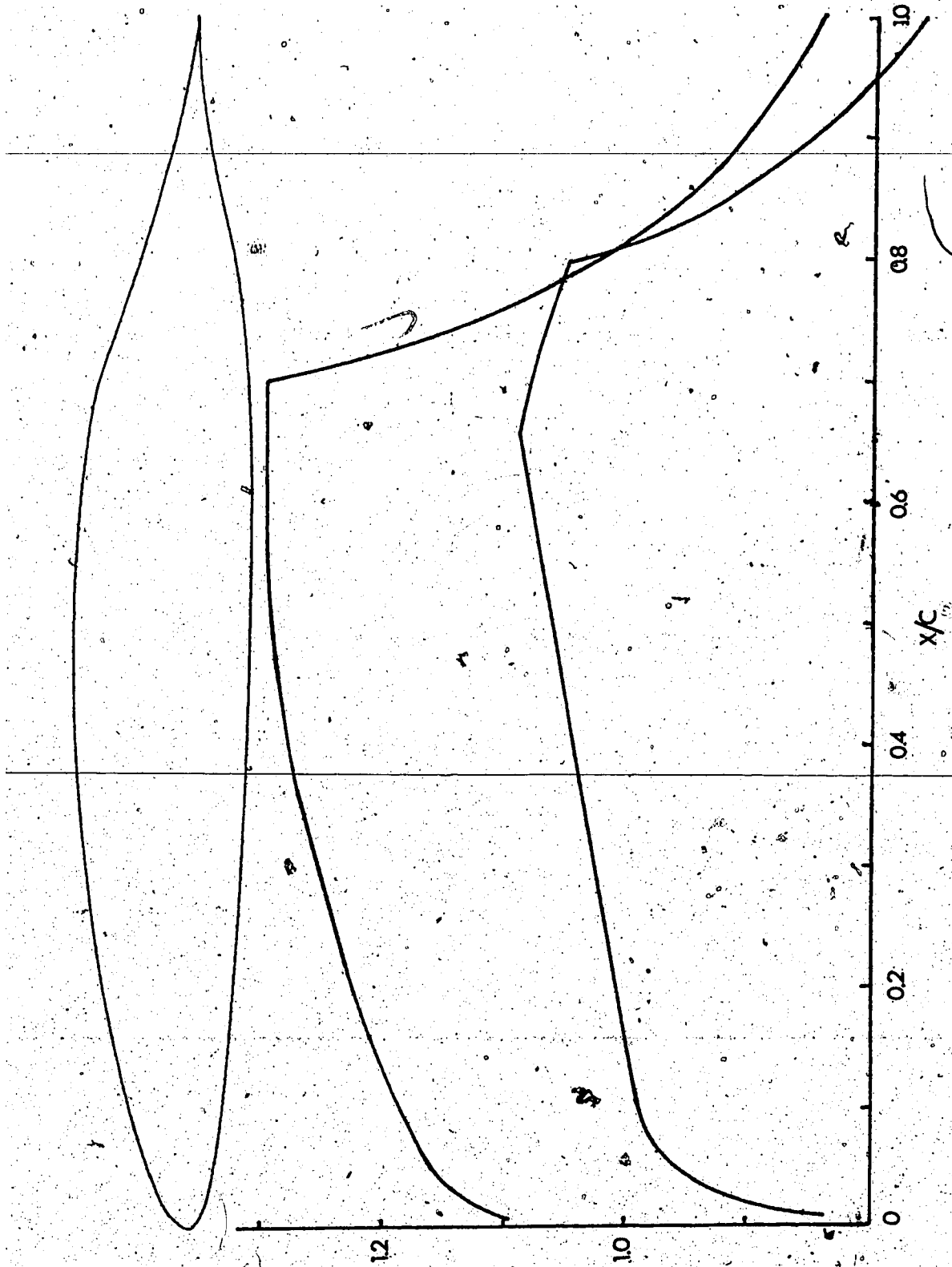
Figure 29. A Low Drag Airfoil Section Designed for
R = 3 x 10⁶.

Figure 30. A Low Drag Airfoil Section Designed for
R = 2 x 10⁶

at about 78% chord on both sides. The design potential lift coefficient was 0.35 and the drag coefficient based on the potential pressure distribution was 0.00325. This compares favorably with other low-drag designs. For the suction side, the boundary layer form parameter in the pressure recovery region was constant at about 1.6 compared to the design pressure recovery of 2.2. (This problem is discussed in Chapter II).

The small nose radius of airfoil number one results in the rapid development of a severe suction peak at the nose. This means that the low-drag range is quite narrow since the optimum conditions disappear rapidly as the suction peak grows.

The second low-drag airfoil was designed for $R = 2 \times 10^6$. This required the inclusion of instability regions on both sides because at this Reynolds number boundary layer transition must be promoted by regions of uniform or slightly increasing pressure. If these regions are chosen correctly (in terms of length and pressure gradient), the transition point will move only slightly with increasing incidence. Consequently optimum pressure recovery is possible over a range of lifts because a fully-developed young turbulent boundary layer will exist at the beginning of the optimum pressure recovery.

For this airfoil the design potential lift coefficient was 0.29 and the calculated drag coefficient was 0.0039.

The relatively sharp nose again results in a sharply defined low-drag range. The instability regions functioned well with the suction side transition fairly stable at 68% chord while the pressure side transition point moved from 66% chord for C_L = 0.128 to 79% chord for C_L = 0.574.

Some experience is required in specifying instability regions. The length of instability regions can be estimated from previous results of others, however the pressure gradient must usually be established by trial and error.

APPENDIX D

Experimental Apparatus and Results

A 12 inch (flap retracted) chord model of the designed airfoil section was tested in the aeronautical open return wind tunnel in the Department of Mechanical Engineering at the University of Alberta.

The test section measured 18.375 inches by 8.375 inches and the model spanned the shorter dimension. The tests were conducted at Reynolds numbers between 0.77 and 0.84×10^6; the wind tunnel test section turbulence level was 0.34%.

Experimental results were obtained for two test section configurations: one with a 75% open area ratio slotted upper wall[48] and one with a normal (closed) upper wall. The flap extended configuration was tested in the slotted test section only while the flap retracted configuration was tested in both test section configurations.

The Slotted Test Section

Williams[48] showed that for a 75% open area ratio upper wall, no wind tunnel corrections are required since wind tunnel interference is reduced to negligible amounts. For these tests the test section was sealed by a second upper wall while the slotted wall consisted of three inch

chord symmetrical airfoil sections with a nine inch

spacing (to give a 75% open area ratio).

Dynamic pressure was measured with a pitot

static tube approximately one chord length downstream of

the model. This value was used for the lift and drag

coefficients. No corrections were applied to the results

obtained in the slotted wall tests.

The Closed Test Section

The data obtained from the closed test section

were corrected using the standard wind tunnel corrections

for solid blocking, wake blocking and streamline curvature

outlined by Pope and Harper.[49]

The three relations for corrections to C_L, C_D and

α for two dimensional testing in a closed test section are:

$$\alpha = \alpha_u + \frac{57.3\sigma}{2\pi} (C_{Lu} + 4C_{M\frac{1}{4}u})$$

$$C_L = C_{Lu} (1 - \sigma - 2\varepsilon)$$

$$C_D = C_{Du} (1 - 3\varepsilon_{sb} - 2\varepsilon_{wb})$$

Here subscript u refers to the uncorrected results or the

experimental results.

$$\sigma = \frac{\pi^2}{48} (\frac{c}{h})^2$$ where $\frac{c}{h}$ is the ratio of model chord

to the tunnel height. For the tests $\sigma = 0.0876$.

ε_{sb} is the term associated with solid blocking

$\varepsilon_{sb} = \Lambda\sigma$ where Λ depends on the thickness to chord ratio

of the wing section and is about 0.3 for the tests, from which $\varepsilon_{sb} = 0.026$.

ε_{wb} is the wake blocking term. $\varepsilon_{wb} = \frac{c}{2h} C_{Du}$.

For the tests C_{Du} was in the neighborhood of 0.0075 so that ε_{wb} was taken as 0.0025. $\varepsilon = \varepsilon_{sb} + \varepsilon_{wb}$

The moment coefficient $(C_{M\frac{1}{4}u})$ about the quarter chord point was about -0.1.

Therefore for the tests:

$$\Delta\alpha = \alpha - \alpha_u = 0.8 \ (C_{Lu} - 0.4)$$

$$C_D = 0.917 C_{Du}$$

$$C_L = C_{Lu} \ (0.855)$$

C_{Lu} was the uncorrected lift coefficient based on the dynamic pressure measured downstream in the slotted test section for the same angle of attack.

Experimental Procedures for Pressure Distribution and Lift

The pressure distribution around the airfoil was measured using a scanivalve and pressure transducer. Static pressures were measured at 43 points on the wing surface; the locations of the taps are given in Table 4. The primed numbers refer to taps on the flap section.

Dynamic pressure was measured with a standard pitot static probe at a point approximately one wing chord downstream of the model. This location is far enough away from the model to be free of the influence of the static pressure field around the model.

TABLE 4

Locations of Pressure Taps on the Model

Retracted Section (Top)

Tap Number	Chordwise Position (inches)
1	0
2	0.115
3	0.318
4	0.619
5	1.011
6	1.489
7	2.044
8	2.667
9	3.344
10	4.070
11	4.829
12	5.608
13	6.392
14	7.171
15	7.929
15a	9.25
4'	10.120
3'	11.000
2'	11.381
1'	11.875

Retracted Section (Bottom)

Tap Number	Chordwise Position (inches)
16	0.280
17	0.619
18	1.011
19	1.489
20	2.044
21	2.667
22	3.344
23	4.070
24	4.829
25	5.608
26	6.392
27	7.171
11'	8.600
12'	9.925
13'	10.940
14'	11.380
15'	11.812

TABLE 4. (Continued)

Flap Section (Top)

Tap Number	Chordwise Position (inches)
9	0
8	0.12
7	0.56
6	1.31
5	2.0
4	2.32
3	3.189
2	3.581
1	4.075

Flap Section (Bottom)

Tap Number	Chordwise Position (inches)
10	0.26
11	0.80
12	2.125
13	3.14
14	3.58
15	4.012

Lift coefficient was determined from an integration
of pressure acting on the surface of the wing

$$C_L = \frac{1}{qc} \left[\int_0^c (P_O - P_{st})_{top} \, dx - \int_0^c (P_O - P_\infty)_{bottom} \, dx \right] \cos \alpha$$

where P_O is the pitot reference pressure for the transducer
and $dx = ds \cos \theta$. θ is the slope of the airfoil surface
and ds is the distance along the surface.

Experimental Procedure for Drag

A pitot traverse measuring total pressure in the
wake approximately one chord length downstream of the model
was used to determine profile drag.

The method of Jones[33] is applicable:

$$C_D = 2 \int_{wake} \sqrt{\frac{g_2 - P_2}{q_\infty}} \left(1 - \sqrt{\frac{g_2 - P_\infty}{q_\infty}} \right) \frac{dy}{c}$$

where g_2 is the total pressure measured in the wake, P_2 is
the static pressure in the wake, q_∞ is the free stream
dynamic pressure and P_∞ is the free stream static pressure.

Since the pitot traverse is well downstream of
the wing, $P_2 = P_\infty = P_{O\infty} - q_\infty$ where $P_{O\infty}$ is the free stream
total pressure. Hence $g_2 - P_2 = g_2 - P_{O\infty} + q_\infty$. If
$P_{O\infty} - g_2 = \Delta P$ (the loss of total pressure in the wake)
then:

$$C_D = \frac{2}{q_\infty c} \int_{wake} \left\{ [(q_\infty - \Delta P) q_\infty]^{\frac{1}{2}} - (q_\infty - \Delta P) \right\} dy$$

ΔP was measured directly at intervals through the wake and the corresponding intervals ΔY were measured simultaneously. Writing $q_\infty - \Delta P = A$ for convenience:

$$C_D = \frac{2}{q_\infty c} \Delta Y \ \Sigma [(Aq_\infty)^{\frac{1}{2}} - A].$$

The corrected experimental results are given in graphical form in Figures 33 and 34. Figures 35 and 36 are a sampling of measured pressure distributions for the slotted top test section case.
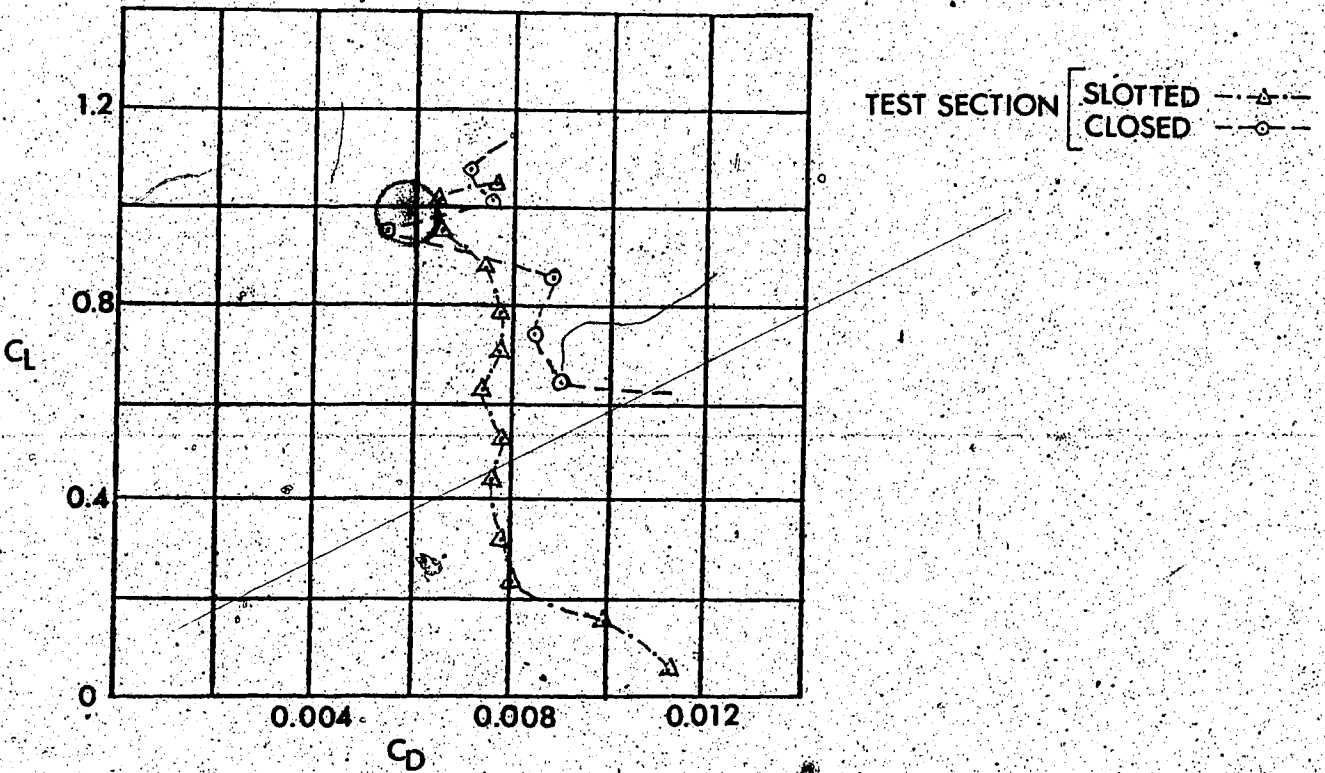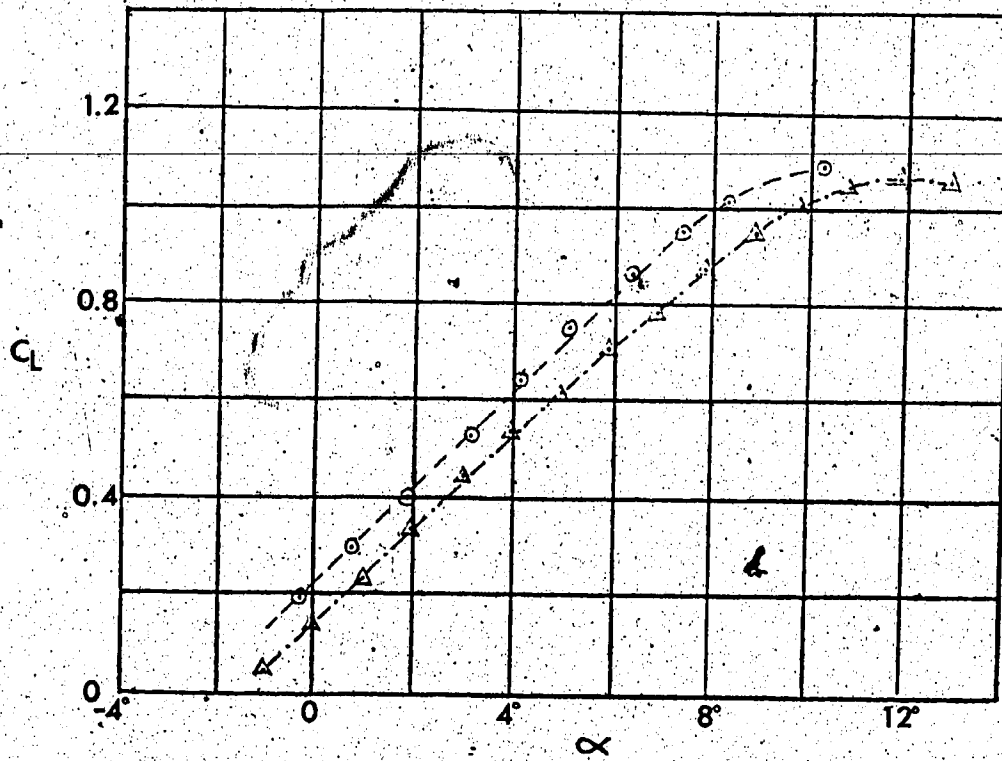
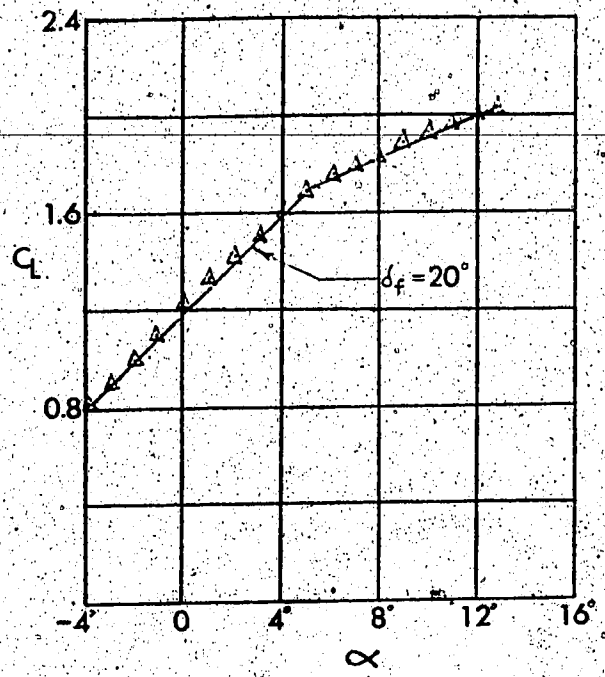**Figure 33.** Experimental Results for the Flapped Airfoil with the Flap Retracted (R = 0.84 x 10⁶)
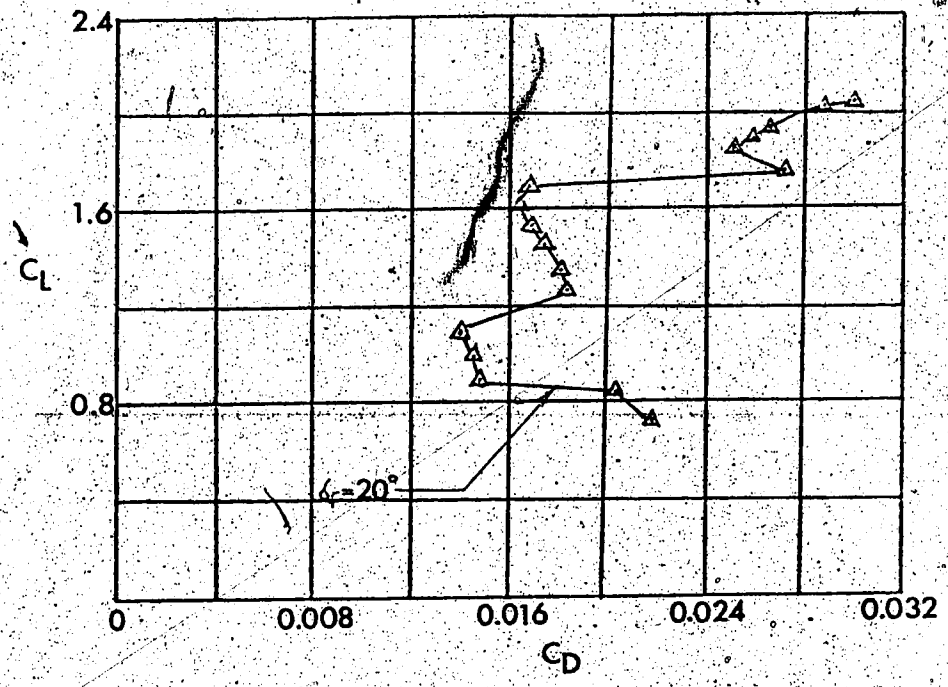
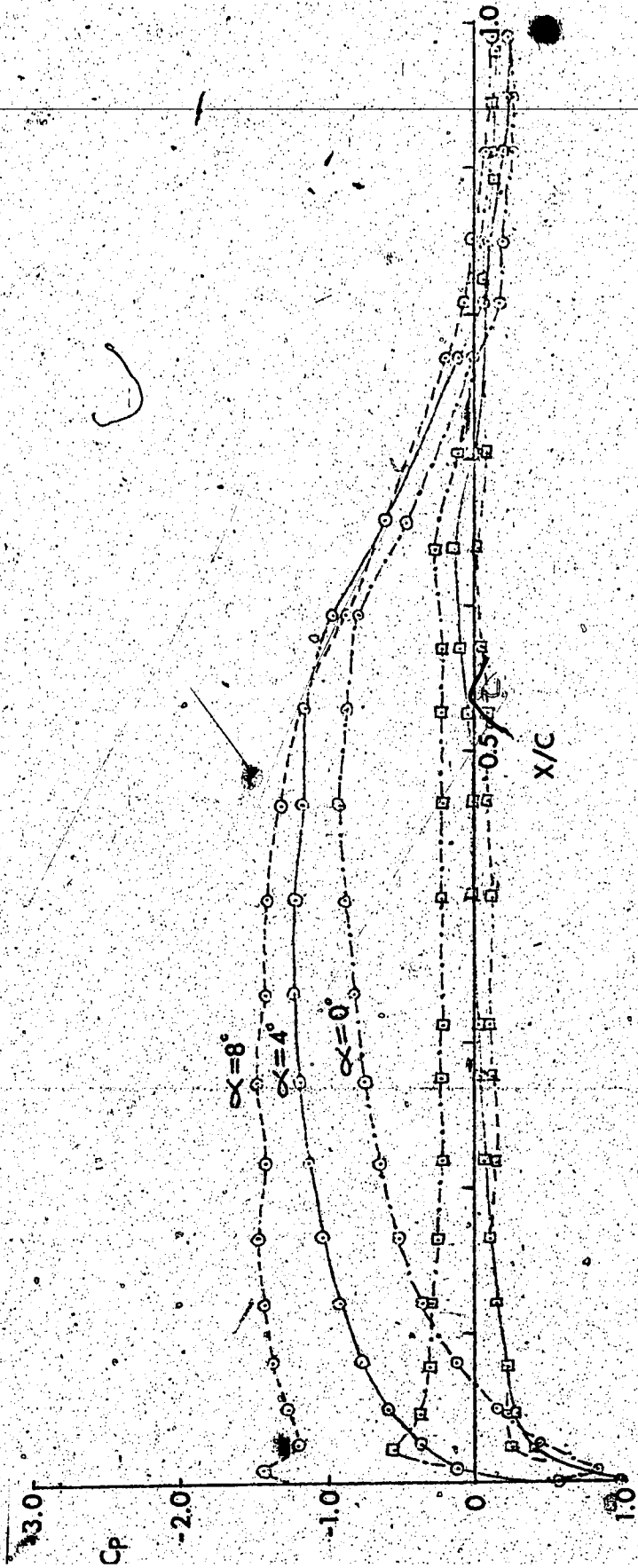Figure 34. Experimental Results for the Flapped Airfoil with the Flap Extended (Slotted Top Test Section, R = 0.84 x 10^6)

Figure 35. Experimental Pressure Distributions with the Flap Retracted (Slotted Top Test Section, R = 0.84 x 10⁶).
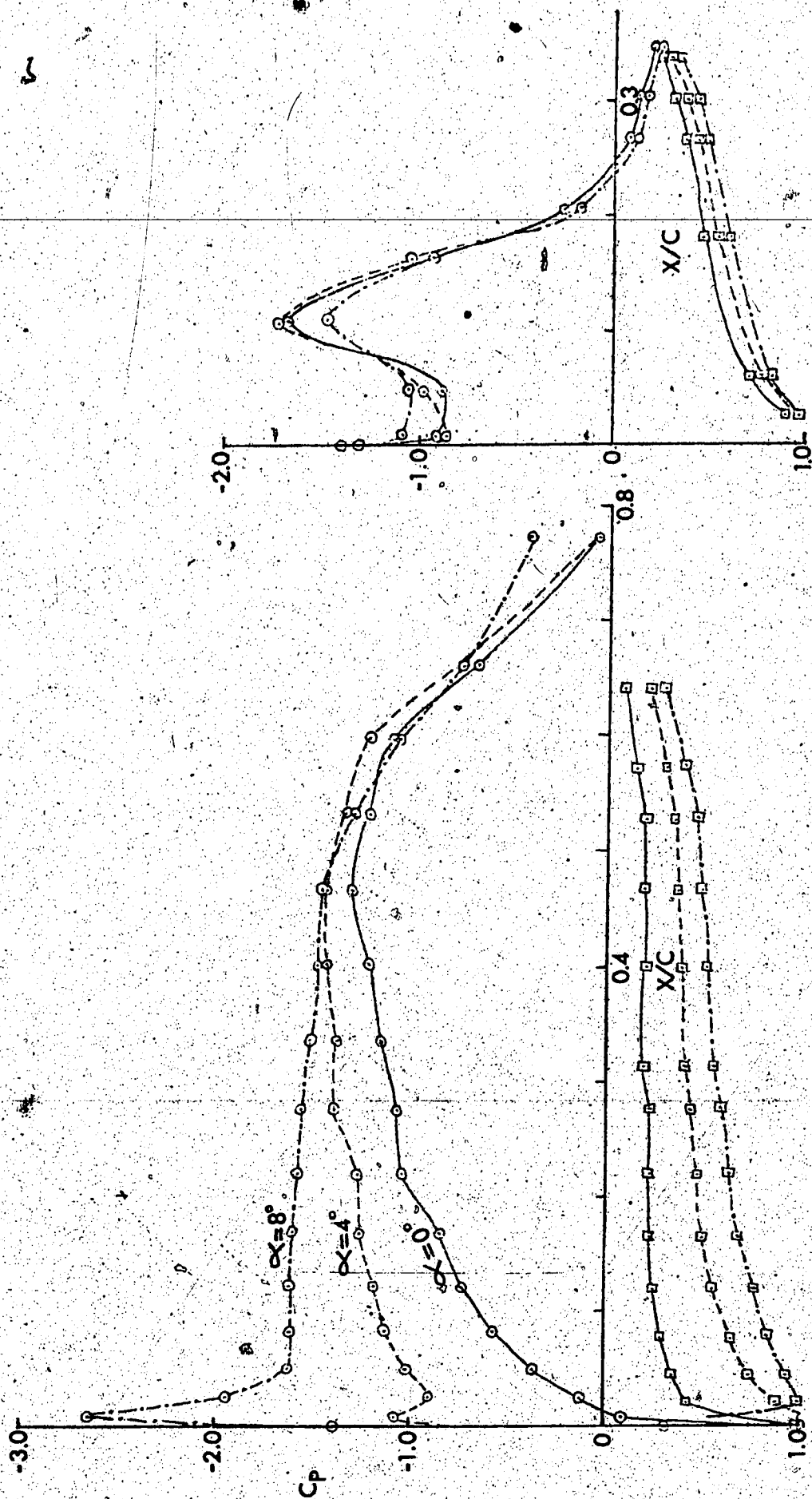
Figure 36. Experimental Pressure Distributions with the Flap Extended (Slotted Top Test Section, $\delta_f = 20^o$, $R = 0.84 \times 10^6$)